ESA/ESTEC

Contracts n° 16023/02/NL/SF
16026/02/NL/SF
16030/02/NL/SF

SOLAR INDUCED FLUORESCENCE EXPERIMENT (SIFLEX)

Final Report

FINNISH METEOROLOGICAL INSTITUTE

Solar Induced Fluorescence Experiment (SIFLEX)

FINAL REPORT

Jose Moreno, University of Valencia
Tuomas Laurila, FMI
Ismael Moya, Lure

FINNISH METEOROLOGICAL INSTITUTE

Solar Induced Fluorescence Experiment (SIFLEX)

FINNISH METEOROLOGICAL INSTITUTE

References

LIST OF PARTICIPANTS

FMI
Tuomas Laurila
Esko Kyrö
Tea Thum
Mika Aurela
Annalea Lohila
Virpi Lindfors
Jarno Kallonen
Juha-Pekka Tuovinen
Kaisa Lakkala
Noora Jaakola
Minna Turunen
Marja-Liisa Sutinen
Gunnar Wingsle

LURE
Ismael Moya
Abderrahmane Ounis
Jean-Marc Ducruet
Juliette Louis
Sebastian Evain

UVAL
Jose Moreno
Luis Alonso
Gloria Fenandez
Soledad Gandia
Jose C. Garcia
Luis Guanter
Jose M. Marti
John Miller
Jose A. Martinez-Lozano
Maria P. Utrillas
Roberto Pedros
Jose L. Gomez-Amo
Jose A. Sobrino
Guillem Soria
Juan Carlos Jimenez-Muñoz
Jauad El-Kharraz
Monica Gomez
Vicente Caselles
Raquel Niclos
Enric Valor
Cesar Coll
Juan Manuel Sanchez



FINNISH METEOROLOGICAL INSTITUTE

LIST OF FIGURES

LIST OF TABLES

1. Introduction to the SIFLEX-2002 campaign

1.1 BACKGROUND

For global change studies, understanding the role of forests as sinks and sources of carbon dioxide, the most challenging greenhouse gas, is of utmost importance. The carbon balance of a forest is the difference between the Gross Primary Production (GPP) and the total respiration (Rtot). A great effort has been made to quantify these components because the information is needed for the estimation and verification of carbon sinks according to the Kyoto Protocol.

Remote sensing is the only tool for achieving a homogeneous analysis on a large scale. Presently there are estimations of GPP from remote sensing observations using simple methods based on the measurements of fractional absorbed photosynthetically active radiation (fAPAR) and incident solar radiation covering the photosynthetically active region (PPFD):

$$GPP = PPFD * fAPAR * E \qquad (1)$$

Here E denotes the photosynthetic yield of plants. Presently it is assumed that E=1 because it is not possible to observe it from the space. In addition, there are no means to observe the ecosystem respiration from the space. This leaves the Net Ecosystem Exchange (NEE), representing the carbon sink, as unknown. To reach NEE balances based on remote sensing observations, a combination of modelling and measurement approaches has to be used. Considering coniferous vegetation, a major drawback in this approach is missing information of the biochemical activity of the trees. In the boreal region, the length of the growing season is one of the most important factors explaining the forest-atmosphere gas exchange. The efficiency of photochemistry during the spring recovery is crucial, because during that season plenty of solar radiation is available for CO_2 assimilation. It is difficult to observe the actual photochemical efficiency of coniferous tree species using traditional reflectance-based remote sensing methods, such as NDVI.

The photosynthetic yield has been measured by chlorophyll fluorescence instruments which give information on the down regulation of the photochemical apparatus e.g. due to dormancy, water stress or excess solar radiation. Fluorescence has been measured traditionally; using excitation light pulses by photodiodes, flash light or lasers. Solar-induced, passive, fluorescence would offer a remote sensing method to obtain direct information on the activity of photochemistry, which is a key factor to improve the estimates of the GPP, water stress or vitality of the plants.

Solar-induced chlorophyll fluorescence is difficult to observe because it is only 1-2 % of the reflected sunlight by the vegetation. The solution to this measurement problem relies on the use of the Fraunhofer lines where the solar spectrum is attenuated by atomic absorption of the solar chromosphere, or by molecular absorption of the telluric atmosphere. The Fraunhofer line method compares the depth of an absorption line in the solar irradiance to the depth of the same line in the radiance of the target. There are several Fraunhofer lines, which are in the chlorophyll fluorescence region of the spectra. Successful demonstrations of fluorescence signal detection by the Fraunhofer Line Principle have used oxygen A (760 nm) and B (687 nm) and H (656 nm) lines (Carter et al., 1990; Moya et al., 1998).

Instead of direct observations of fluorescence, another remote sensing method for obtaining information on plant functioning have been proposed by Bilger et al. (1989). Xanthophyll cycle carotenoids in the leaf tissue participate in excess solar energy dissipation undergoing de-epoxidation transformations (Demmig-Adams and Adams, 1996). The epoxidation state, which is calculated from the carotenoid concentrations in the leaves, has been related for a wide range of plant species to the so-called Physiological Reflectance Index (PRI) defined as the normalised difference of reflectance at 531 nm and 570 nm (Gamon et al. 1997).

Usually these passive methods have been tested for the plant material on the leaf level. For an operational remote sensing method these observational methods should be applicable on the canopy and landscape level. Evain et al. (2002) made a comparison between different passive methods and net CO_2 assimilation for a maize canopy. Coniferous forest canopies represent a very different kind of target, which has a very complex hyperspectral radiation distribution.

For the development of operative passive fluorescence instruments further studies are needed to find out the appropriate methods. Validation of the fluorescence signals for different plant types and environments on canopy level is urgently needed. For this purpose, the European Space Agency organised the first field campaign SIFLEX-2002 for observing solar-induced fluorescence in a boreal forest during the spring recovery of Scots pine. The campaign belongs to the FLEX-studies funded by ESA, originally proposed as a Fluorescence Mission to explore the feasibility of the detection and scientific use of the remote sensed fluorescence of terrestrial vegetation by Stoll et al., (1999a, 199b).

In this chapter, we will shortly describe the objectives, participants, and site of the SIFLEX-2002 study and also the climatic conditions during the campaign. In the end of the chapter we will show, using observations of meteorological parameters and maximal photochemical efficiency and gas-exchange modelling, the seasonal life-cycle of our target forest and how fluorescence

observations may improve the estimation of the seasonal evolution of GPP, serving as an introduction to what kind of environmental processes we are looking for. The most important SIFLEX-2002 components, the hyperspectral radiation and active and passive chlorophyll fluorescence observations, will be presented in the other chapters.

1.2 OBJECTIVES

One of the most demanding environments for a chlorophyll fluorescence instrument testing is the observation of the spring recovery of the photosynthesis of coniferous trees in the northern boreal region. For advancing technical development and scientific understanding of passive fluorescence instruments, the European Space Agency organised a field campaign at the Arctic Research Centre, Sodankylä in northern Finland.

The main goal of this SIFLEX campaign was to understand whether solar-induced fluorescence measurements might someday be used to monitor and map the photochemical activity of boreal forests from space. More specifically the objectives were:

- to measure and quantify the solar-induced fluorescence flux in the A and B oxygen absorption bands during spring thaw in a boreal forest
- to collect complementary measurements for fluorescence interpretation and radiative modelling purposes, for example spectral reflectance and solar irradiance data
- to collect a CO_2 flux dataset for the study of linkage between photosynthetic activity indicators (e.g. fluorescence and PRI) and CO_2.

1.3 PARTICIPANTS AND THE CAMPAIGN SCHEDULE

The European Space Agency made contracts with three institutes for conducting the SIFLEX-2002 campaign. M. Davidson (ESA, EOP/FS, ESTEC, Noordwijk, The Netherlands) acted as the campaign co-ordinator.

The three main participating institutes were:

- Laboratoire pour l'Utilisation du Rayonnement Electromagnetiqué (LURE) in Paris, France
- University of Valencia, Valencia, Spain
- Finnish Meteorological Institute (FMI), Helsinki, Finland

From LURE, the persons involved were I. Moya, A. Ounis, J. Louis and J.-M. Ducret. They had the most demanding task of developing methods and observations of chlorophyll fluorescence using passive and active methods. Numerous scientists from the University of Valencia participated in the study: J. Moreno, V. Caselles, J. Sobrino, J. Martinez-Lozano, L. Alonso, R. Pedros, J.C.

Jimenez, J.L. Gomez, G. Soria, R. Niclos, J. El-Kharraz. Also J. Miller from the University of York, Canada actively participated in the study. The central tasks of the University of Valencia team were studies on spectral observations of sky radiation and radiation reflected from the forests including the short wave and infrared regions of the spectra. From FMI, the persons involved included T. Laurila, T. Thum, M. Aurela, A. Lohila. FMI provided the observations of CO_2 fluxes between the forest and the atmosphere together with other meteorological parameters and also the infrastructure, such as the measurement towers.

The teams arrived in Sodankylä on the 23rd of April 2002 when the installation and testing of the instruments started. In the beginning we agreed on the final experimental plan. Most of the instruments were running in the beginning of May. The daily observational period of the hand-operated instruments was 10h00-16h00. The campaign database was updated at regular intervals during the campaign. Additional measurements, including the canopy structure, were conducted during the intensive study period on the week June 3rd-10th. The campaign ended on June 10th.

1.4 SODANKYLÄ SITE IN THE NORTHERN BOREAL ZONE

The Arctic Research Centre of the Finnish Meteorological Institute is in the North Boreal zone, 100 km north of the Arctic Circle (67° 21' 42.7" 26° 38' 16.2", 179 m a.s.l, Figure 1.1). The Research Centre is located in a Scots pine forest close to the river Kitinen. The Scots pine forest represents well the ecosystems in the area. Pine is the most common tree species in Lapland, with forests dominated by Scots pine covering 75 % of the forestland area.

The study forest is a pure Scots pine forest, which is naturally generated after forest fires. The oldest trees in the area are more than 300 years old. A large number of the trees originate from the warm 1930's after which there have been no forest fires. The forest fire frequency before that was around 40 years. The average tree age is 103 years. The height and diameter of these trees are about 10 m and 10 cm, respectively. The highest trees are about 21 m and their breast height diameter is over 60 cm. The tree density is 2100 trunks per ha and the total leaf area is 3.7, resulting in a projected leaf area of 1.2. The ground vegetation is 73 % lichens, 12 % mosses, and 15 % small shrubs. The soil type of the forest is fluvial sandy podzol.

At the observatory, routine meteorological observations include for example synoptic weather reports, PTU soundings, a weekly ozone sounding and continuously recorded UV-spectral radiation and broad band radiation components and meteorological parameters. Close to the research centre, carbon dioxide exchange between the atmosphere and a Scots pine forest are measured using the micrometeorological eddy-covariance method (Aurela et al., 2002; Laurila et al., 2000) on half-hourly resolution as part of a

CARBOEUROPE study. Downward and reflected solar radiation and Photosynthetic Photon Flux Density (PPFD), net radiation, and gradients of the CO_2 concentration, temperature, humidity and wind speed are measured in a 48 m high micrometeorological mast.
The fluxes of CO_2, latent and sensible heat and momentum are measured at the height of 23 m.

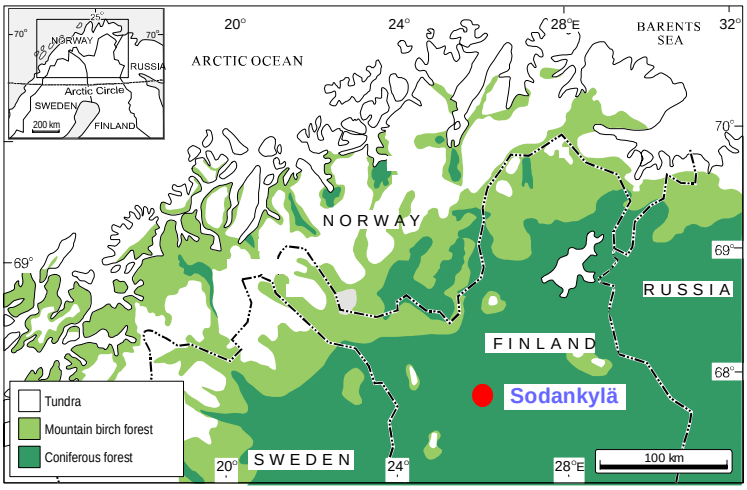

Figure 1.1. Sodankylä is located in the central part of Lapland in a coniferous forest region.

In the Köppen's climate classification northern Finland belongs to the area of a snow and forest climate characterised by moist, cold winters. Yearly averages (1961-1990) of temperature and precipitation are –1.0°C and 500 mm, respectively. The monthly averages of air and soil temperature, precipitation, cloudiness and snow depth on the 15th day of the month and the monthly-accumulated global radiation show very seasonal changes typical for the boreal area (Table 1.1).

Table 1.1. Monthly averages of temperature, precipitation, cloudiness, and snow depth on 15th of the month (1961-1990) and global radiation (1981-1990).

	Air T	Soil T 20cm	Precipitation	Cloudiness	Snow depth on 15th	Global radiation
	°C	°C	mm	%	cm	MJ m-2
Jan	-15.1	-3.42	30.7	74	51	6
Feb	-15.6	-3.71	25.5	74	67	50
Mar	-8.5	-3.08	25.2	70	72	176
Apr	-2.1	-1.17	23.6	68	69	389
May	5.0	2.66	34.5	70	15	490
Jun	11.6	11.04	55.9	71		542
Jul	14.1	14.72	64.7	70		497
Aug	11.2	12.51	62.8	75		342
Sep	5.9	6.81	55.3	78		175
Oct	-0.3	1.59	50.9	80	3	64
Nov	-7.4	-1.36	39.4	79	15	12

Dec	-13.1	-2.71	30.8	74	34	1

For the SIFLEX campaign we chose a period from the end of April to the beginning of June. Weather in the end of April is usually characterised by freezing temperatures, at least during the night, high snow depth and soil frost. In the beginning of June night frosts are not common anymore and based on the CO_2 flux measurements in 2000 and 2001, the net CO_2 uptake by the forest is representative of typical summer values.

Spring 2002 was exceptionally warm. During the very warm period in the end of April, temperatures reached 15°C (Figure 1.2). Between 20th of April and May 5th, night frost was observed only on May. The snow cover thawed during this warm period and the site was snow free on May 1st. Net CO_2 uptake during the day was observed already on April 24th. On the last days of April, it reached levels usually observed in the summer. After this warm period, cool, cloudy weather prevailed in May for nearly three weeks. Net CO_2 uptake values during the day were lower than those in the end of April because of cloudy weather and low temperatures. Night frosts were observed during several nights. The monthly average temperature in May was 7.2°C. On May 27th, the weather changed. Sunny weather prevailed for a week and the maximum temperature on the 30th was very high, 27.0°C. High daily UV radiation doses were observed during this period. In the beginning of June, daytime net CO_2 uptake was at the full summer level.

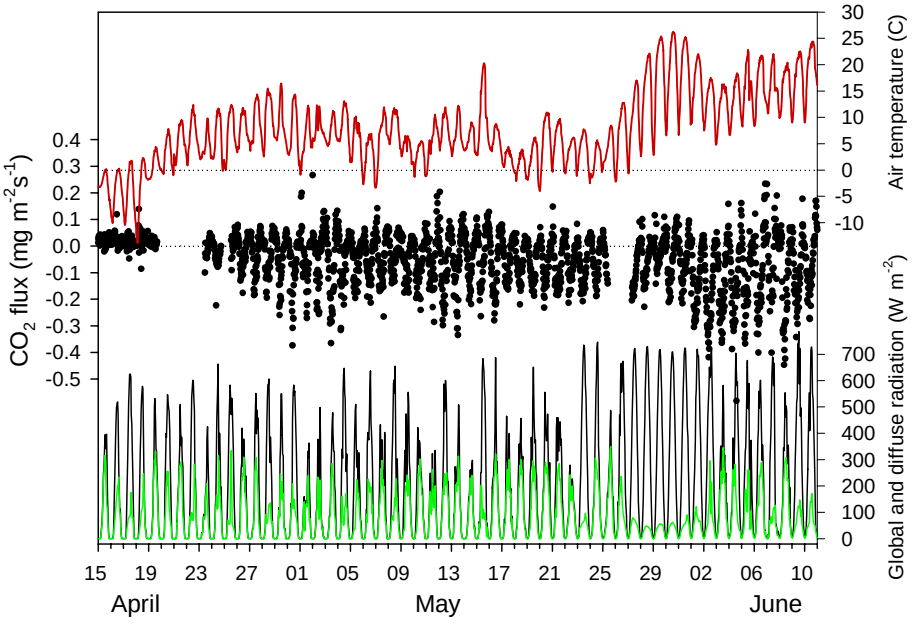

Figure 1.2. The air temperature (red), net CO_2 fluxes (dots), and global and diffuse (green) radiation during the SIFLEX-2002 campaign. Positive CO_2 fluxes denote net total respiration, negative values indicate net CO_2 uptake by the forest.



FINNISH METEOROLOGICAL INSTITUTE


Considering the original planning of the campaign period, it was a drawback that the commencement of photosynthesis was already actively going on before the dedicated fluorescence and spectral radiation instrumentation was running. However, the alternative might have been very harsh weather that would have prevented the installation of the instruments and measurements. Before the campaign, the snow surface, which has a high albedo, was considered a significant problem. This was, however, eliminated by the very early thaw.

1.5 LOCATIONS OF THE SIFLEX-MEASUREMENTS

Measurements specifically for the SIFLEX project were conducted at seven locations within 700 m (Figure 1.3):

1) Main experiment: 20 m tower erected for SIFLEX, top level holds PMFD, ASR field spectrometer, 6m level holds Cimel temperature sensors
2) Main Target (25 x 25 m): Holds target trees pointed at by PMFD, ASR; 3D reconstruction of canopy geometry, measurement of radiation budget, measurement of canopy temperature
3) Single-tree level fluorescence measurements, small tree used as target for fluorescence measurements with FIPAM, BD
4) Micromet tower: 48 m tower providing CO_2 flux measurements and other meteorological data
5) Needle level active fluorescence measurements
6) 10 m tower: spectrally resolved direct and global irradiance, supporting meteorological measurements such as broadband radiation components
7) Long-term needle level fluorescence measurements.

Description of the instruments and measurements will be given in the other chapters of this report.

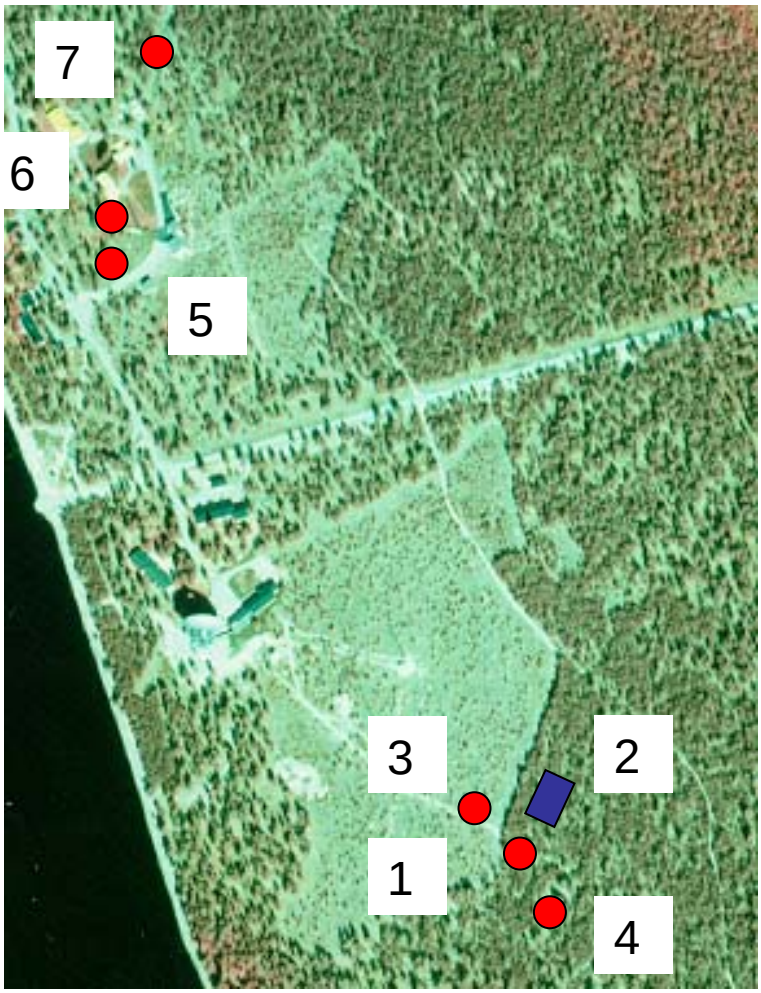

Figure 1.3. Aerial view of the Arctic Research Centre and the surrounding forest. The measurement locations are indicated by numbers which are explained in the text above.

1.6 SEASONAL DEVELOPMENT OF GROSS PRIMARY PRODUCTION

Coniferous forests in the boreal region have adapted to the harsh conditions during the winter by down regulating their photosynthetic apparatus to the winter dormancy. In spring, there is abundant solar radiation for photosynthesis but the trees have to postpone the release of winter dormancy because freezing temperatures would damage the photosynthetic system and the needles would dry out because of the lack of water due to the frozen soil and stems. Growing season in the boreal region is short and the coniferous trees have to optimise between the risks related to the early spring recovery and abundant solar radiation providing good potential for GPP. Many studies have shown that early date of the commencement of photosynthesis is the most important parameter explaining the interannual variability of the carbon sink

of coniferous forests.

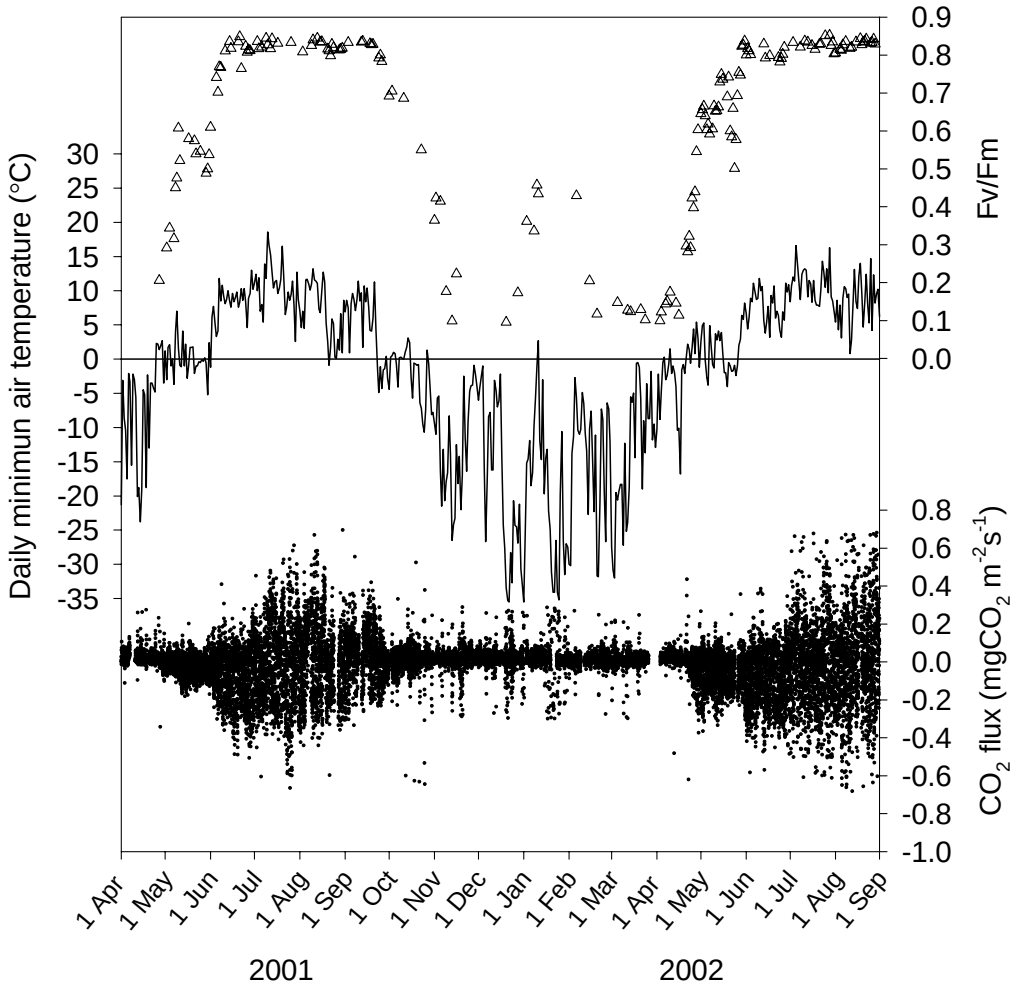

Figure 1.4. The maximal photochemical efficiency (Fv/Fm) of pine needles (triangles) and the eddy covariance CO_2 exchange together with the daily minimum temperature at Sodankylä during 1 April 2001 – 1 September 2002. The maximal photochemical efficiency Fv/Fm from needles was measured at location 7 (Figure 3) using leaf clips by a HANSATEC fluorometer. Four trees of different ages, at least three samples from each tree, were measured before noon.

In the northern boreal region, air temperature is the most important factor controlling the NEE at the seasonal scale (Figure 1.4). After the small, relatively steady respiration during winter, the first signals of photosynthesis as negative, downward CO_2 fluxes, are observed in April. In May the daytime CO_2 uptake increases during warm days but the full uptake potential is not reached before night frosts are over. The highest uptake and total respiration rates are observed in July-August. This is followed by a clear decline after the first below zero temperatures in September. These results are in accordance with flux

studies on Scots pine forests in the southern boreal zone (Markkanen et al., 2001) and in western Siberia (Lloyd et al., 2002). The ratio of the variable component to the maximal fluorescence (Fv/Fm) increases from the late winter values of about 0.2 in the end of April to the summer values of about 0.8 in June (Figure 1.1). The gradual increase occurs during warm spells, with the night frost causing temporary declines. The canopy scale CO_2 uptake at noon follows Fv/Fm closely during the spring recovery. In autumn, both Fv/Fm and CO_2 uptake at noon decrease concomitantly after cold weather with freezing temperatures.

Solar radiation north of the Arctic Circle has a remarkable seasonal cycle with polar night during the winter (Figure 1.5). We used equation (1) to estimate the seasonal progress of GPP from the PPFD radiation absorbed by the vegetation (PPFD*fAPAR), which can be observed by using remote sensing techniques. The biophysical changes of needles during the spring recovery and autumn were taken into account by introducing measured Fv/Fm as a scaling factor. When we add this direct information on the photosynthetic yield, the resulting values compare very well with direct estimates calculated from the micrometeorological observations (Figure 1.5).

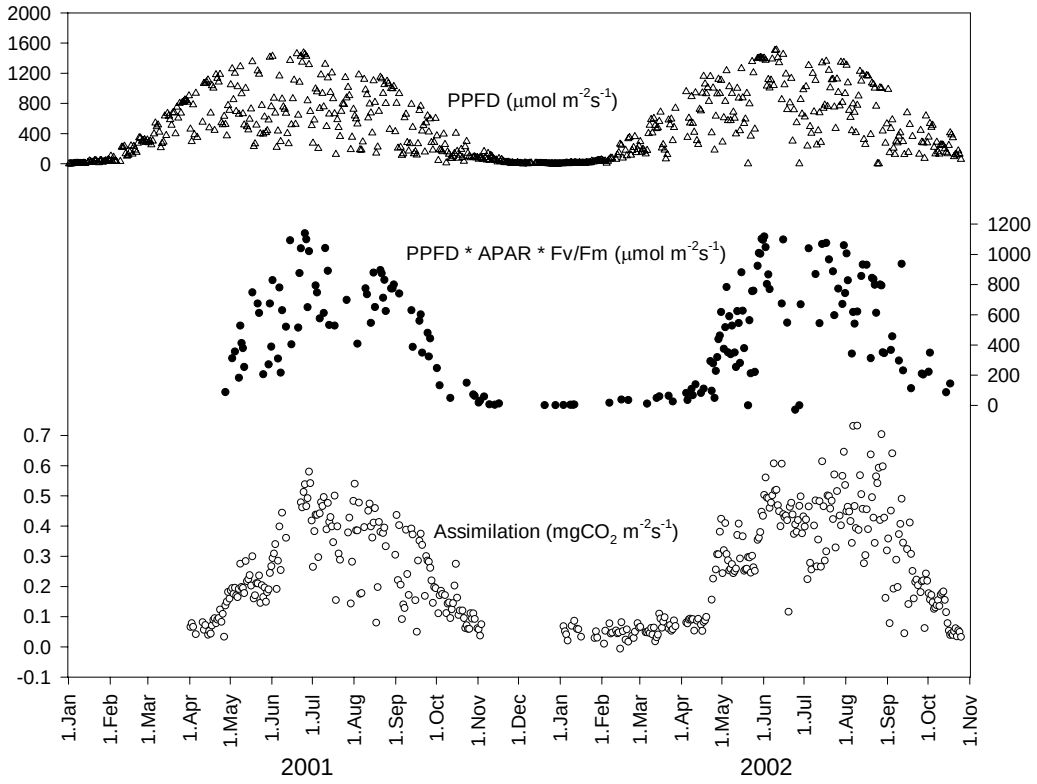

Figure 1.5. The seasonal course of Photosynthetically active Photon Flux Density (PPFD), the estimation of GPP potential as PPFD times fractional absorbed photosynthetic radiation (fAPAR) times the maximal photochemical efficiency (Fv/Fm), and the CO2 assimilation (GPP) estimated from micrometeorological flux measurements. The data represent noontime conditions.

In addition to the direct estimation of GPP from micrometeorological flux data, we simulated GPP using a gas exchange model. The model is based on the idea of optimal control of the gas exchange (Cowan, 1977). The model optimises the stomatal control of gas exchange by finding out a level in which the loss of water is minimal and the gain of carbon is maximal. Application of the model for cuvette measurements have been described by Hari et al. (1986) and Aalto and Juurola (2001). Aalto et al. (2002) present a comparison of optimal stomatal regulation model to a biochemical model using Scots pine cuvette data from Värriö, which is also located in Finnish Lapland at the same latitude as Sodankylä. We use a version of the model adapted to be used together with meteorological input data. In this study, we parameterise the seasonal changes in the gas exchange using the measured maximal photochemical efficiencies Fv/Fm scaled from 0 in winter to 1 in midsummer.

Simulated GPP for the campaign period are depicted in Figure 1.6. Seasonal changes of the GPP are in accordance with the micrometeorological CO_2 flux data (Figures 1.2 and 1.5) keeping in mind that the micrometeorological fluxes include total respiration. This modelling exercise shows that chlorophyll fluorescence observations are very valuable data for taking into account the biochemical changes during the spring recovery. For the biochemistry models, this kind of information is difficult to obtain otherwise. Certainly, remote sensing observations of chlorophyll fluorescence would improve the remote sensing estimates of GPP considerably.

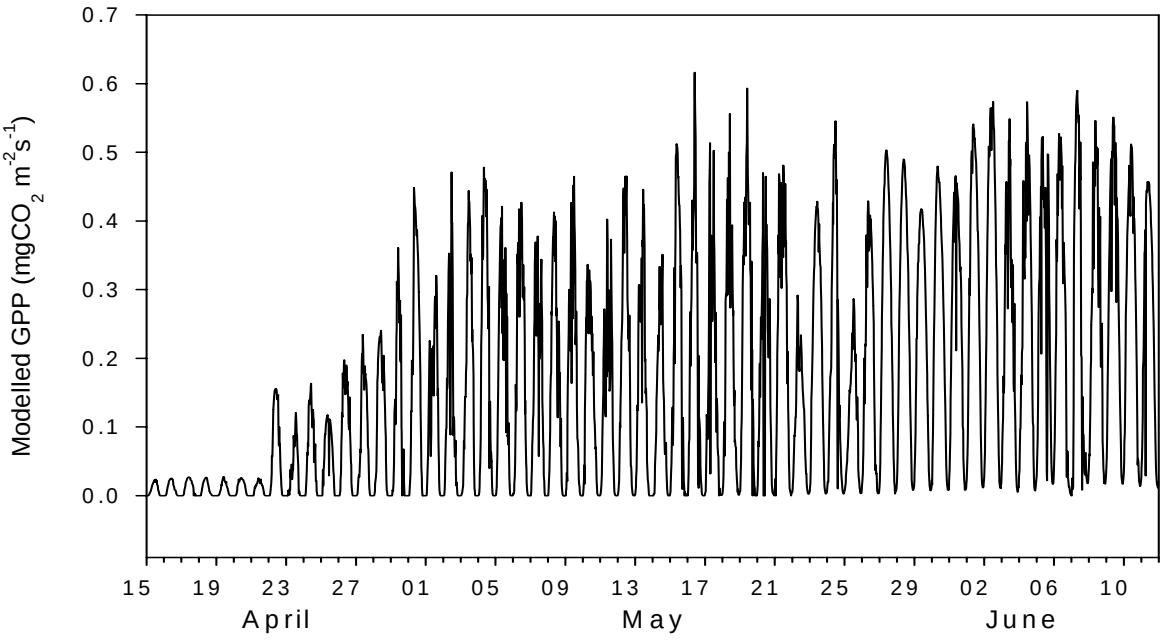

Figure 1.6. Gross Primary Production of the Scots pine canopy for the campaign period simulated by the optimal regulation model which uses measured Fv/Fm as parameter to describe the seasonal changes in biochemistry.

2. Measurements by FMI

This chapter describes the data collected at the FMI-Arctic Research Centre at Sodankylä, Finland as part of the SIFLEX-2002 project in response to the ESTEC Contract No. 16026/02/NL/SF. The campaign period was from late April to early June 2002. The objective was to follow the spring recovery of the photochemistry of Scots pines. We collected direct observations of carbon dioxide, latent heat and sensible heat fluxes using micrometeorological methods above a Scots pine forest at a test site. In addition, we collected data on maximum photochemical efficiency using a fluorometer and spectral radiances together with standard meteorological observations. In addition to the measurements stated in the contract, the FMI group made cuvette CO2 flux measurements, further biomass measurements using tree harvesting, forest inventory and hemispheric photography, and participated in the collection and analysis of needle pigments.

In spring 2002, the weather was much warmer than the climatological average. After a cold spell on April 14–18, a very warm weather thawed the snow, which disappeared before May 1 variable but warmer than normal weather prevailed in May. Night frosts were common. In the end of May, very high temperatures with the daily maxima exceeding 25 °C were observed. The maximum PSII photochemical efficiency of Scots pine needles increased during the warm period from below 0.2 in the first half of April to 0.6 in late April. Night frosts in May prevented the maximum photochemical efficiency from reaching the summer values (about 0.8) before the end of May. The carbon dioxide assimilation rates of the Scots pine canopy were estimated from the micrometeorological measurements by subtracting the estimated total respiration from the measured net flux. The midday CO_2 assimilation was close to zero before the warm spell in April, after which it increased to about 0.25 mg m^{-2} s^{-1} and in June to about 0.35 mg m^{-2} s^{-1}. The assimilation rates followed the air temperature similarly to the maximum photochemical efficiency. The main discrepancy occurred during the very warm days in the end of May when the CO_2 exchange was limited by the reduced stomatal conductance due to very low atmospheric humidity. Air temperature was the key factor explaining the spring recovery of pines. All the measured parameters (maximal photochemical efficiency Fv/Fm, epoxidation state of the xantophyll cycle, micrometeorological net CO_2 uptake) showed an increase after the warm days, but decreased when freezing temperatures were observed. Epoxidation state seems to react to warm temperatures at a higher rate than the net CO_2 uptake and the maximal photochemical efficiency measured by the fluorometer.

2.1 MEASUREMENTS BY THE FINNISH METEOROLOGICAL INSTITUTE DURING SIFLEX-2002

The overall goal of the campaign was to study the feasibility of observing solar induced fluorescence from boreal coniferous canopies during the spring recovery and summer. The observed signal will be compared to the photochemical activity of the forest which was measured using traditional methods and to the reflectance spectra which is comparable to existing remote sensing methods.

The Finnish Meteorological Institute provided micrometeorological flux and other meteorological parameters to support and compare with the measurements by the other project partners. Scots pine dark-adapted fluorescence, ground reflectance spectra, CO_2 exchange of Scots pine shoots using cuvettes and forest biomass parameters were measured.

Personnel of the Finnish Forest Research Institute collected Scots pine needles. Pigments were collected under supervision by Marja-Liisa Sutinen (Finnish Forest Research Institute) and Minna Turunen (Arctic Research Centre). Pigments were analysed by Gunnar Wingsle at the Umeå Agricultural University.

2.2 METEOROLOGICAL CONDITIONS AND CO_2 FLUXES BETWEEN THE PINE FOREST AND THE ATMOSPHERE

In the Introduction chapter, we provided an overview of the site, climatology, weather and the observed and modelled CO_2 fluxes during the campaign. In this chapter, we will present more meteorological parameters related to the SIFLEX research topics.

2.2.1 METEOROLOGICAL MEASUREMENTS CLOSE THE OBSERVATORY BUILDING

Meteorological observations were conducted at two locations. Routine observations were made at Location 6 in Figure 3 of Introduction (WGS-84 co-ordinates 67° 22’ 00”, 26° 37’ 41.5”, 182.2 m a.s.l.). An automatic weather station (Vaisala MILOS 500) recorded in 1-min resolution basic meteorological parameters such as air temperature, pressure, humidity, dew point, wind speed and direction, visibility and rain intensity, and automatically produced the weather code. Synoptic observations of clouds and weather were conducted on 3-hourly intervals.

Broadband radiation components were measured in 1-min resolution at the top of the 17-m tower. Attached to the sun-tracker (Kipp Zonen 2APGD) there were sensors of direct (Eppley NIP), global (Kipp Zonen CM11), and diffuse

(Kipp Zonen CM11) solar radiation and a sun ON/OFF sensor. Reflected solar radiation (Kipp Zonen CM11) was measured in a nearby open clearing at a height of 2 m.

UV-radiation and total ozone were measured by a spectrophotometer (Brewer MKII) and a broad band UV-meter (SL-501) on a roof of a nearby building. Atmospheric soundings of temperature, humidity and wind were conducted twice a day (00 and 12 UTC) (Vaisala RS-80) and ozone soundings once a week (Science Pump, ECC sensor).

2.2.2 CO_2 FLUX AND SUPPORTING MEASUREMENTS AT THE 48 M MICROMETEOROLOGICAL TOWER IN THE SCOTS PINE FOREST

The micrometeorological 48-m tower is located in the Scots pine forest (Location 4 in Figure 2.3 of Introduction), WGS-84 co-ordinates 67° 21' 42.7", 26° 38' 16.2", 179.3 m a.s.l).

The eddy-covariance fluxes of CO_2, H_2O, heat and momentum were measured using a LICOR-7000 analyser and a SATI-3Sx sonic anemometer at 23 m above the ground. The eddy-covariance methodology has been described by Aurela et al. (2001) and Aurela et al. (2002). In addition, heat and momentum fluxes were measured using four Solent sonic anemometers at 47 m, 32 m, 8 m and 3 m.

Global and reflected photosynthetically active photon flux density (PPFD) (Li-Cor 190SZ), global and reflected short wave radiation (Kipp&Zonen CM11), upward IR-radiation (Eppley PIR), net radiation (REBS Q-7) and radiation temperature of the canopy (Everest Interscience 4000.4GL) were measured at 46 m. Air temperature and humidity were measured at 48 m, 32 m, 18 m, 8 m and 3 m, and wind speed at 47 m, 38 m, 25 m and 18 m (Vaisala HMP 45).

Soil parameters were monitored in the vicinity of the tower including soil temperature and volumetric soil moisture profiles, soil heat fluxes, and air temperature and humidity 10 cm above the surface. Snow depth was recorded using an automatic sensor.

2.2.3 METEOROLOGICAL PARAMETERS

An overview of meteorological conditions during the campaign was presented in the Introduction, and this chapter will provide additional data.

The warm period in the end of April thawed the snow, which is very well illustrated as a decrease in the albedo observed over the forest and over a forest clearing (Figure 2.1). During the snow cover period, global radiation albedo is 0.23 above the Scots pine canopy and between 0.6 and 0.7 above the forest clearing below the canopy level. After the thaw, albedo above the

clearing is about 0.13 and slightly less above the forest, 0.11–0.12. Albedo in the photosynthetically active region above the forest canopy is 0.18 during the snow cover period and 0.04 after thaw.

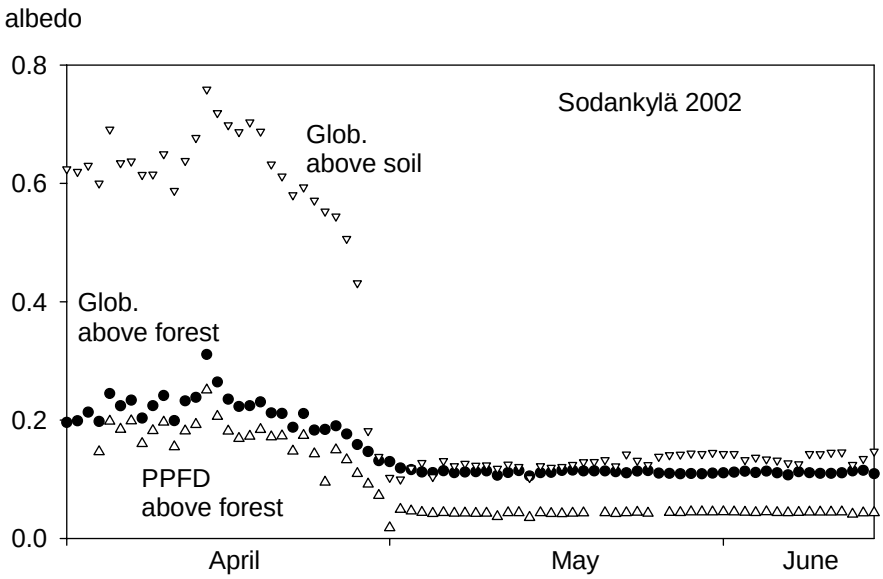

Figure 2.1. Time series of three albedos representing different surfaces and spectral regions. 'Global above soil' is measured in a small forest clearing. 'Above forest' denotes the observations from the top of the 48-m mast. 'Global' denotes the total solar radiation spectra and 'PPFD' is the photosynthetically active part of the spectra. The daily values are three-hourly averages centered at noon.

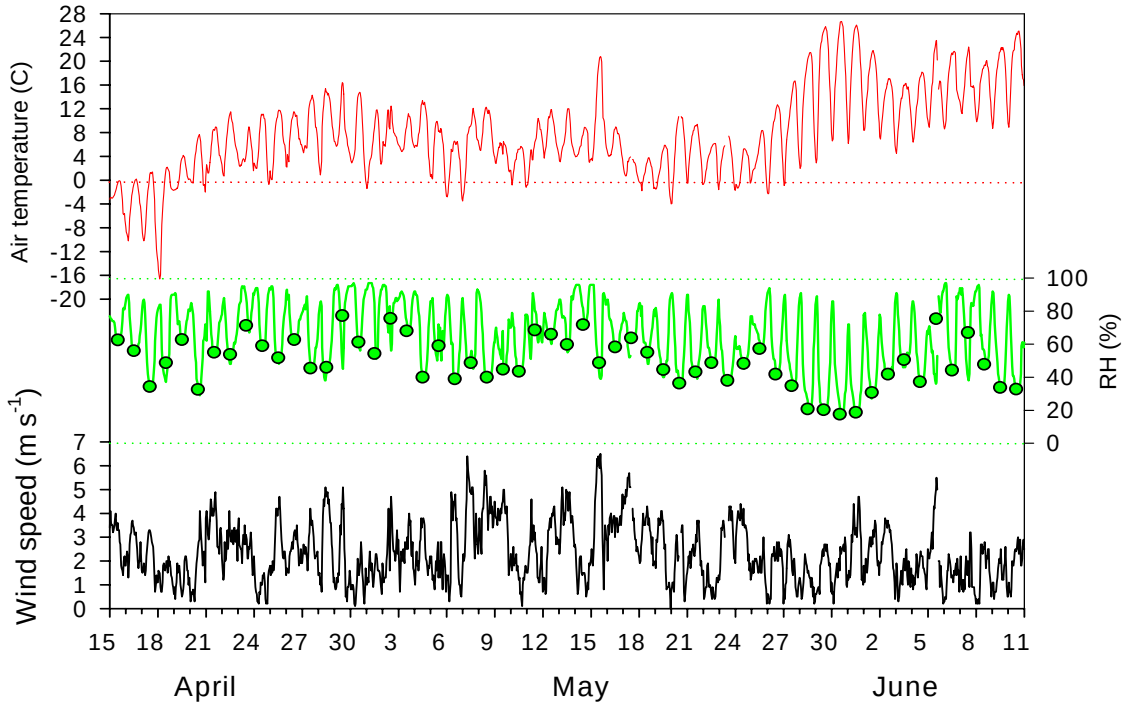

Figure 2.2. Air temperature (red), relative humidity (green, RH at noon marked as a dot) and wind speed in

spring 2002.

After the very warm period in the end of April, cool and mostly cloudy weather prevailed until May 26 (Figure 2.2). Only on May 15, the weather was sunny and temperatures rose to 21 ºC. May 17 is an example of a day when cold advection was strong. The weather map indicates snow showers and winds from northern Russia (Figure 2.3).

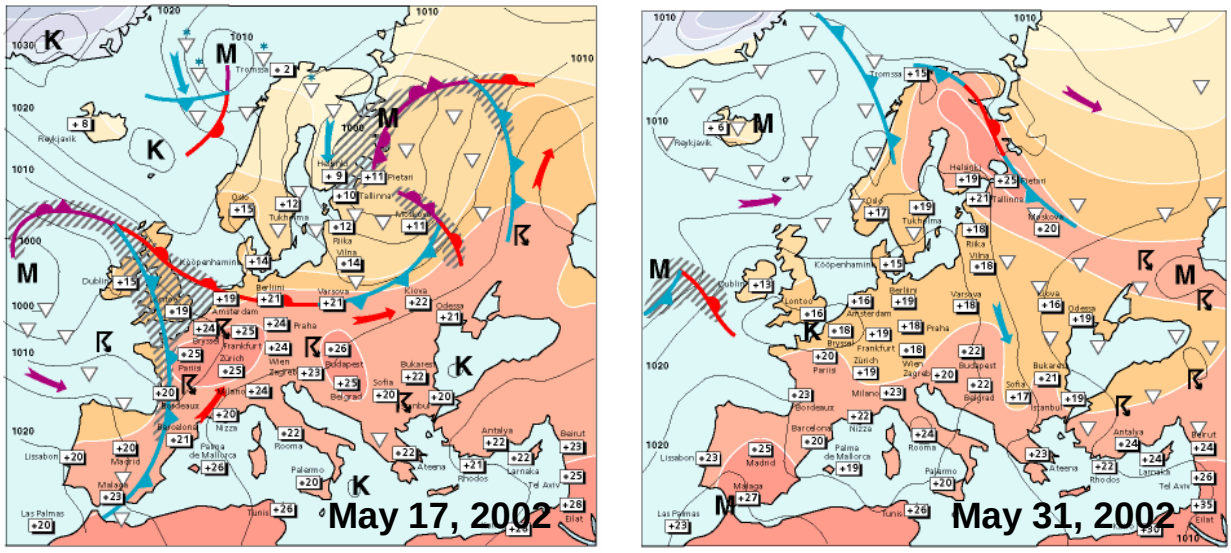

Figure 2.3. Weather maps on May 17 and May 31. M and K denote the centers of low and high pressure area, respectively.

The highest daily temperatures were only about 3 ºC. The high-pressure area began to strengthen on May 26. Cloud free conditions prevailed until the beginning of June. The radiation components on May 28 are shown as an example (Figure 2.4). The highest air temperatures reached 26 ºC on May 31 (Figure 2.5). During this sunny period, relative humidity at noon was often very low, around 22%. A period of variable weather and cloudiness began in the beginning of June (Figure 2..4), representing typical summer conditions. The rain amount between April 23 and June 10 was 54.3 mm, which is rather normal.

2.2.4 CANOPY SCALE FLUXES OF CO_2

In the beginning of the campaign on April 23–24, when there was still a continuous snow cover, we observed negative net CO_2 fluxes of about -0.05 mg $m^{-2}s^{-1}$ at noon (Figure 5). Already then, the CO_2 uptake by the canopy exceeded the total respiration. The warm weather advanced the development of Scots pines, and in the end of April, the net CO_2 fluxes at noon reached the -0.3 mg $m^{-2}s^{-1}$ level. During the cool period in May, when temperatures at noon varied between 3 ºC and 12 ºC and were below or around 0 ºC at night, the net CO_2 fluxes at noon were only -0.15 mg $m^{-2}s^{-1}$.

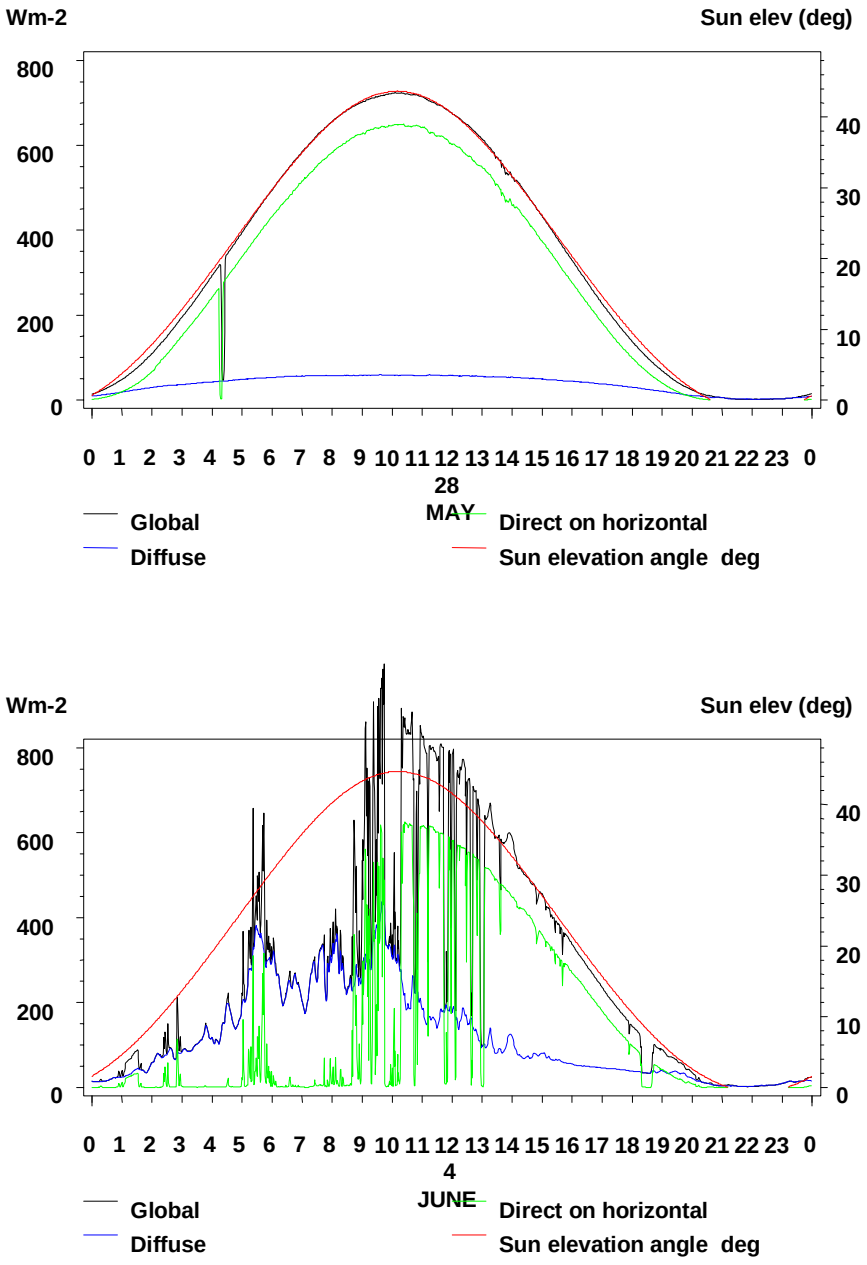

Figure 2.4. Global, diffuse and direct radiation, and solar elevation angle on May 28 and June 4.

The light response curve (Figure 2.6) illustrates the relatively high net uptake in the end of April, considering the fact that there was still snow on the ground. This warm period was followed by uptake periods of alternating intensity. Net uptake was high in the middle of May, after which it decreased during the colder period that followed (Figure 2.6). The nocturnal freezing temperatures were over on May 27 (Figure 2.7). Despite the very warm weather in the end of May, the net CO_2 uptake remained low. After June 2, the net CO_2 fluxes at noon increased to -0.4 mg $m^{-2}s^{-1}$, which is a typical value in summer. A comparison of light response curves reveals the difference in the net CO_2 fluxes between the sunny period, when humidity was very low, and the later period when humidity was higher (Figure 2.8).

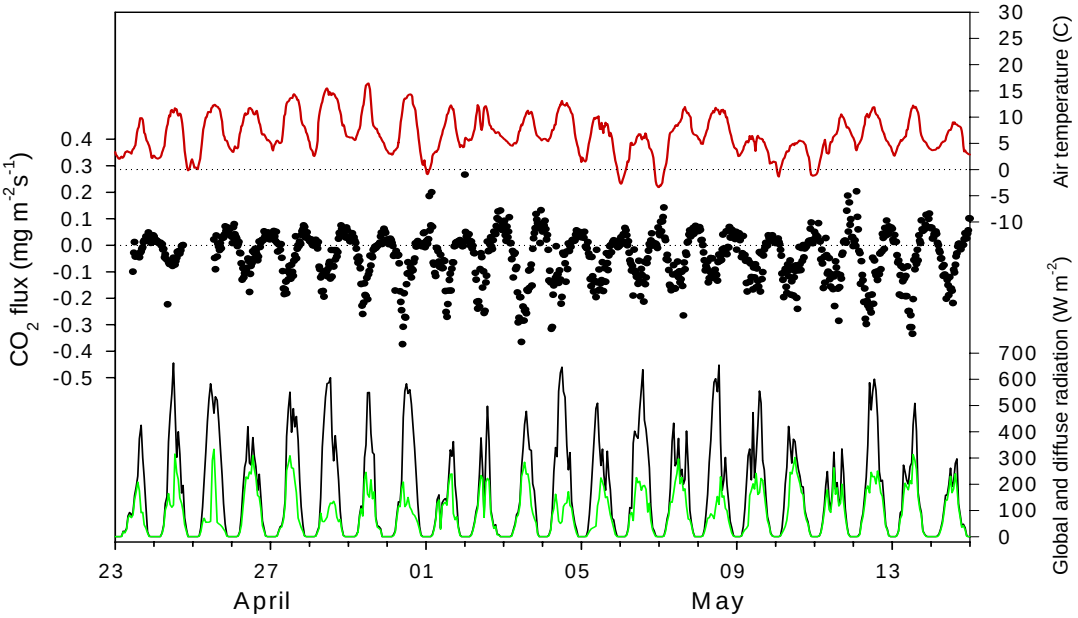

Figure 2.5. Air temperature (red line), half hourly net CO_2 flux (dots), and global (black line) and diffuse (green line) radiation on April 23 – May 14. A negative net CO_2 flux indicates net uptake (flux downward) by the forest.

The water vapour conductances of the canopy were calculated from the micrometeorological fluxes measured on May 27 – June 4 (Figure 2.9). The conductances were very low during the warm and sunny days in May. The lowest values were observed on May 29, when the afternoon conductances were only 0.1 cm s^{-1}. Thus, the stomatal regulation of the needles seems to be the most probable reason for the reduced CO_2 uptake observed during this period.

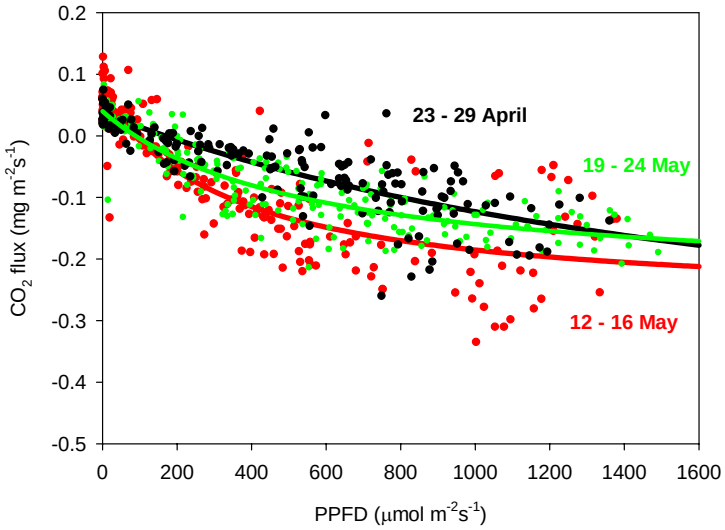

Figure 2.6. Light response of half-hourly net CO_2 fluxes on April 23–29, May 19–24 and May 12–16.

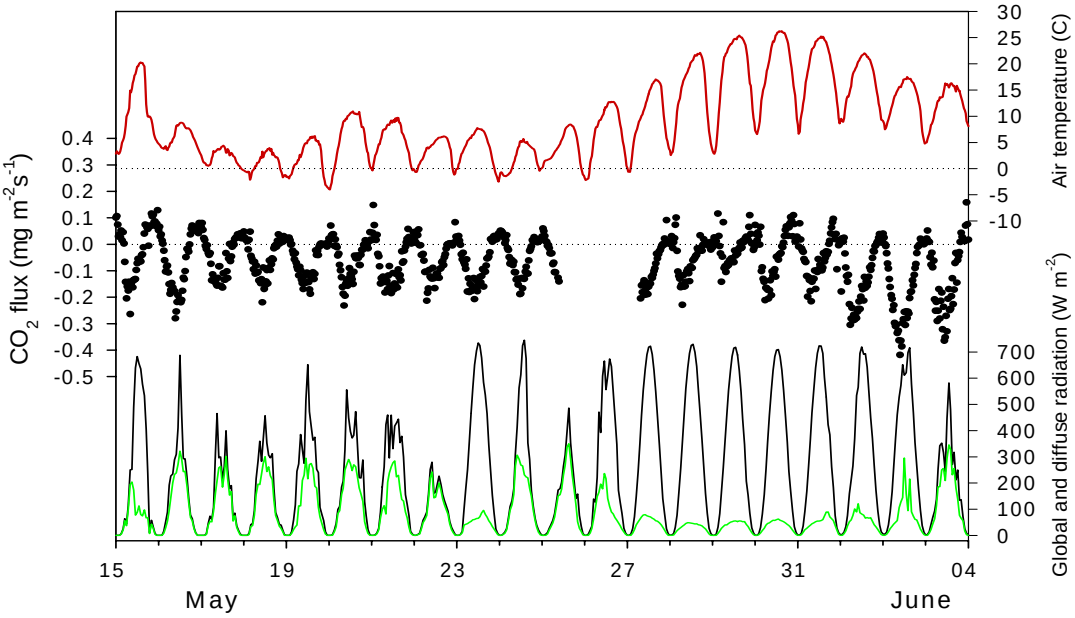

Figure 2.7. Air temperature (red line), net CO_2 flux (dots), and global (black line) and diffuse (green line) radiation on May 15 – June 4.

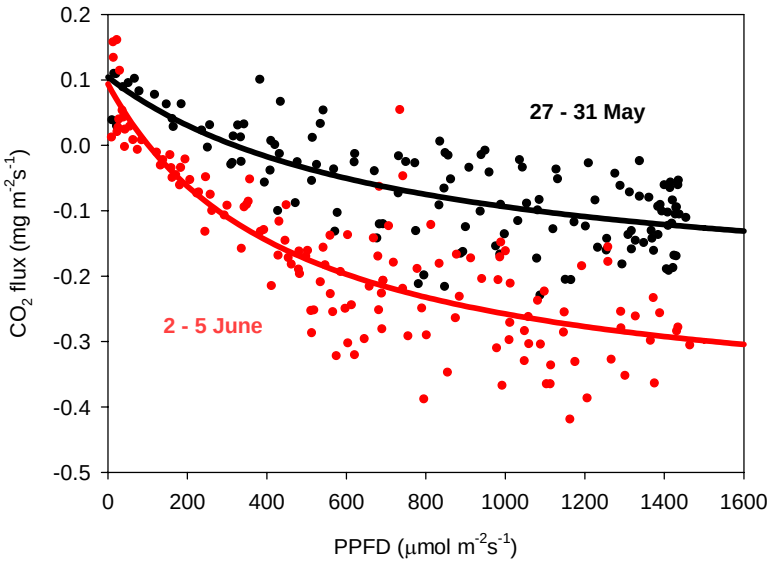

Figure 2.8. Light response of half-hourly net CO_2 fluxes on May 27–31 and June 2–5.

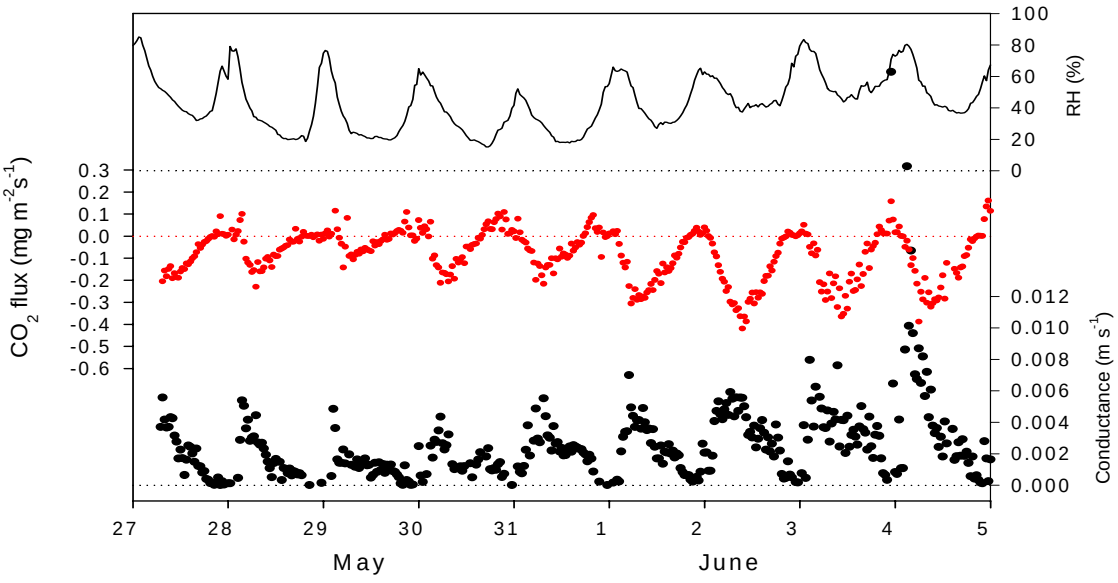

Figure 2.9. Relative humidity, net CO_2 fluxes and canopy scale H_2O conductances on May 27 – June 4.

FINNISH METEOROLOGICAL INSTITUTE

2.3 MAXIMUM PHOTOCHEMICAL EFFICIENCY (FV/FM) MEASUREMENTS

The maximum photochemical efficiency of Scots pine needles has been measured at Sodankylä not only during the SIFLEX-campaign but also through the years 2001 and 2002. These data provide essential information on the seasonal changes in Photosystem II performance, which may be compared with the micrometeorological CO_2 flux data.

2.3.1 INSTRUMENT PEA HANSATECH FLUOROMETER

The instrument used in the measurements was Plant Efficiency Analyzer (PEA) made by Hansatech. PEA is a portable fluorometer to be used after dark adaptation using leaf clips. The sensor unit has a source for powerful illumination by light emitting diodes that provide red light with a peak wavelength of 650 nm and a detector for the fluorescence signal. The instrument calculates the fluorescence parameter Fv/Fm. Measurements with the PEA were made daily. The main limitation was the rain, as the needles need to be dry for the measurement. Measurements were made at three different sites. One of these was the FMI seasonal site (Location 7), where fluorescence is measured throughout the year. The four pine trees were measured at this site. The second site was next to the 17-m tower, where one pine tree was measured (Location 6). Five trees were measured at the third site located close to the 20-m tower (Location 3). Ambient PPFD on the shoot was also recorded before the PEA measurements in order to determine the light environment of each shoot. Three measurements were made for each tree.

The maximum photochemical efficiency of the Scots pine is around 0.2 in winter and above 0.8 in summer. These seasonal changes were discussed in the Introduction chapter. We used the long-term observations of Fv/Fm to model Gross Primary Production through the years 2001 and 2002. These model calculations showed that the CO_2 uptake was correctly simulated during the transition period in spring and fall, when Fv/Fm was used as a seasonally changing parameter.

We observe that the air temperature is the key factor explaining the changes in Fv/Fm (Figure 2.10). Fv/Fm was below 0.2 in April when temperatures were below 0 ºC. As the period of warm weather began on April 20, Fv/Fm started to rise. After 25 April, no night frost occurred until May 1, and Fv/Fm reached

values between 0.45 and 0.7 by the end of the month. The weather was more variable in May. During this mostly cool and cloudy period, Fv/Fm was alternating between 0.45 and 0.8. The highest Fv/Fm was observed after the warm day of May 15, which was preceded by four days without night frosts. The lowest values in May were observed on May 26, after nine days with night frosts. After that, the period of very warm weather, especially at noon, intensified the development, and on 30 May, Fv/Fm exceeded 0.8 at all sites.

It was also observed that some trees may have systematically higher or lower Fv/Fm values during the spring recovery, but generally the trends are remarkably similar.

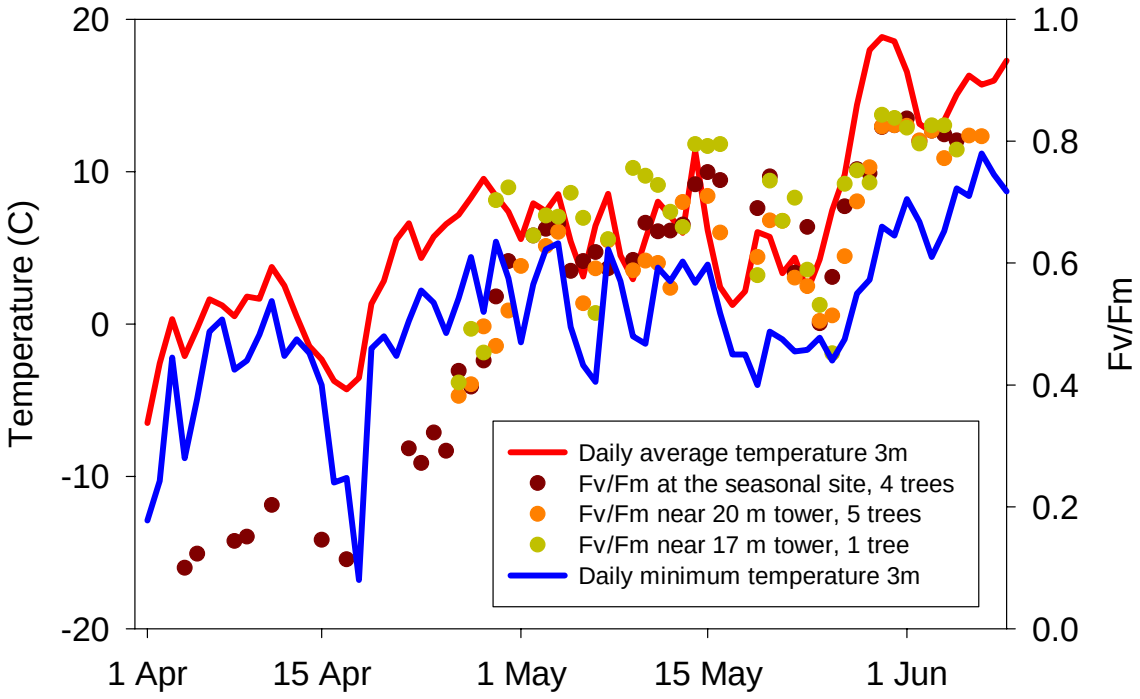

Figure 2.10. Maximum photochemical efficiency of Scots pine needles measured at three locations together with daily average and daily minimum temperatures.

2.4 GAS EXCHANGE MEASUREMENTS OF SCOTS PINE SHOOTS

Cuvette gas exchange measurements were made using a LICOR 6262 together with custom made shoot chambers and a LICOR 6400 Photosynthesis measurement system. In addition to the measurements made during the campaign, we measured in July 2002 gas exchange and fluorescence parameters using a LICOR 6400 and a Walz PAM2000 fluorometer.

2.4.1 INSTRUMENTATION AND MEASUREMENT PROCEDURES

The shoot cuvette was made of transparent plastic, and there were two LICOR PPFD sensors inside the cuvette. The relative humidity and temperature of the ambient air were measured using a Vaisala HMPY5A/D sensor. Gas concentrations in the cuvette were measured using a LICOR 6262 CO_2 and H_2O gas analyzer. Data were collected through a Vaisala QLI50 data logger; from the LICOR 6262 the data go directly to the computer.

Measurements were taken from four pine trees on over 20 days during the campaign. Two of the trees were located at the site where FMI measures fluorescence (Location 7). From these two trees, one twig per tree was measured. The two other trees were situated near the main tower (Location 3). From these, two twigs were measured for each tree.

Measurements were made at three different light levels: full ambient light, dim and dark. Two measurements were made for each light level. Assimilation rates and dark respiration parameters were calculated from these data. After the campaign, needles were collected and their surface area was estimated. Fluxes are presented per needle surface area.

The light response of CO_2 exchange of a pine shoot shows uptake of -0.09 mg CO_2 $m^{-2}s^{-1}$ at full light (Figure 2.10). The light response of a shoot is much steeper than that of the whole forest shown in Figure 2.8. In the beginning of the campaign (April 26–27), the CO_2 assimilation rate in full light was close to 0.1 mg CO_2 $m^{-2}s^{-1}$, increasing to 0.19 mg $m^{-2}s^{-1}$ on April 30 and to 0.22 mg $m^{-2}s^{-1}$ on May 4. After that, when the weather was cool, lower and more variable CO_2 assimilation rates were observed. During the last two days of May, CO_2 assimilation was approaching 0.3 mg CO_2 $m^{-2}s^{-1}$.

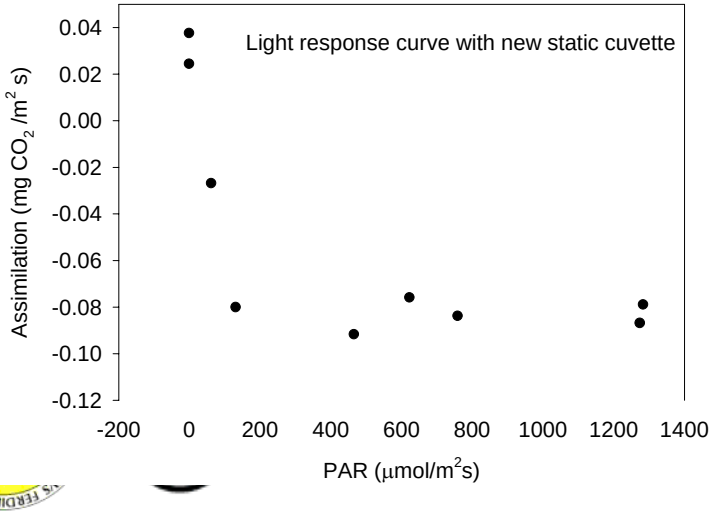

Figure 2.11. Light response of the CO_2 exchange of a Scots pine shoot measured using a static chamber on June 7.

In July, the carbon dioxide and water vapour exchange of a pine shoot were measured using a LICOR 6400. At the same time, the fluorescence parameters were measured from the needles of the year 2001 (old) and 2002 (new) using a WALZ PAM-2000. Figure 12 shows a 47-min sequence of photosynthesis, fluorescence yield and Electron Transport Rate (ETR) measurements under natural variable light (PPFD) conditions on July 20. Fluorescence yield is 0.6–0.7, when PPFD is lower than 1000 µmol $m^{-2}s^{-1}$. Yield decreases to below 0.3, when light intensity is increased to 1400 µmol $m^{-2}s^{-1}$. Net photosynthesis increases together with the increasing PPFD, but at high light levels the assimilation rate saturates. Leaf temperature and conductance are kept constant by the LI-6400. The light response of net photosynthesis, ETR and the intercellular CO_2 concentration (Figure 2.13) show that assimilation is limited by the intercellular CO_2 concentration, which decreases to 180 ppm, when PPFD is greater than 700 µmol $m^{-2}s^{-1}$. ETR saturates when PPFD exceeds 1000 µmol $m^{-2}s^{-1}$.

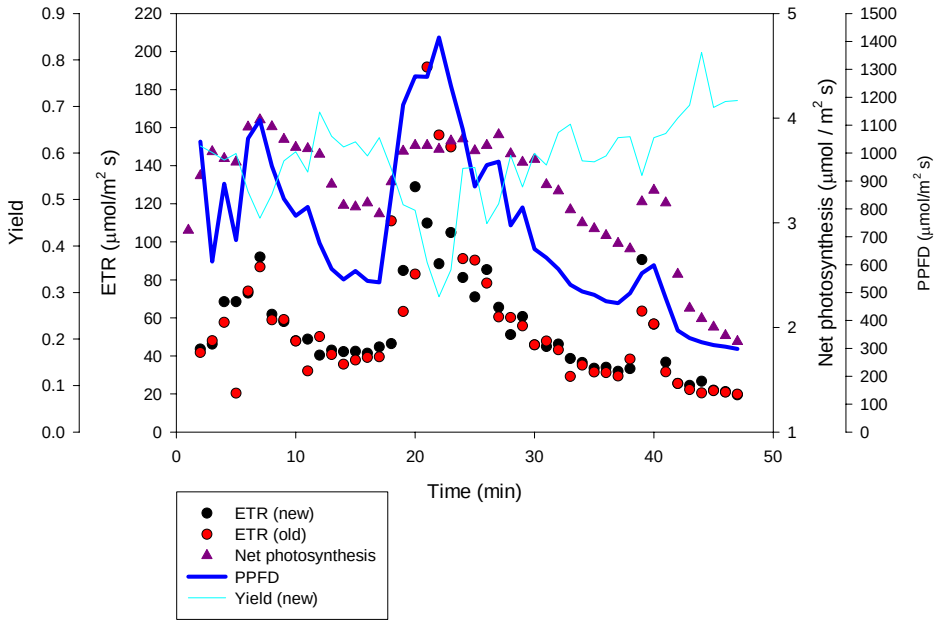

Figure 2.12. Conifer chamber measurements of CO_2 net photosynthesis, fluorescence yield and electron transport rate from current and one-year old needles (ETR).



FINNISH METEOROLOGICAL INSTITUTE

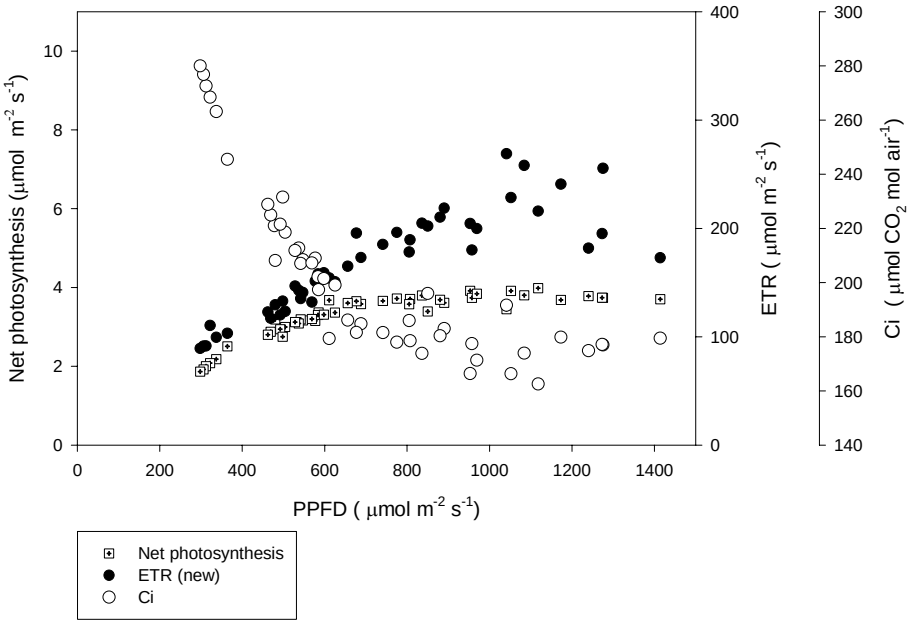

Figure 2.13. Light (PPFD) response of CO_2 net photosynthesis, electron transport rate (ETR) for current-year needles and internal CO_2 concentration (Ci) measured on July 20 using the conifer chamber.

2.5 SEASONAL CHANGES IN CHLOROPHYLL AND CAROTENOID CONTENTS OF THE NEEDLES

Needle samples were collected for an analysis of Chlorophylls and carotenoids concentrations to be used within studies on radiative transfer and the seasonal changes in the xanthophyll cycle. In winter and freezing temperatures, when the photosynthetic apparatus is not able to use solar energy, quenching form carotenoid pigments, antheraxanthin and zeaxanthin, instead of violaxanthin, absorb the excess solar energy. This transformation of xanthophyll cycle carotenoids to their quenching forms is called de-epoxidation. Often at full sunlight at noon, there is excess radiation resulting in partial photoinhibition. Then de-epoxidation safely dissipates excess energy. Towards the evening, when light levels become lower, epoxidation and recovery from photoinhibition takes place.

2.5.1 NEEDLE COLLECTION AND ANALYSIS

Needles were collected from four trees close to the observatory, where seasonal changes of maximum photochemical efficiency are monitored, and from four trees close to the special study forest plot. Ten needles from each tree were sampled once a week from April 30 to June 12. The sampling took place between 9:00 and 11:00 local time. The needles were put into liquid nitrogen tank and transferred to the Kolari research station. After the

campaign, all needles were transferred to Umeå for analysis. Prof. Gunnar Wingsle conducted pigment analysis using HPLC at the Swedish Agricultural University in Umeå. Fresh weight contents of Cholorophyll *a* and *b*, antheraxanthin, zeaxanthin, violaxanthin, lutein, neoxhantin, and alfa and beta-carotenes were analysed.

2.5.2 RESULTS

In May during the spring transition, the needle concentrations of Chlorophyll a and b were relatively constant, after which they increased, as depicted in Figure 2.14 for the three Scots pines growing closest to the experiment forest.

Carotenoid concentrations have been shown to change seasonally and over the diurnal cycle (Demmig-Adams and Adams, 1996; Ottander et al., 1995). Xanthophyll cycle carotenoids protect via epoxidation processes the sensitive parts of photosystem from damage induced by too high radiation levels. During winter or at noon when there is excess solar radiation, violaxanthin concentrations are low relative to the all xanthophyll cycle carotenoids (violaxanthin (V), antheraxanthin (A) and zeaxanthin (Z)). The epoxidation state EPS = (V+0.5*A)/(V+A+Z) of xanthophyll pigments is close to 1 in summer and shade conditions when the photosynthesis apparatus may safely use all radiation energy and there is no need to dissipate excess energy.

As an example of needle carotenoids we show concentrations in early June when the trees had already reached a CO_2 assimilation potential typical for the summer period. Lutein, beta-carotenes, and violaxanthin have highest concentrations (Figure 2.15). The epoxidation state has a value of is 0.87.

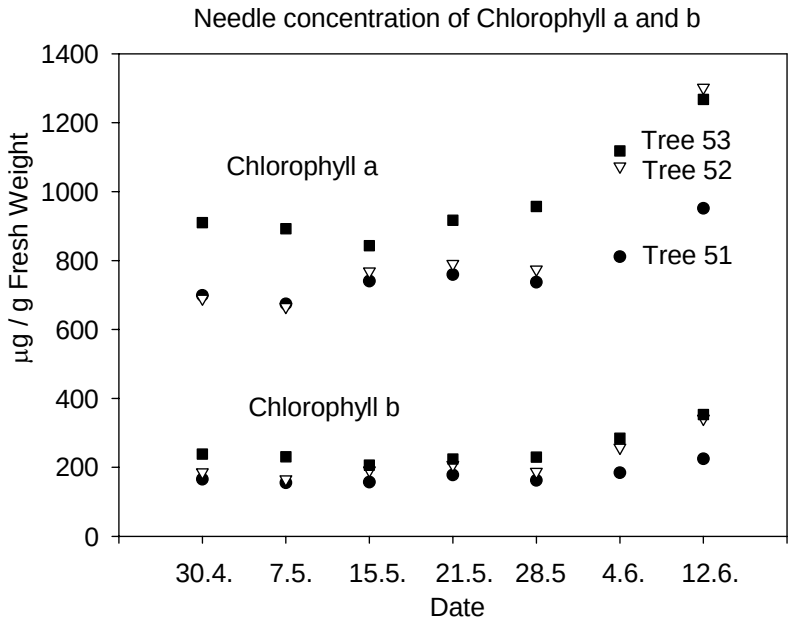

Figure 2.14. Chlorophyll a and b concentrations in needles of the trees 51, 52 and 53.

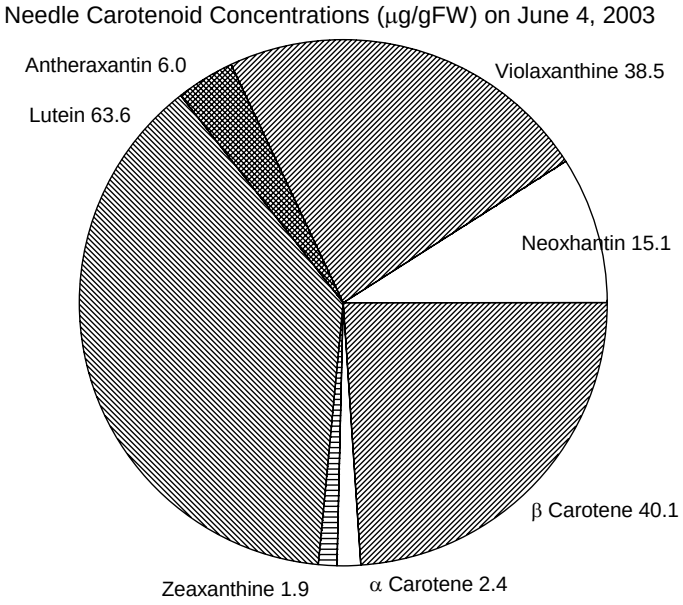

Figure 2.15. Average needle carotenoid concentrations on June 4. The average is taken over all nine-sample trees.

In the previous chapters we showed that the maximal photochemical efficiency (Fv/Fm) of pine needles increased seasonally from about 0.2 in late winter to about 0.82 in summer. The EPS ratio is expected to have a similar increase during spring. During the SIFLEX-campaign period, the epoxidation state does not show the same kind of gradual increase as the maximal photochemical efficiency (Figure 2.16). In fact, the highest value (0.915) was observed in the end of April. We may look for the reason for this apparent contradiction from the unusual weather conditions in 2002. Weather was very warm in the end of April. Before the sampling date of April 30, there was night frost on the 25th (only -0.6 ºC) and on the 21st. Daily average temperatures were between 7 ºC and 10 ºC. On April 30, the CO_2 assimilation rate estimated from the micrometeorological measurements was close to the summer levels (Figure 5). The maximal photochemical efficiency increased from 0.28 on 23 April to 0.6–0.7 on the 30th. This data suggest that the spring recovery of Scots pine was nearly complete by the end of April.

Night frosts were common after May 1, when a period of alternating development began. In May, EPS varied between 0.52 and 0.91. It seems that the variation is related to the temperature conditions before the sampling. In Figure 16, we have plotted the number of days without night frosts before the sampling. This number seems to describe a large part of the variation. We also

calculated the Effective Temperature Sum (ETS, accumulated daily average temperatures above 0 ºC) since the last night frost. This index had a value of 42.9-degree days on April 30 when the first sample was taken. This value was not exceeded until June. The ETS in May had a value of 27.0 and 9.6 degree days on the 15th and 28th, respectively. The low EPS values of the 7th and 21st of May were observed when night frost had occurred in the previous night, a few hours before the needle sampling.

In addition to the seasonal changes, the intensity of solar radiation also affects the xantophyll cycle. Lower relative violaxhantin values are observed when solar intensity is high. The needle samples show chemical composition at the ambient light intensity because the samples were put into liquid nitrogen immediately after detaching. The maximal photochemical efficiency (Fv/Fm) was observed in the dark-adapted needles. The modulation of the xantophyll cycle by the solar radiation is reflected in the EPS values. On June 4 and 12, the Scots pines are in their summer state, as determined by the micrometeorological CO_2 assimilation rates and the maximal photochemical efficiency. The EPS is lower on a sunny day (the 12th, PPFD = 620 µmol $m^{-2}s^{-1}$) than on a cloudy day (4th, PPFD = 1100 µmol $m^{-2}s^{-1}$) (Figure 2.4).

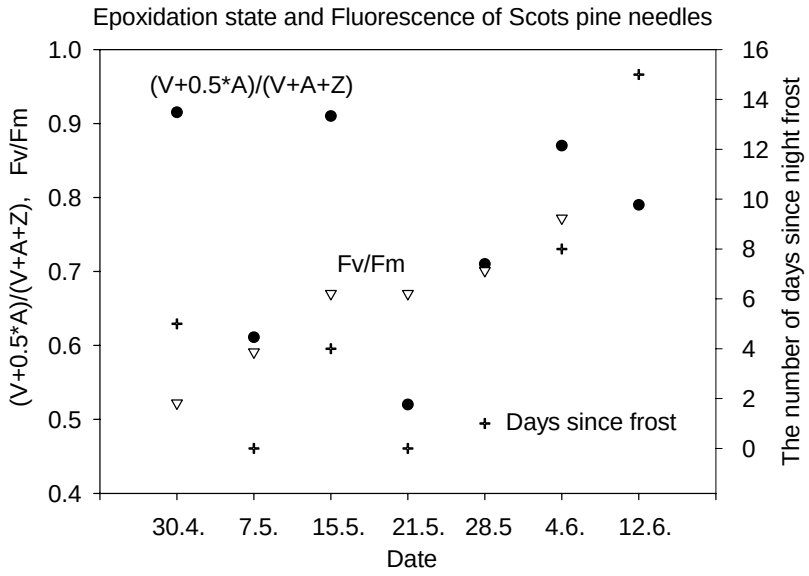

Figure 2.16. Epoxidation state ratio (dots) and the maximal photochemical efficiency Fv/Fm (triangles) of pine needles during the campaign. On the right axis is shown the number of days since the latest night frost (+). The values are averages of the trees 51, 52, and 53.

2.6 LEAF AREA INDEX MEASUREMENTS USING LICOR LAI-2000

Leaf area index (LAI) measurements were made twice at the 12 points located in the 25m x 25m main target forest. LAI was measured using a LICOR

LAI-2000, which calculates the leaf area from radiation measurements made with an optical sensor having a field-of-view of 148 degrees. We used a 90-degree view cap for azimuthal masking. First the reference was taken in the open area on the road and then LAI was measured at three points close to the marked point. The measurement dates were May 15 and 22. The average LAI of the 12 points was 1.15 on May 22, when cloudiness was more even than during the first measurements.

2.7. HEMISPHERIC PHOTOGRAPHY

Hemispheric photographs of the Scots pine canopy were taken using both 6 mm and 15 mm lenses for estimating canopy structure parameters in the main target forest and also in other parts of the Scots pine forest.

Photographs were taken in both cloudy and partially cloudy conditions on the 15th of May using a Canon FTb camera with a Canon FD 15 mm lens and Kodak Gold 200 film.

On May 31, photographs were taken using a Canon F-1 camera with a Canon 6 mm fish-eye lens and Kodak Gold 200 film. Weather conditions were mostly partially cloudy. At the 12 points located in the 25m x 25m main target forest, photographs were taken pointing the camera upwards on a level at a height of 75 cm. The bottom of the camera was in the north-south direction, the right side of the picture pointing to the north.

Projected LAI was analysed from digitised pictures using a Gap Light Analyzer v2.0 programme (Figure 2.17). The LAI from the analysed pictures was typically 1.2, which is close to the LAI-2000 values. These optical measurements have difficulties in differentiating between the green biomass from stems and branches. In our case, a substantial part of the sky shading is due to the other than needle surfaces.

Figure 2.17. Hemispheric photograph taken on May 31 in the main target forest.

2.8 SAMPLE TREE BIOMASS MEASUREMENTS AT SODANKYLÄ

The forest biomass of the Scots pine forest, which acts as a source area of the micrometeorological measurements, has been presented in the introduction. After the SIFLEX campaign on June 25–27, we harvested 3 trees in the main target forest for a more accurate estimation of the needle biomass and tree structure. One of the trees (number 10) was the target of the solar induced fluorescence measured from the 20-m tower. In this chapter we will describe the biomass of those three trees, which were chosen to represent the tree population in that area.

2.8.1 TRUNK, BRANCH AND NEEDLE MEASUREMENTS

Trees 10, 13, and 577 were felled on June 25–27. Twigs and shoots were measured and needles were collected and dried. The trunk diameters below all living whorls and at breast height were measured. All the diameter measurements were done above the bark. These measurements were carried out using a standard calliper with an accuracy of 1 mm used in forest measurements. Three discs per tree were cut, one at stump, one at breast height and one at crown base. The diameter increment and the age were measured in the laboratory.

The diameters of all living branches were measured below the lowest living whorl of sub-branches and above the beginning of the branch. Branch diameter measurements were carried out with an accuracy calliper (accuracy 0.05 mm), measuring the diameters above the bark. The heights of each whorl of branches were measured including the height of lowest living

whorl and total tree height.
A sample of eight branches per tree was randomly selected from the branches of the sample trees. The dry needle weights of all sample branches were measured for analyses of branch diameter and needle mass relationship. The needle lengths and weights of a single needle of every sample branches were determined as a mean of 20 needles per sample branch.

2.8.2 BIOMASS CALCULATIONS

Needle masses for the sample trees were estimated by using regressions shown in Figure 18. The ratio between the stem cross-sectional area below living crown and sum of total tree branch cross-sectional area (Figure 2.19) was used in stand-level measurements. The regressions in Figure 2.18 are different than the average regression, which has been used for the stand-level calculations. The ratio between the needle masses per unit cross-sectional area is based on measurements and is different between the stands.

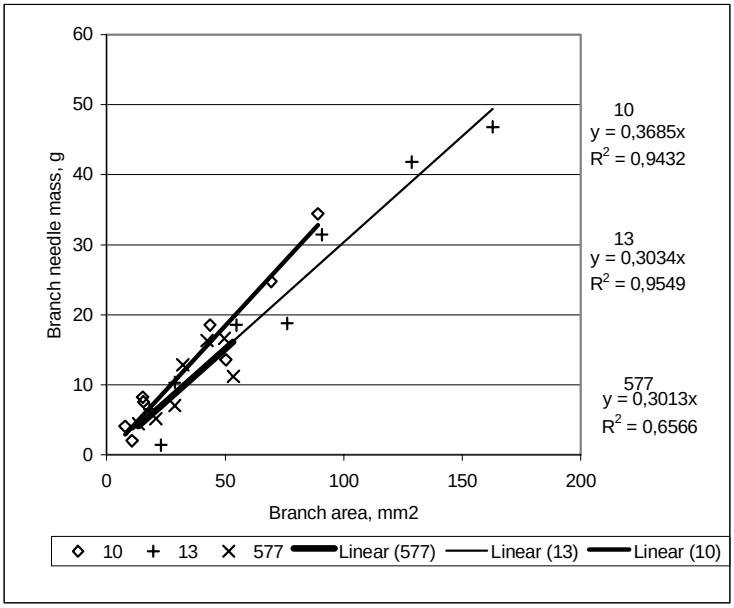

Figure 2.18. Relationships between branch cross-sectional area and foliage mass for the sample trees.

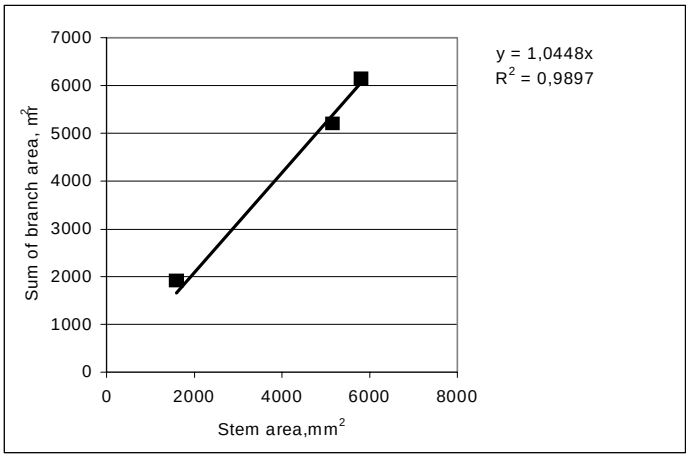

Figure 2.19. Relationship between total tree branch cross-sectional area below the lowest living whorl of sub-branches and stem cross-sectional area below living crown.

The same cross-sectional area at the crown base in younger trees, or in trees having a better position within a stand, can support a bigger needle mass. In unevenly aged forests, which are common in Lapland, there may be variations in the relationship between sapwood and heartwood. The differences between needle masses calculated by the regressions for individual trees and the regression for the whole forest area (Figure 2.20) were approximately 20%.

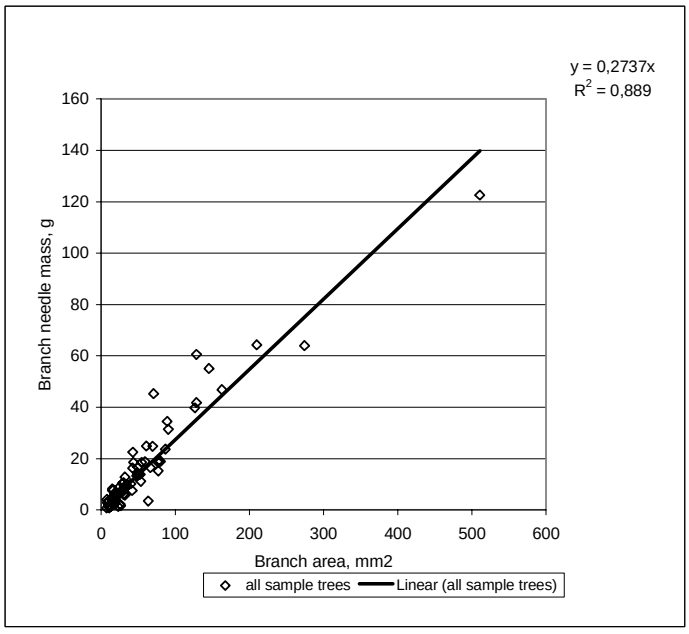

Figure 2.20. The relationship between branch cross-sectional area and foliage mass Regressions for forest area. One outlying observation removed.

We calculated needle areas of every branch using the mean length (Figure 2.21) and weight of 20 needles. The all-sided surface area of a needle was calculated from the needle length (l_N, in mm) by applying an empirical formula

$$S_N = A_1 l_N + A_2 l_N^2 \qquad (2)$$

where the coefficients are A_1=0.03 and A_2=0,120 (based on measurements by Eero Nikinmaa).

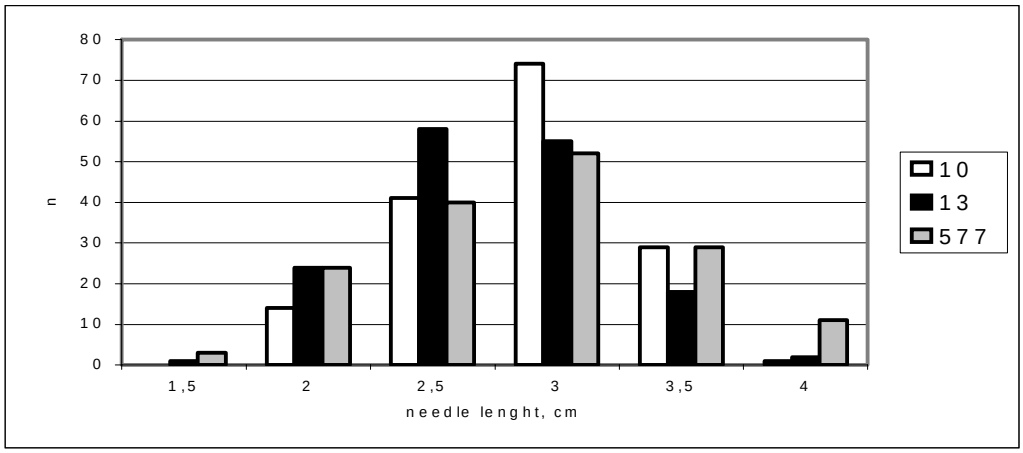

Figure 2.21. The needle length distribution of the sample trees.

The growth of the trees is slow, which is common in the northern boreal zone. The annual diameter increment varies between 0.2 and 0.8 mm (Figure 2.22) and the annual height increment varies between 10 and 30 cm (Figure 2.23).

Close to the 20-m fluorescence measurement tower, the forest structure is rather even. The height of the pines varies between 4.5 and 12 m, the mean height being 8.3 m. The crown bases of the smallest and the tallest pines are on the average at 2 and 7.5 m, respectively. The dry needle mass is 4728 kg ha^{-1}, which corresponds to a total leaf area of 6.9, which is nearly twice the average of the whole pine forest area.

A summary of the parameters of the sample trees is presented in Table 1. The sample tree 10, which was measured using the fluorescence instrument, was one of the tallest trees in that part of the forest. As compared to the other two sample trees, it had a higher needle biomass and growth rate.

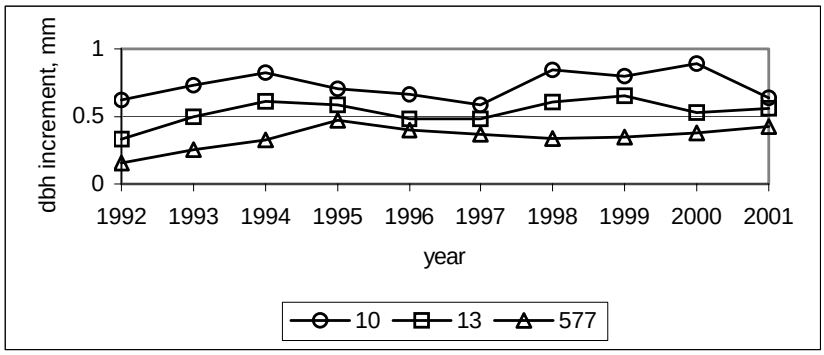

Figure 2.22. The annual diameter increment at breast height, mm yr^{-1}.

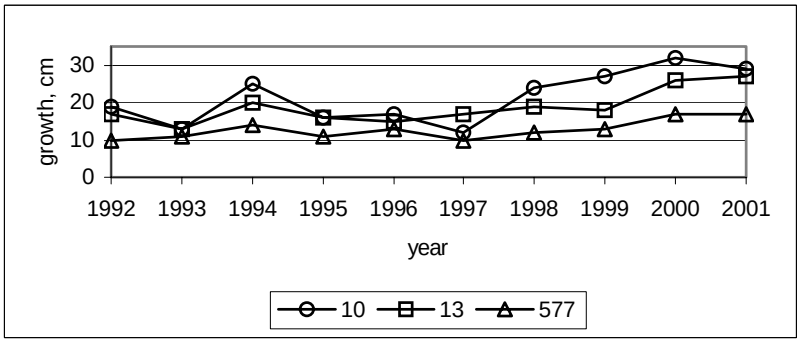

Figure 2.23. The annual height increment, cm yr^{-1}.

Table 2.1. Biomass and growth parameters of the sample trees 10, 13 and 577.

		10	13	577
Diameter at breast height (1.3 m)	mm	105	108	67
Height	cm	1163	1097	798
Height of the crown base	cm	444	527	491
Crown ratio	%	62	52	38
Diameter below living crown	mm	86	81	45
Stem volume	m^3	0.0522	0.0525	0.0157
Volume growth (over time period of 10 years)	$dm^3\ yr^{-1}$	1.46	1.27	0.35
Height growth (over time period of 10 years)	cm yr^{-1}	21.4	18.8	12.8
Branch cross-sectional area	mm^2	6149	5213	1919
Needle mass	g	2266	1582	578
Total needle area	m^2	17.4	20.5	5.0
Age	years	68	63	64

2.9. GROUND SPECTRA MEASUREMENTS WITH THE ASD PERSONAL SPECTROMETER II

2.9.1 MEASUREMENTS

Ground spectra were measured using a Personal Spectrometer II (Analytical Spectral Devices), which is a semiconductor-based passive non-imaging high spectral resolution field spectroradiometer. The spectrometer measures reflectance at 512 different channels between 320 and 1050 nm. The bandwidth of one channel is 1.4 nm. Ground spectra were measured weekly at four different locations. Different targets in different locations were measured. Measurements were taken during days when there was constant cloudiness or when it was completely sunny.

Before each measurement, the dark current was subtracted and the white reference was taken using a Spectralon panel. In most measurements, a foreoptic of 15 degrees was used. The spectra were taken keeping the foreoptic at a 10 cm distance from the target. Two spectra averaged from four consecutive measurements each were recorded per target. There was a break of one second between these two measurements, and the same dark current subtraction and white reference were used.

2.9.2 RESULTS

The study site is on a nutrient poor sandy soil where lichens (Cladina), cowberry (Vaccinium vitis-idea) and crowberry (Empetrum nigrum) are common. The ground vegetation in Finnish Lapland is very much affected by the freely grazing reindeers. Only a very thin layer is actually present, because the ground vegetation is the preferred feed of the reindeer. We measured lichen (Cladina arbuscula) and cowberry plots in the central part of the forest in a fenced area, where reindeers have not been grazing for decades. This fenced area is located 250 m eastwards from the observatory. Outside the fenced area, only a very thin lichen layer is present. The reflectance spectra of these two plots and that from a moss plot inside the fenced area are shown in Figure 24. On May 29, the weather was sunny and the ground surfaces were very dry.

The reflectance of lichen surfaces is within 0.08–0.1 in the spectral region 450–680 nm, except for the thick lichen surface in the fenced area which has a higher reflectance (above 0.1) in the spectral region 580–680 nm. Above 680 nm, the thick lichen surface has a lower reflectance. The dry moss surface has a lower reflectance below 680 nm than the lichen surfaces, and a higher

reflectance in the longer wavelength region. The red edge inflation points were 706.5, 703.7 and 695.1 nm for the lichen surfaces inside and outside the fenced area and for the moss surface inside the fence, respectively. In the BOREAS study, Bubier et al. (1997) measured a higher visible reflectance for lichen surfaces than for moss. They also found a reflectance minimum at 405 nm for the lichen surface. Dry organic soil, covered with some plant material such as dry needles and small amounts of lichens, has a low reflectance in the entire spectral region (Figure 2.25). The reflectance of a sand surface resembles that of the soil surface, but is considerably higher.

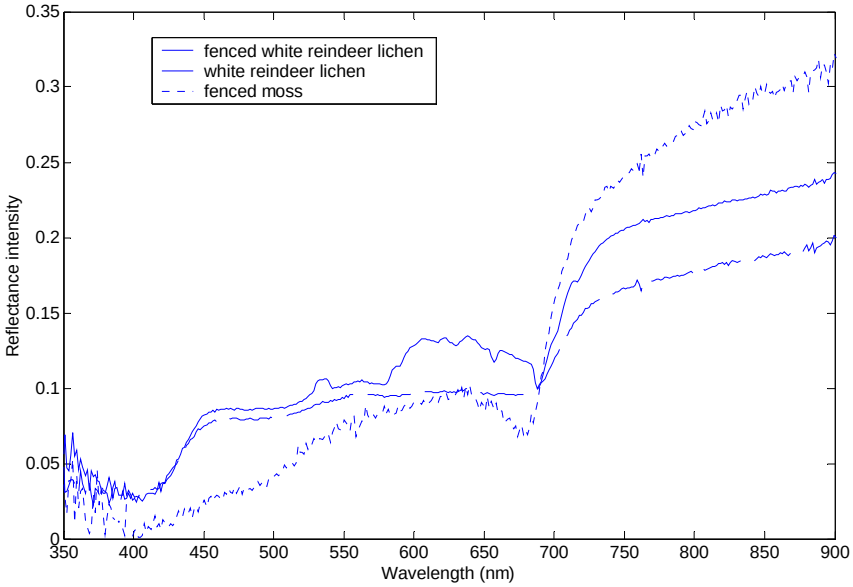

Figure 2.24. Reflectance spectra of lichen surfaces inside and outside the fenced area and of a moss dominated surface in the fenced area on May 29th.

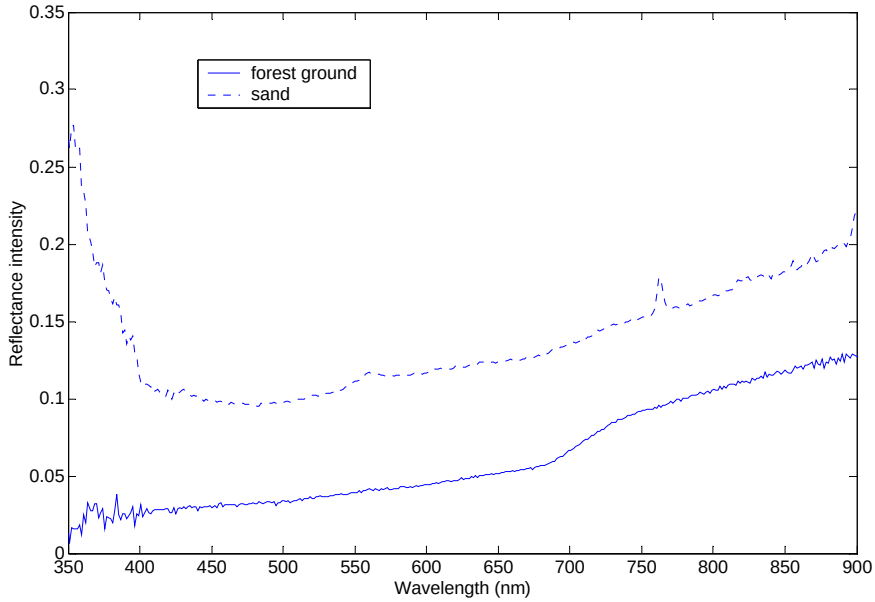

Figure 2.25. Reflectance spectra of bare forest soil and sand surfaces on May 29.

3. Measurements by LURE

The contribution of LURE team to the SIFLEX-2002 campaign, which has been held in the boreal forest at Sodankyla, Finland (26° 39' longitude East, 67° 22' latitude North), from 23 April 2002 to 10 June 2002, consisted to test the technical feasibility of passive fluorescence remote sensing (fluorosensing) methods at the level of tree canopies. During this campaign we tested two passive fluorescence instruments, the Passive Multi-wavelength Fluorescence Detector (PMFD) and the Bi-detector (BD), based on the Fraunhofer line principle applied to the atmospheric oxygen absorption bands. We monitored daily cycles of solar-induced chlorophyll fluorescence, NDVI (Normalized Difference Vegetation Index) and PRI (Physiological Reflectance Index) on Scots pine trees (*Pinus sylvestris* L.) during the spring recovery of vegetation. We also used two micro-FLIDAR (Fluorescence LIght Detection And Ranging) systems to monitor the laser-induced chlorophyll fluorescence on Scots pine at scale levels of needles and trees. The micro-FLIDARs "Laser-PAM" and "FIPAM" were mainly used as reference and calibration tools for passive fluorescence measurements, and also to provide complementary information on the photosynthetic activity and the constraints on the vegetation.
In addition to the above-mentioned equipments and measurements, collaborative investigations have also emerged with the University of Valencia team (Spain) and the FMI (Finnish Meteorological Institute, Finland) team.

3.1 INTRODUCTION

The objective of the SIFLEX-2002 campaign was to study the technical feasibility of passive fluorescence remote sensing (fluorosensing) methods at the level of tree canopies, and to observe, for the first time, the solar-induced chlorophyll fluorescence (ChlF) signal over a northern (26° 38' longitude East, 67° 22' latitude North, Sodankyla, Finland) boreal coniferous forest of Scots pine (*Pinus sylvestris* L.). The campaign period covered the spring recovery of pine trees from winter dormant to summer fully active state of photosynthesis. During this project, the contribution of our group (LURE team) was mainly to provide specific instrumentation for passive fluorescence measurements and to perform active fluorescence measurements with micro-LIDAR systems, in addition to the expertise provided for data processing and interpretation.
The solar- and laser-induced fluorescence signals observed at different scale levels of the forest, from pine needles to trees canopies, and also reflectance indexes have been compared to carbon dioxide fluxes measured on the same site using specific methods (Eddy covarience) and provided by the Finnish Meteorological Institute (FMI). These measurements were also compared to the canopy temperature, which was available from infra-red emisivity measurements provided by the University of Valencia team.
The instrumentation developed by the LURE team and provided during the campaign was mainly:

- Two passive fluorescence instruments based on the Fraunhofer line principle applied to the atmospheric oxygen absorption A and B bands, at 760 and 687 nm, respectively.
- Two micro-FLIDARs for near-field measurements of ChlF: FIPAM (Flexas *et al*., 2000) and Laser-PAM (Ounis *et al*., 2001).

3.2 INSTRUMENTATION AND SET-UP

3.2.1 THE PASSIVE MULTI-WAVELENGTH FLUORESCENCE DETECTOR (PMFD)

The PMFD is the main instrument used during this campaign to assess the chlorophyll fluorescence fluxes. The instrument is based on the Fraunhofer line principle, applied in the atmospheric oxygen absorption A and B bands (760nm and 687nm, respectively) (Evain et al., 2001). The output parameters are the stationary fluorescence fluxes at 687 and 760 nm, and also the NDVI = (R760-R687) / (R760+R687), where R760 and R687 are the canopy reflectance at 760 and 687 nm, respectively. Thanks to two additional channels available on this sensor, at 531 and 570 nm, it was also possible to monitor the PRI=(R531-R570)/(R531+R570), where R531 and R570 are the canopy reflectance at 531and 570 nm, respectively.
The aim of the experiment using this instrument was mainly to monitor simultaneously, on the same target, the variation of chlorophyll fluorescence fluxes at 687 and 760 nm as a consequence of photosynthetic activity changes during the spring recovery period and diurnal variation of incident

light.

3.2.2 MEASUREMENT PROCEDURE OF CHLF FLUXES, NDVI AND PRI WITH THE PMFD

The PMFD sensor (see Figure 3.1) was installed on the top of the main tower (20-m height) and maintained in the same viewing direction during all the campaign. The zenith angle of the viewing direction was about 120 degrees, and the instrument was south-to-north oriented.

The PMFD acquired automatically and continuously the reflectance and fluorescence signals from the forest canopy (3 or 4 tress) (see Figure 3.2). The sensor was alternatively oriented towards the target and towards a small reference panel (30×30 cm) installed near the instrument (about 1 m distance). We first tested a vertical and a 30-degree orientation of the panel, and then we maintained a horizontal orientation during the campaign.

Figure 3.1. Experiment involving the main passive instrument, the PMFD. View of the PMFD instrument without protection (A), the PMFD installed at the top of the 20-m high tower (B), which was about 10 m above the crown of the trees canopy (C).

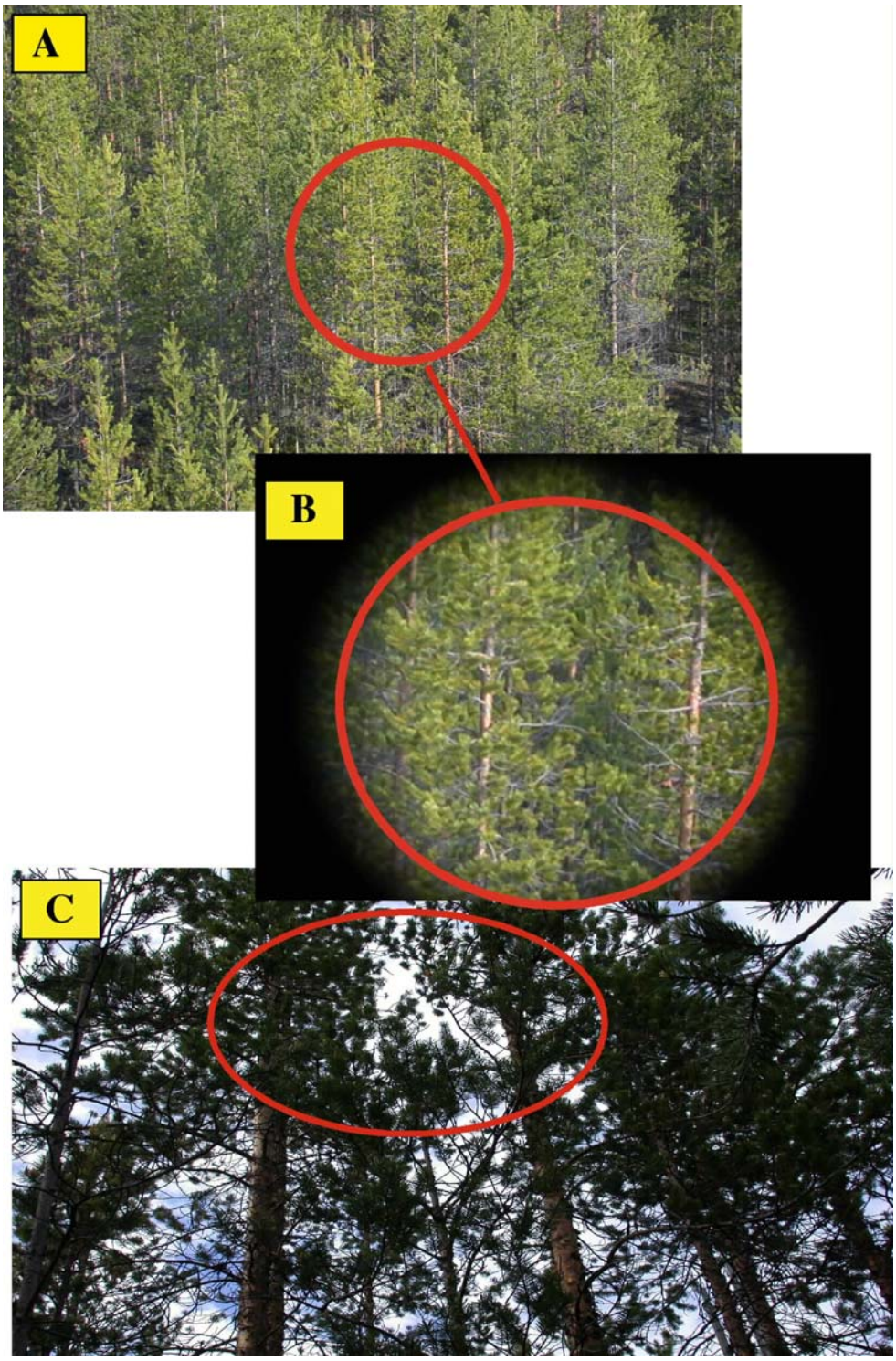

Figure 3.2. Photographs of the PMFD target. Target photographed from the 20-m high tower (A), viewing of the exact measured zone as photographed through the field of view of the PMFD instrument (B), and the target seen from ground (C).

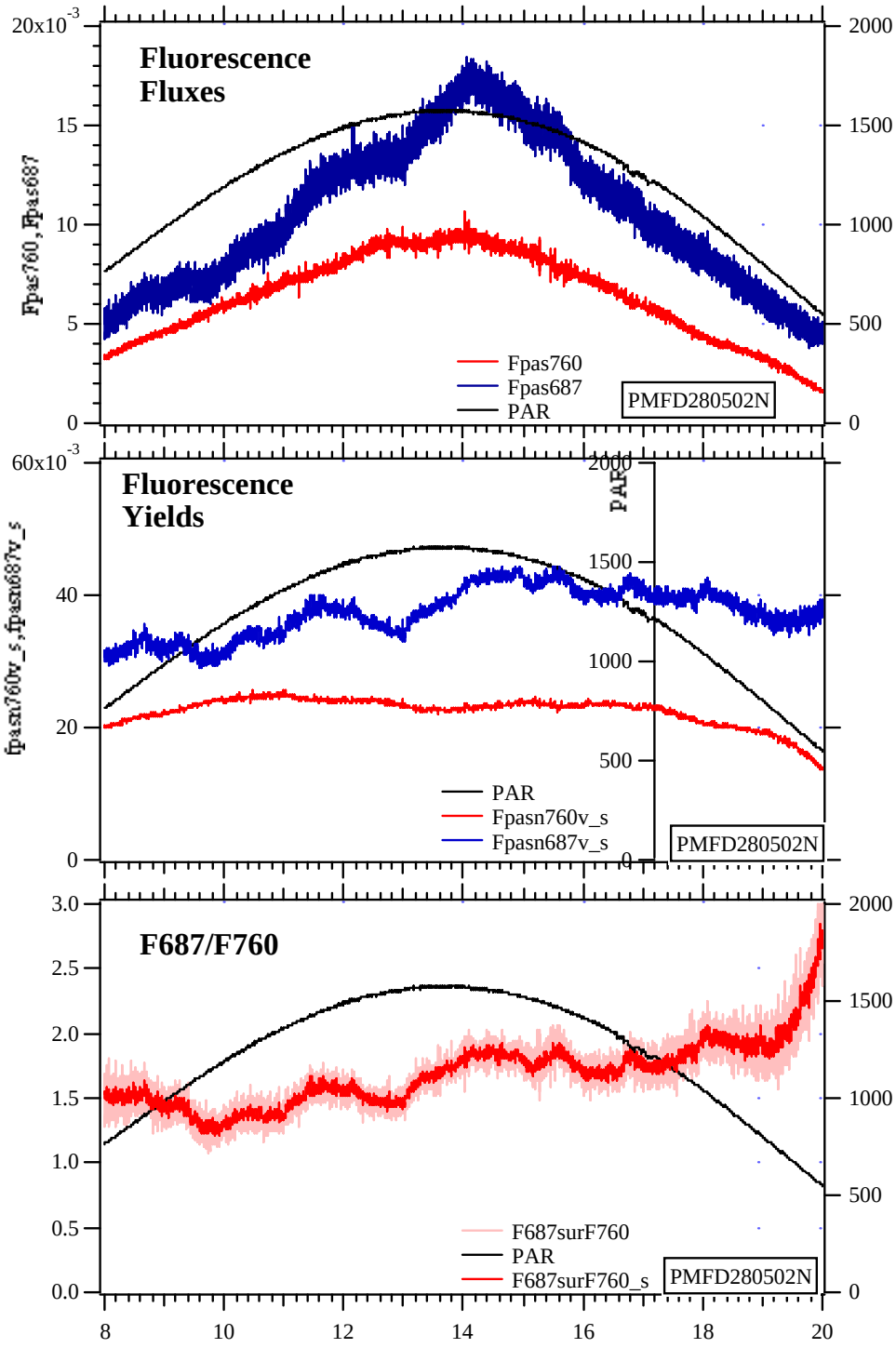

Figure 3.3. Diurnal cycle of stationary fluorescence fluxes at 687 and 760 nm (Fpas687 and Fpas760, respectively), apparent fluorescence yields at 687 and 760 nm, and the fluorescence index F687/F760 recorded with the PMFD during a sunny day, on the 28th of May 2002. The PAR is also plotted during the

diurnal cycle. All smoothed signals have a "_s" suffix. The time (bellow) is indicated in hours (UT + 3).

As shown in Figure 3.3 and 3.4, the output parameters of the PMFD are the stationary fluorescence fluxes at 687 and 760 nm (Fpas687 and Fpas760, respectively), and the canopy reflectances at 687 and 760 nm (R760 and R687, respectively) and also at 531 and 570 nm (R531 and R570, respectively). These parameters were recorded during a diurnal cycle, on a sunny day (on the 28th of May 2002). Using these parameters, it was then possible to deduce and monitor the apparent fluorescence yields at 687 and 760 nm, the fluorescence index F687/F760, the PRI and the NDVI (not shown). For comparative purposes, the same signals recorded during a cloudy day (22nd of May 2002) are shown in Figure 3.5 and 3.6. More details related to these experiments are presented in chapter 5.

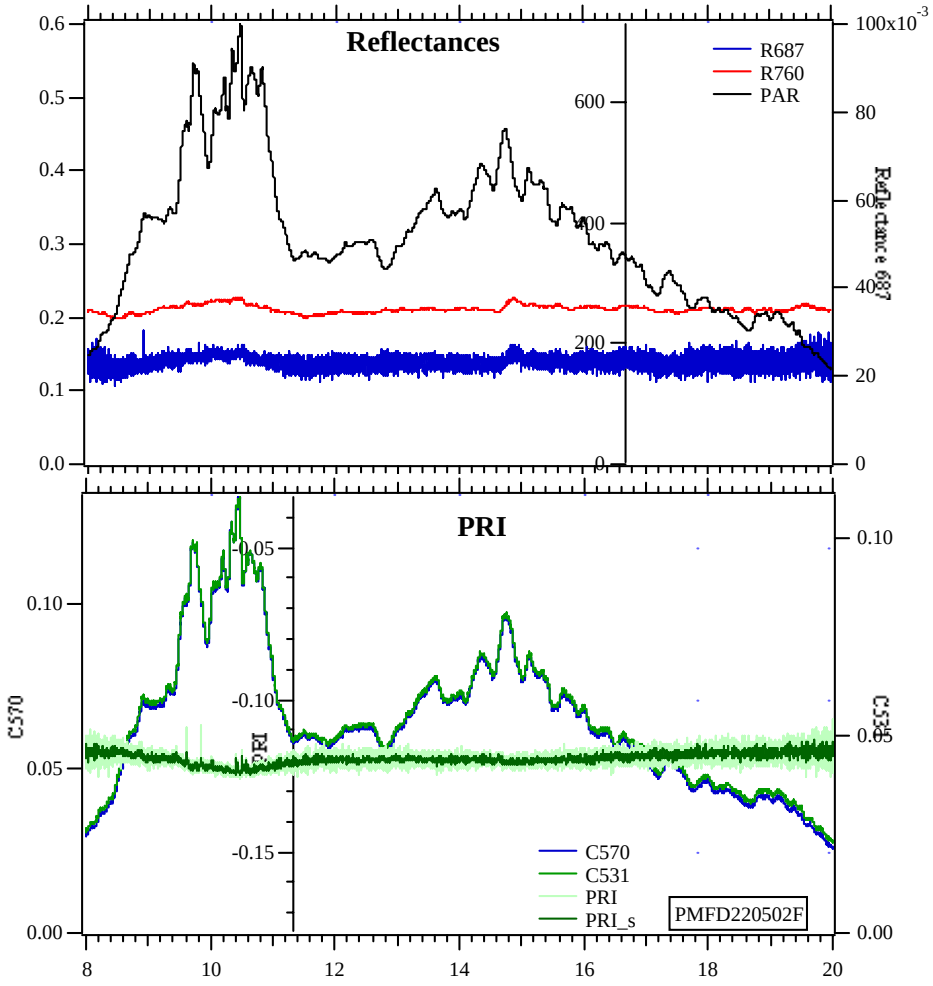

Figure 3.4. Canopy reflectances at 687 and 760 nm (R760 and R687, respectively) and also at 531 and 570 nm (R531 and R570, respectively) recorded with the PMFD during a cloudy day, on the 22nd of May 2002. The calculated PRI is also plotted during the diurnal cycle. The "_s" suffix denotes the smoothed signals. The time (bellow) is indicated in UT + 3

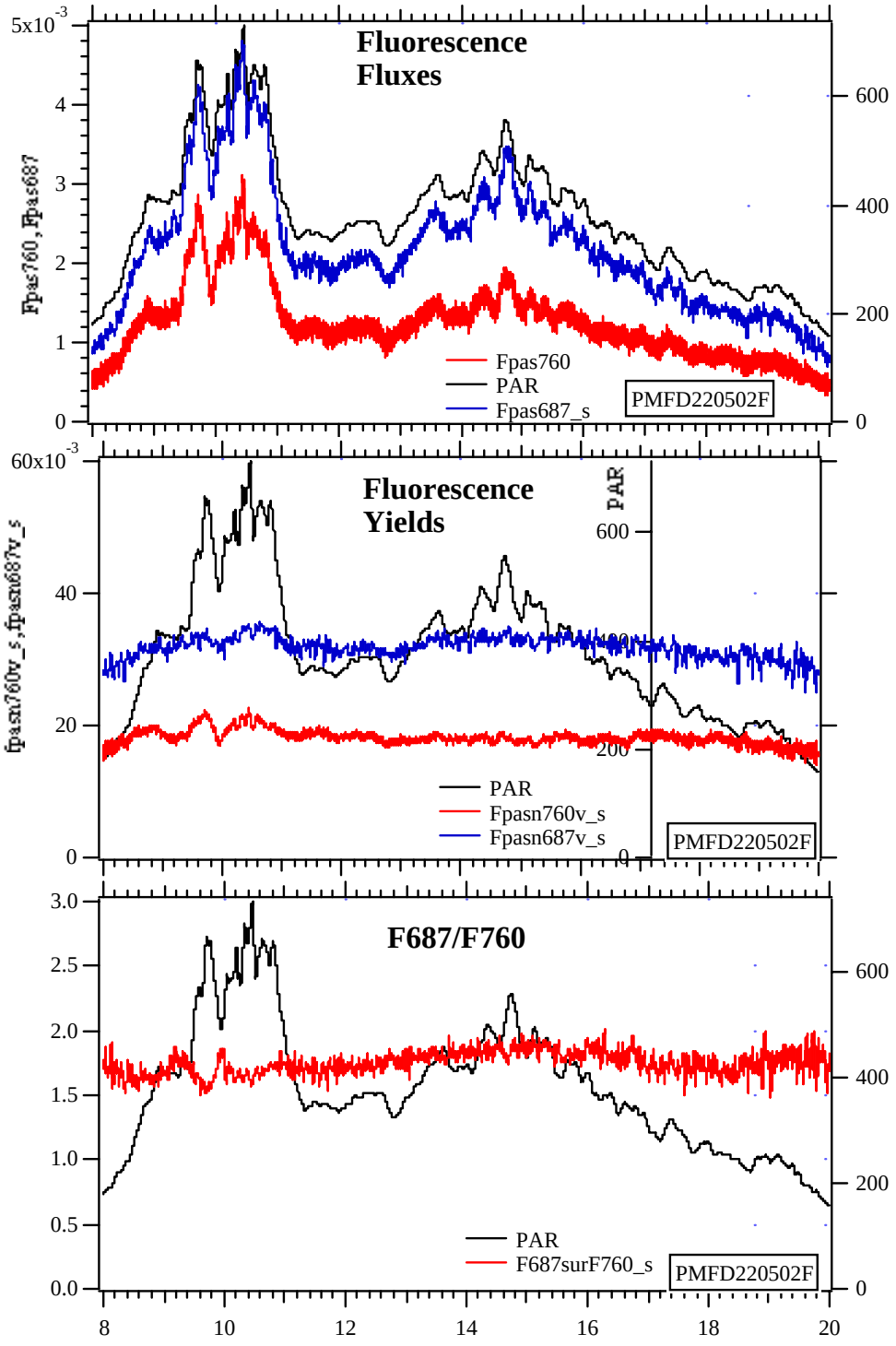

Figure 3.5. Stationary fluorescence fluxes at 687 and 760 nm (Fpas687 and Fpas760, respectively), apparent fluorescence yields at 687 and 760 nm and the fluorescence index F687/F760 recorded with the PMFD during a cloudy day, on the 22nd of May 2002. The PAR is also plotted during the diurnal cycle. All smoothed signals have a "_s" suffix. The time axis (bellow) indicated in hours is in UT + 3.

3.2.3 BI-DETECTOR (BD)

The Bi-detector is the second passive fluorescence sensor operating in the atmospheric oxygen A band at 760 nm. This detector was used to perform complementary measurements at a scale level of one tree. These measurements were performed simultaneously with the micro-FLIDAR Laser-PAM (see below, and Figure 3.9 and 3.10).

3.2.4 MEASUREMENT PROCEDURE OF CHLF FLUXES WITH THE BD

The BD sensor was first installed on the top of the meteorological 17-m high tower to detect fluorescence and reflectance signals at a scale level of a tree. However, we changed the configuration of the experiment by installing this detector on the ground (20 may 2002). The BD was south-to-north oriented during all the campaign.
The sensor was alternatively oriented towards the target (spot size of about 30 × 30 cm) and a reference panel installed near the Scots pine tree. We also performed measurements with a flat black panel installed behind the target to minimise the contribution of transmitted sunlight by the pine tree.

3.2.5 THE MICRO-FLIDAR LASER-PAM

Originally, the Laser-PAM is an adaptation of the commercialised fluorometer "PAM–101" (Heinz Walz, Effeltrich, Germany) that we modified to perform non-invasive remote measurements of chlorophyll fluorescence on single leaves and needles (Ounis et al. 2001). During SIFLEX-2002 campaign, we used a new version of the Laser-PAM based on a 300 mW-laser diode, with a field of view of 25 mrad (1.5°) (Figure 3.9). The main improvement of this new version concerns the measurement of chlorophyll fluorescence and photosynthetically active radiation (PAR) on small canopies (50 × 50 cm) up to a distance of 10 m (Figure 3.10). As an additional improvement of the instrumentation used during SIFLEX campaign, the Laser-PAM was completely remote controlled by a master-computer by mean of a radio frequency connection (IEEE 802.11b, 2.4 GHz). Indeed, this new possibility is very helpful and well suited for field measurements, especially when several instruments are located at different places in the experimental site, or installed on high towers.

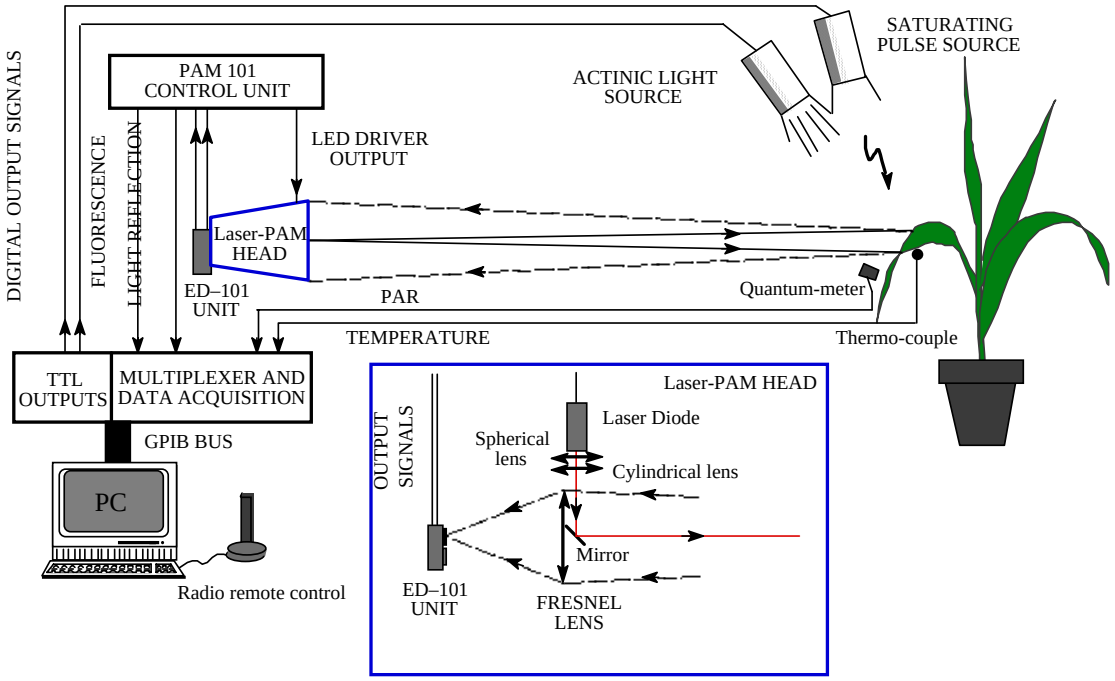

Figure 3.6. Schematic diagram of the Laser-PAM system, used for remote sensing and non-invasive laboratory measurements. During SIFLEX campaign, the temperature of the laser diode was regulated at 10 °C. The optical filter used for ChlF and PAR detection was a 1-mm thick red glass filter (RG9, Schott, Clichy, France) and an interference filter (710DF80, Omega optical, Brattleboro, Vermont, USA).

Figure 3.7. New version of the Laser-PAM head, using a 300–mW laser diode (emitting at 660 nm) for small canopy measurements.

3.2.6 MEASUREMENT PROCEDURE OF STEADY-STATE LASER-INDUCED CHLF, PAR AND TEMPERATURE WITH THE LASER-PAM

During SIFLEX campaign, the Laser-PAM was first installed on the top of the meteorological 17-m high tower to detect chlorophyll fluorescence at a scale level of a tree. However, we changed the configuration of the experiment by installing this Micro-FLIDAR on the ground (20 may 2002).
The Laser-PAM was mainly used as reference and calibration tool for passive chlorophyll fluorescence measurements (Bi-Detector) at a scale level of a Scots pine tree (spot size of about 30×30 cm) (see Figure 3.9 and 3.10). The Laser-PAM was south-to-north oriented during all the campaign.
The measurements were performed everyday, 24 hours a day, with no interruption, except for minor technical problems or when we had exceptional electric cuts on the experimental site (general electric interruption) (see Figure 3.11).

Figure 3.8. Simultaneous measurement of laser-induced ChlF with the Laser-PAM (on the left) and solar-induced ChlF with the Bi-detector (on the right) on a Scots pine tree. The quantum-meter was positioned in a vertical position to detect the incident PAR coming from the top.

Figure 3.9. Experimental set-up of Laser-PAM and Bi-detector systems for laser- and solar-induced ChlF monitoring on a Scots pine tree. The measurements were performed on the same target, at a distance of 4 m, with a south to north direction. At this distance the target dimensions were

about 30 × 30 cm.

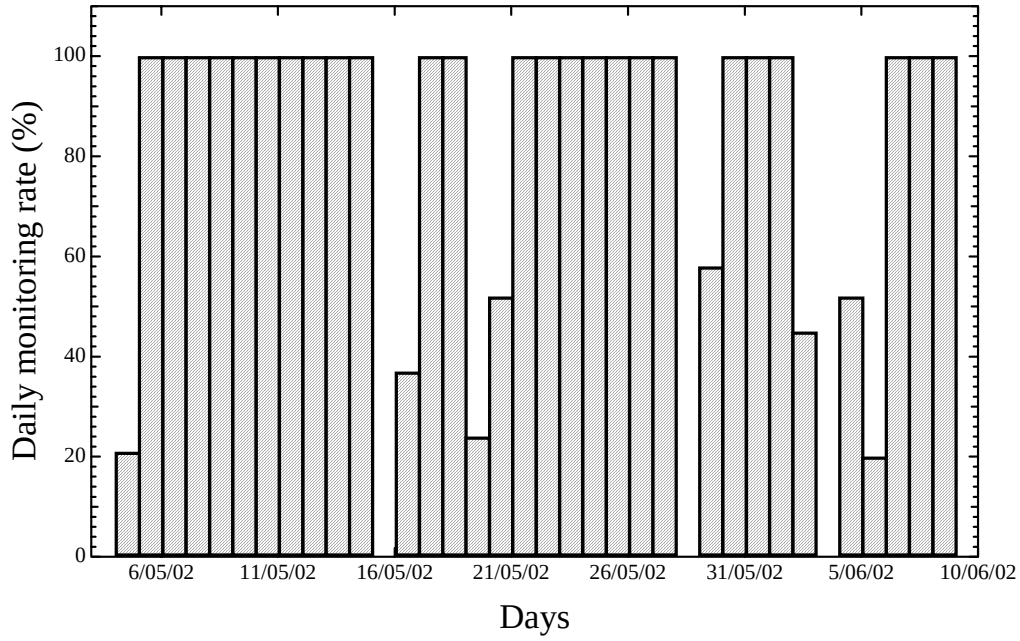

Figure 3.10. Experimental set-up of Laser-PAM and Bi-detector systems for laser- and solar-induced ChlF monitoring on a Scots pine tree. The measurements were performed on the same target, at a distance of 4 m, with a south to north direction. At this distance the target dimensions were about 30 × 30 cm.

3.2.7 THE FREQUENCY-INDUCED PAM (FIPAM)

The FIPAM, a second micro-FLIDAR used during SIFLEX-2002 campaign, is a laboratory-made instrument (Flexas et al. 2000, Ounis 2001) (see Figure 3.12). The particularity of the FIPAM (Figure 3.13) is that the laser diode excitation source is frequency-modulated. Hence, at very low frequency (e.g. 0.5 Hz) the average light power density is weak enough not to induce any increase of minimal steady state chlorophyll fluorescence (Fs, or Fo for dark-adapted vegetation). At high frequency excitation (100 kHz), the average light power density (or the Photosynthetic Photon Flux Density, PPFD) on the sample can reach up to 5000 μmol photons m^{-2} s^{-1}, which saturates the photochemical conversion and then allows the measurement of the maximal fluorescence yield (Fm', or Fm for dark adapted vegetation). Using these parameters, it is then possible to deduce the optimal photochemical yield (Fv/Fm = (Fm-Fo)/Fm), the actual photochemical yield (ΔF/Fm' = (Fm'-Fs)/Fm') and the non-photochemical quenching (NPQ = (Fm-Fm')/Fm'). As an additional improvement during SIFLEX campaign, the FIPAM was also completely remote controlled by a master-computer by mean of a radio frequency connection.

Figure 3.11. The FIPAM operating in the field at Sodankyla (Finland)

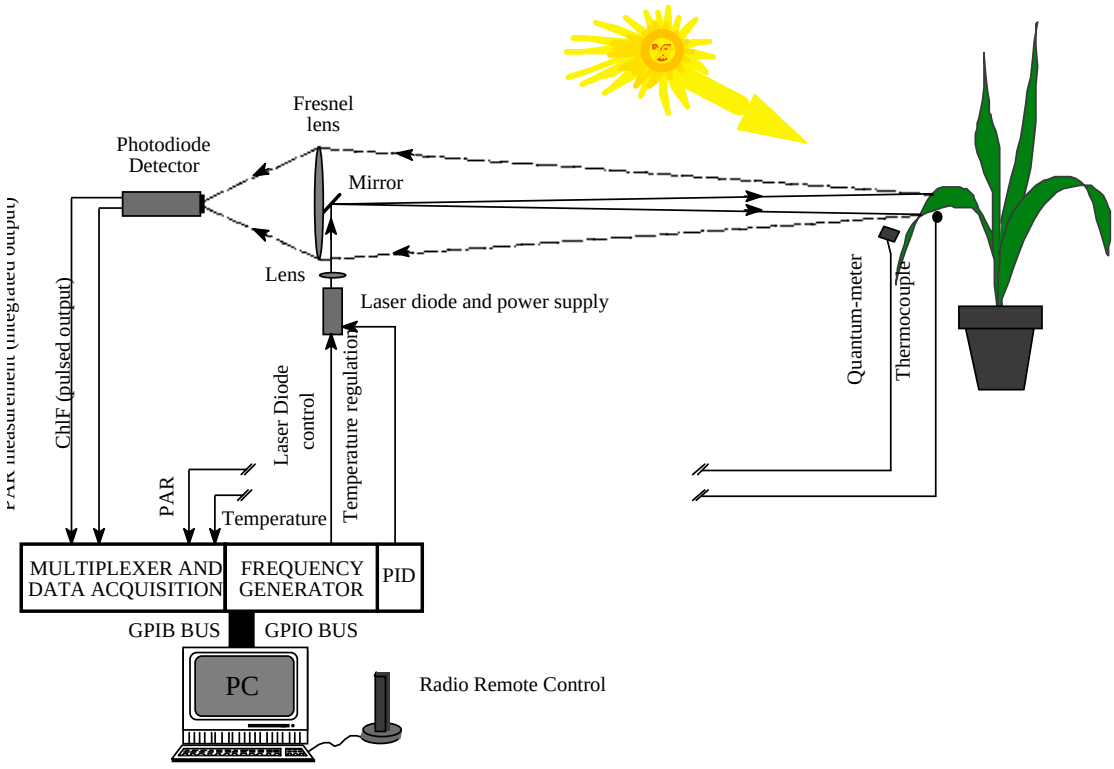

Figure 3.12. Schematic diagram of the micro-FLIDAR FIPAM using a 300 mW-laser diode at 660 nm. During SIFLEX campaign, the temperature of the laser diode was regulated at 10 °C. The optical filter used for ChlF and PAR detection was a 1-mm-thick red glass filter (RG9, Schott).

3.2.8 MEASUREMENTS PROCEDURE OF LASER-INDUCED CHLF PARAMETERS, PAR AND TEMPERATURE WITH THE FIPAM

During SIFLEX campaign, the micro-FLIDAR FIPAM was mainly used as a reference and a calibration tool for passive fluorescence measurements, and also to provide complementary information on the photosynthetic activity and the constraints on the vegetation.

The measurements carried out with the FIPAM were performed at a scale level of some needles (20×3 mm) (see Figure 3.14) due to the average power density needed to saturate the photochemical conversion. The measurements were carried out continuously (24 hours a day), except for some days, where we had some technical problems (see Figure 3.15). These measurements were performed at a short distance (2.5 m) on a single small tree, from a tripod situated on the ground (see Figure 3.12). The recorded measurements allowed us to continuously monitor the photosynthetic electron transport rate (Fv/Fm or ΔF/Fm') and the non-photochemical quenching. These measurements were carried out on two different locations: near the main 20-m high tower, and then next to the 17-m high tower.

Figure 3.13. Chlorophyll fluorescence and PAR monitoring on Scots pine needles with the FIPAM system. The quantum-meter was positioned in the same direction as the target. The needles were maintained with a clamp.

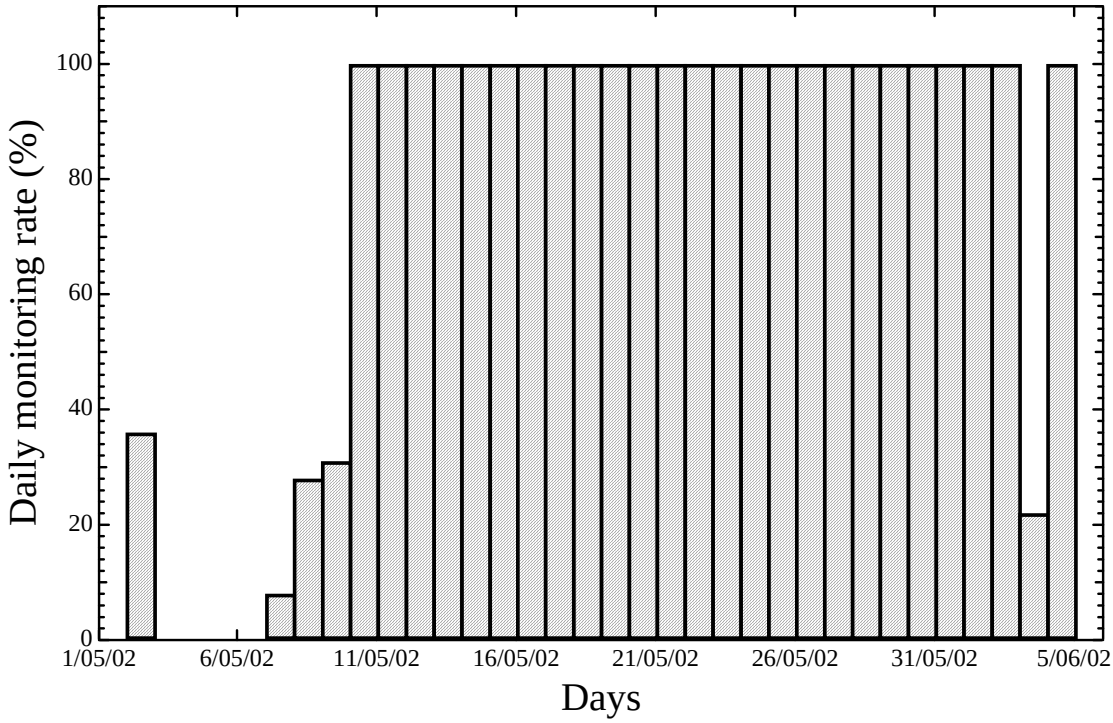

Figure 3.14. Daily monitoring rate of the FIPAM, during SIFLEX-2002 campaign. The average monitoring rate was 77 %.

The measurements performed with the FIPAM in the boreal forest during SIFLEX campaign showed an increasing level of the maximal photochemical yield (Fv/Fm) after the snow melting period, from 0.60 to 0.80, and hence an increase of the photosynthetic activity (see chapter 5 for more details). These measurements showed also that during sunny days, for example on 27 May 2002, the non-photochemical quenching recorded during a diurnal cycle (see Figure 3.16-B) was relatively high with values up to 2. At the same time, the effective photochemical yield (ΔF/Fm') decreased strongly as expected, and reached values up to 0.2. In Figure 17A, Fs and Fm' were strongly quenched by the non-photochemical conversion, when PAR became high (above 600 μmol photons m^{-2} s^{-1}). Fs decreased even below Fo level around midday. The decrease of Fs recorded early in the morning (around 4 am) (Figure 3.16-A), which lasts about 2 hours (see also Figure 3.18 and 3.19), could be due to an optical effect caused by a water vapour condensation on the target or due to the frost of needles. Indeed, at this time the needles temperature was – 0.4 °C, and the ambient temperature was + 0.7 °C. This interpretation could also be corroborated by the simultaneous decrease of Fm', because at that time ΔF/Fm' did not decrease, showing that the photochemical yield has not been affected. As complementary information, one can see the maximal and minimal temperature of the air recorded by the FIPAM during the campaign (Figure 3.17). These measurements show that during sunny days, the

temperature can reach up to 32 °C.

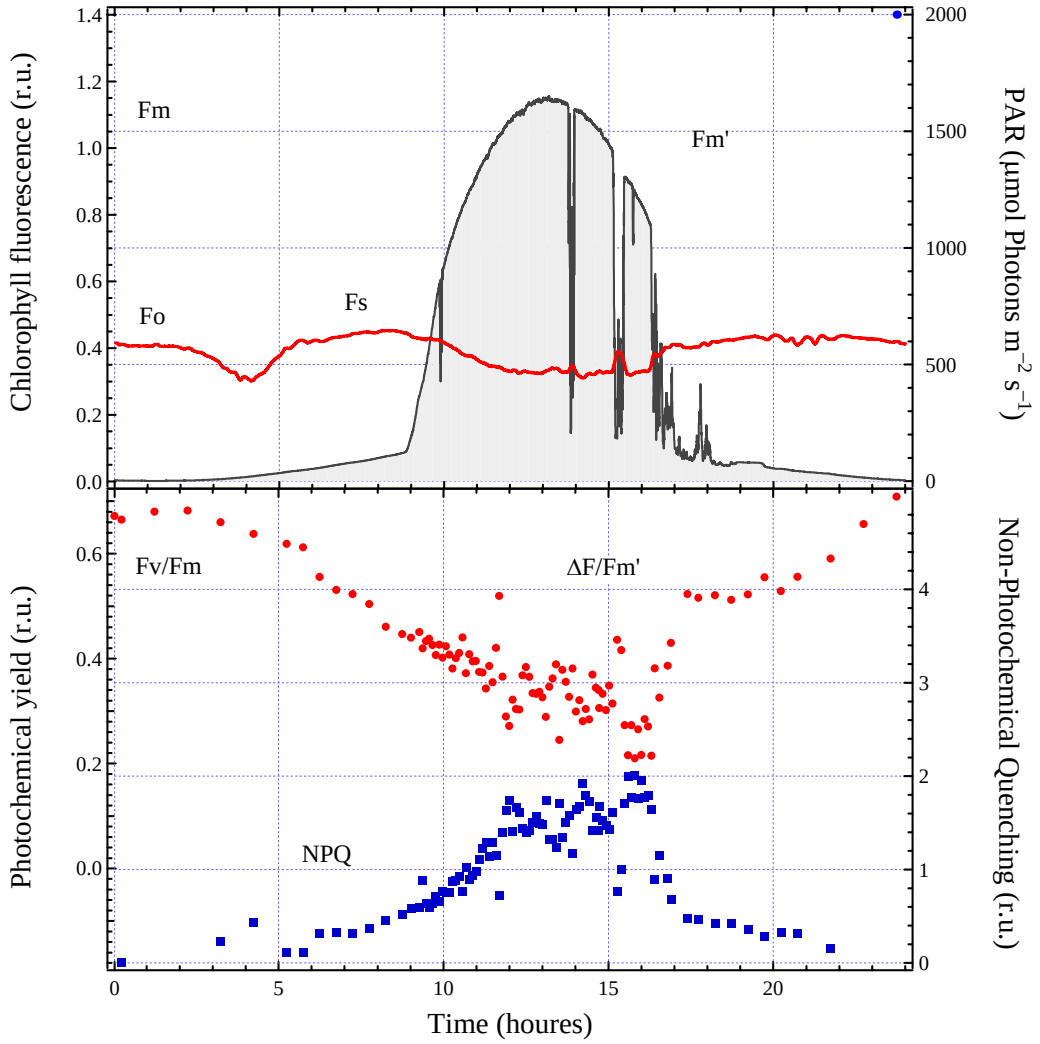

Figure 3.15. Diurnal cycle measurements performed with the FIPAM during a sunny day (27 May 2002). The time is indicated in UT + 3.

The anti-parallel correlation between Fs and PAR, observed during sunny days (Figure 3.16-A), shows that the needles were under the control of the non-photochemical conversion. Due to a strong increase of the non-photochemical quenching, Fs decreased at noon, and also increased when the samples were under shadow (see Figure 3.18-B for more details). Compared to that, during cloudy days (e.g. 21 May 2002), the NPQ was relatively low (see chapter 5). As a consequence, the negative correlation between Fs and PAR was less pronounced (see Figure 3.18-A).

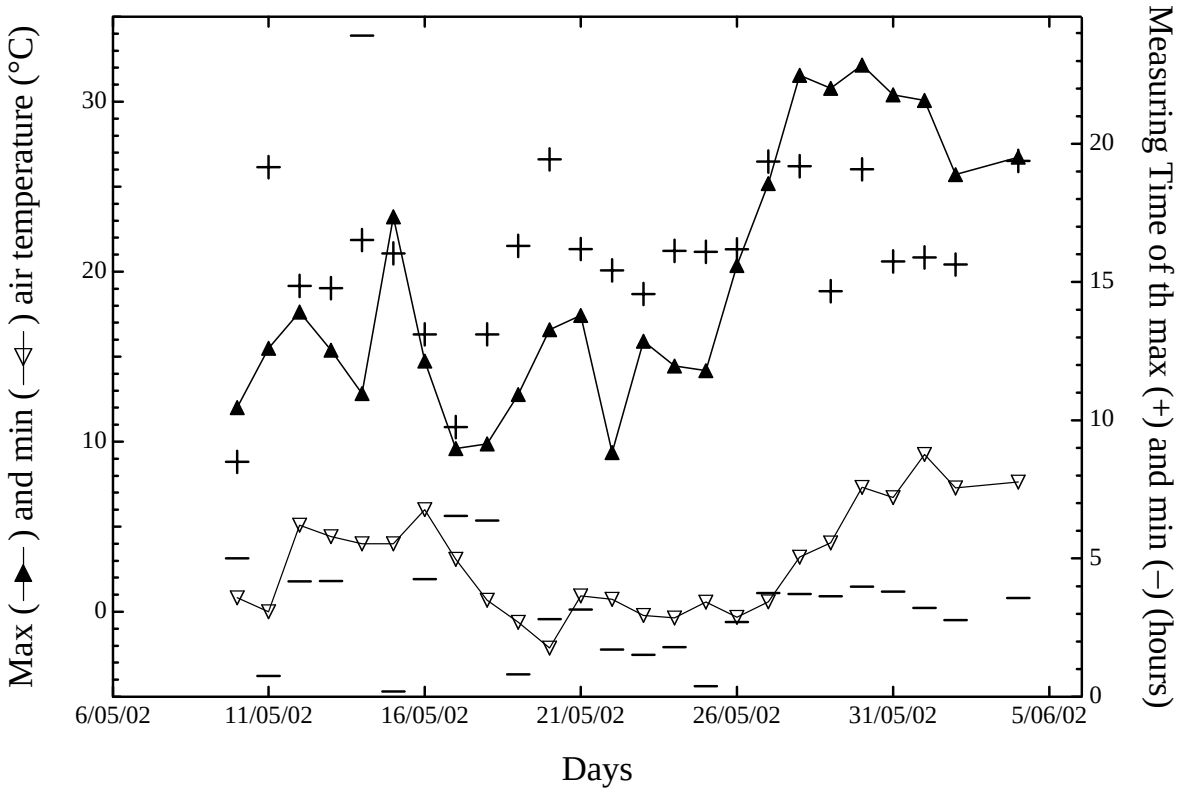

Figure 3.16. Maximal and minimal temperature of the air, and the corresponding time, recorded by the FIPAM during SIFLEX campaign.

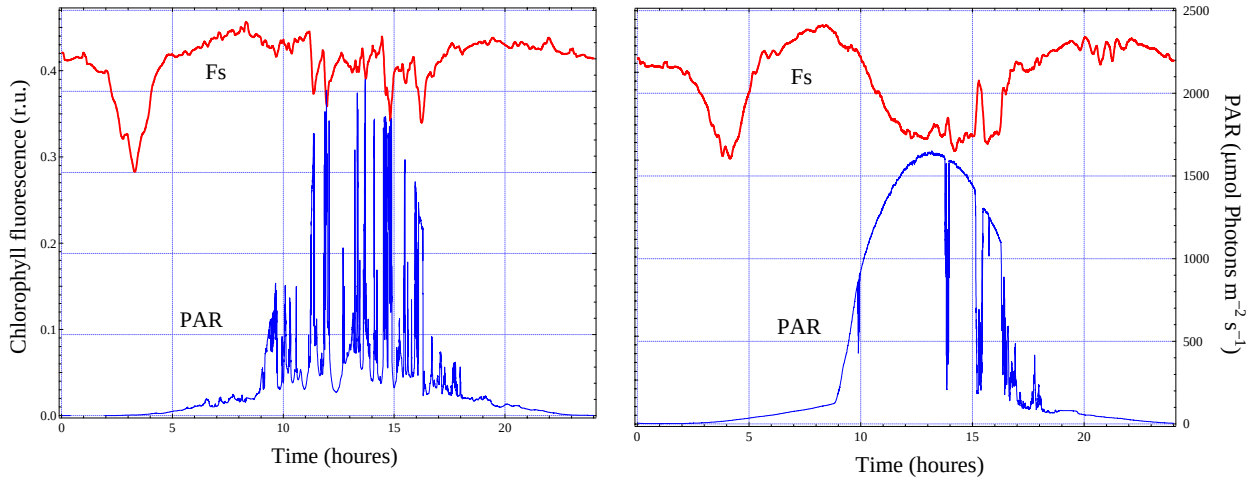

Figure 3.17. Diurnal cycle measurements carried out with the FIPAM during a cloudy day (21 May

2002) and a sunny day (27 May 2002). The measurements were performed at a scale level of some needles. The variations of the PAR during the sunny day are due to the shadow from other Scots pine trees.

The experiment concerning simultaneous measurements of solar-induced ChlF and laser-induced ChlF, performed with the Laser-PAM, at a scale level of a pine tree, showed similar correlation and results as the FIPAM experiment even with different scale of measurements, different pine trees, and different locations (Figure 3.19, see also Figure 3.20). During cloudy days (see Figure 3.19-A), any increase of the PAR was correlated with an increase of Fs (positive correlation), indicating that the vegetation was under the control of the photochemical conversion. On the other hand, the correlation between Fs and PAR recorded with the Laser-PAM, during sunny days, indicated that the vegetation was under the control of the non-photochemical conversion.
In Figure 3.20, we plotted simultaneous measurement of Fs performed with FIPAM on some needles, and Laser-PAM on a tree. These measurements showed similar correlation and results even with different scale of measurements, different pine trees, and different locations (Figure 3.20). However, one can see some differences in the amplitude of Fs variations when the measurements are performed on a bigger target (Laser-PAM measurements). These differences may be due to the integration of ChlF coming from illuminated needles and from others under shadow. The shifting observed between both Fs variations is mainly due to the time-shifted variation of the PAR at different locations on the site.

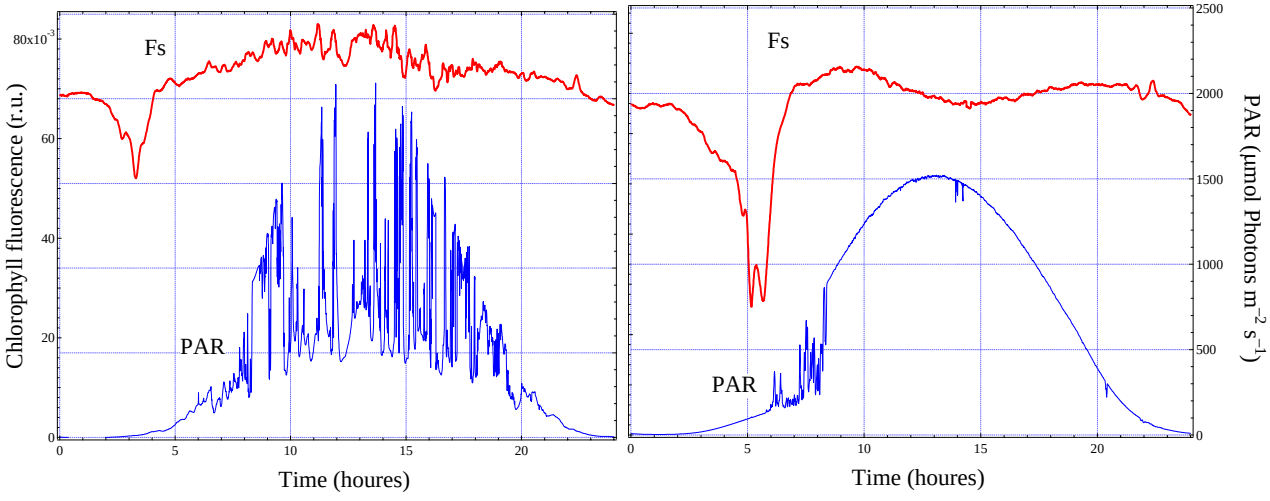

Figure 3.18. Diurnal cycle measurements carried out with the Laser-PAM during a cloudy day (21 May 2002) and a sunny day (27 May 2002). The measurements were performed at a scale level of a tree. The variations of the PAR in the morning are due to the shadow from other Scots pine trees.

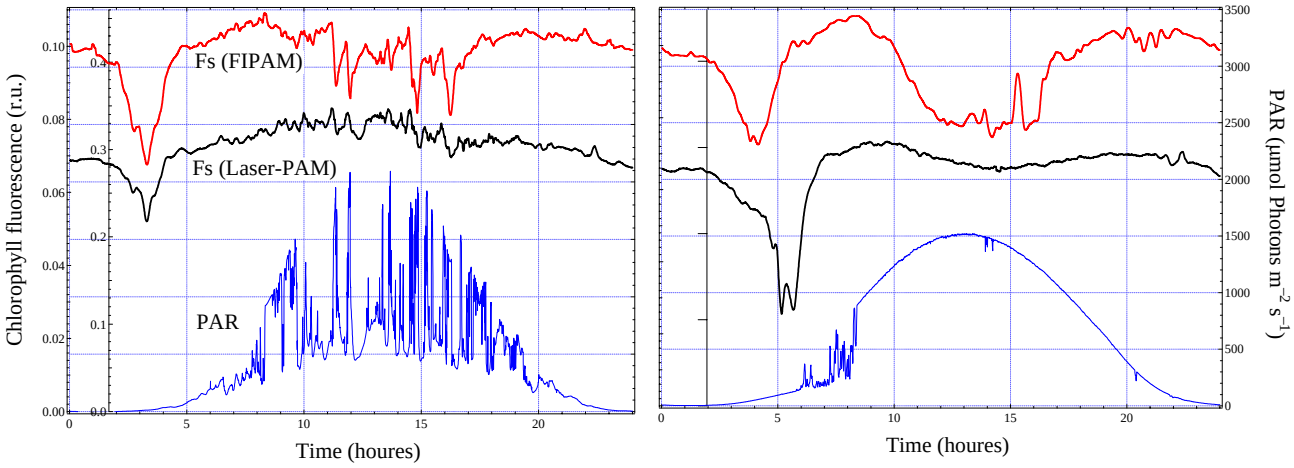

Figure 3.19. Diurnal cycle measurements carried out with the FIPAM and the Laser-PAM during a cloudy day (21 May 2002) and a sunny day (27 May 2002). The measurements were performed at two different scale levels, on pine needles (with FIPAM) and on a pine tree (with the Laser-PAM), and two different locations on the experimental site. The plotted PAR corresponds to measurements performed with the Laser-PAM.

3.3 CONCLUSIONS

The main objective the SIFLEX campaign, which has been held in the boreal forest at Sodankyla (Finland), from 23 April 2002 to 10 June 2002, consisted to test the technical feasibility of passive fluorescence remote sensing methods at the level of tree canopies. During this campaign we tested two passive fluorescence instruments, the Passive Multi-wavelength Fluorescence Detector (PMFD) and the Bi-detector (BD), based on the Fraunhofer line principle applied to the atmospheric oxygen absorption A and B bands (at 760nm and 687nm, respectively). Despite the difficulties related to the geometrical structure of pine trees, from needles to the canopy, and also despite the weather conditions in the boreal forest, we performed continuous monitoring of solar-induced chlorophyll fluorescence, NDVI (Normalized Difference Vegetation Index) and PRI (Physiological Reflectance Index) on Scots pine trees (*Pinus sylvestris* L.). The campaign period covered the spring recovery of pine trees from winter dormant to summer fully active state of photosynthesis. During this campaign, we also used two micro-FLIDARs (Fluorescence LIght Detection And Ranging) systems to monitor the laser-induced chlorophyll fluorescence on Scots pine at scale levels of needles and trees. The micro-FLIDARs "Laser-PAM" and "FIPAM" were mainly used as reference and calibration tools for passive fluorescence measurements, and also to provide complementary information on the photosynthetic activity and the constraints on the vegetation. Thanks to the data provided by the FIPAM and the Laser-PAM, which are mainly Fv/Fm, ΔF/Fm', NPQ, and also Fs, it was possible to monitor the photosynthetic activity of the boreal forest under different

constraints of light exposure and temperature, and also at different scale levels of integration. The results of the measurements showed a good correlation with different instruments on different targets, different scales of measurements, and different locations.

The active measurements showed an increase of the photosynthetic activity after the spring recovery of vegetation, and also an increase of the non-photochemical quenching during sunny days where the temperature was high. These measurements showed also that the correlation between Fs and PAR is a potentiel indicator for the presence of constraints and stress on the vegetation.
The solar- and laser-induced fluorescence signals observed at different scale levels of the forest, from pine needles to trees canopies, and also reflectance indexes have been correlated to carbon dioxide fluxes measured on the same site using specific methods (Eddy covariance). The comparison of the optical signals and gas exchange parameters recorded on the boreal forest are presented separately in chapter 5.

4. Measurements by UVAL

This chapter describes the solar radiation measurements carried out during SIFLEX-2002 held at Sodankylä (Finland) from 23 April to 10 June. The objective of the Solar Radiation Group was to measure the spectral radiation incident to the ground and canopy system by separating its components (direct and diffuse).
In collaboration with the Finnish Meteorological Institute the atmospheric components, particularly ozone, water vapour and aerosols, were characterised.
One of the Solar Radiation Group's instruments was also used to measure some properties, which were considered relevant during the campaign, without modifying the main objectives though.

Note: In this chapter the time is given in local time (LT) as it was used for most of the participants in the campaign. In the solar radiation database the time is given in solar time relative to the 30º meridian (local solar time). The Finnish Meteorological Institute routinely uses UTC (Co-ordinated Universal Time).

4.1 CHARACTERIZATION OF THE SPECTRAL RADIATION (SUN IRRADIANCE AND SKY IRRADIANCE) AND ATMOSPHERIC COMPONENTS DURING THE SIFLEX CAMPAIGN

4.1.1 MAIN OBJECTIVE

Measurement of the solar radiation incoming to the system canopy + ground. The measurements took place in the FMI radiation 17m tower (coordinates 67.37N, 26.63W), which is above the canopy in order to prevent shadows from the trees from, appear.

4.1.1.1 Measurements.

Carried out with a Li-Cor 1800 spectroradiometer with a single monocromator. Sensor: silicon photocell. Full Width at Half Maximum (FWHM) of the instrument: 6 nm. Spectral resolution: 1nm

-Global horizontal spectral irradiance ($I_{g\lambda}$). Optical entrance: teflon dome.

-Direct normal spectral irradiance ($I_{d\lambda}$). Optical entrance: teflon dome + collimator with FOV 4.5º

The diffuse component ($I_{d\lambda}$) is obtained by substraction where θ_z is the solar zenith angle

$$I_{d\lambda} = I_{g\lambda} - I_{d\lambda} I \cos\theta_z \qquad (3)$$

4.1.1.2 Protocol of measurements.

Range:

[300, 1100] nm @ 1 nm

Measurement time:

- 10:00 – 16:00 (Local Time) measurements every 15 min
- 17:00 – 21:00 (Local Time) measurements every hour

Required weather conditions:

- Global horizontal spectral irradiance: no precipitation, which could damage the instrument
- Direct normal spectral irradiance: no clouds covering the sun disk

Figure 4.1 shows an overview of such measurements during the campaign

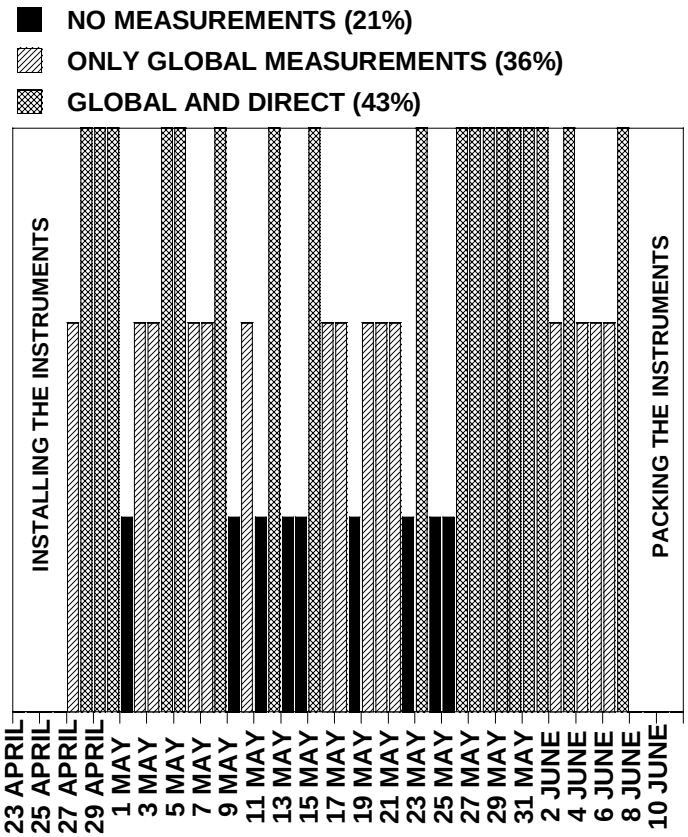

Figure 4.1. Overview of the solar radiation measurements carried out with the Li-Cor 1800 during the campaign

4.1.2 SECONDARY OBJECTIVE

As a secondary objective the Solar Radiation Group carried out measurements to characterise the aerosols. Two kinds of measurements were made: Firstly measurements of the extinction of the radiation in order to obtain the aerosol optical depth and the size distribution. Secondly measurements of the multiple scattering due to the aerosols to retrieve the aerosol refractive index, the aerosol size distribution in a wider range of radii - as well as other radiative properties (phase function, single scattering albedo).

Extinction of the radiation:

Direct normal spectral irradiance: see main objective

Multiple scattering:

Diffuse sky radiance measurements with an Optronic 754-O-PMT spectroradiometer with a double monochromator. Optical entrance: reflex telescope 8X, FOV 1.2º. Sensor element: photomultiplier. FWHM 1.9 nm. Spectral resolution 0.25 nm.

Protocol of measurement:

Range of measurement:

{369, 500, 675, 776} nm, with 0.25 nm spectral resolution, in the almucantar plane of the sun (orthogonal to the principal plane) for scattering angles [0, 40º]. (see figure 3).

Measuring time:

10:00 – 21:00 every 30 min whenever the sky conditions are good enough.

Required weather conditions:

No clouds in the almucantar plane of the sun (see figure 4.3)

Figure 4.2 shows and overview of diffuse sky radiance measurements during the campaign. As it can be seen from the number of measurements carried out, the required conditions were difficult to obtain in the site.

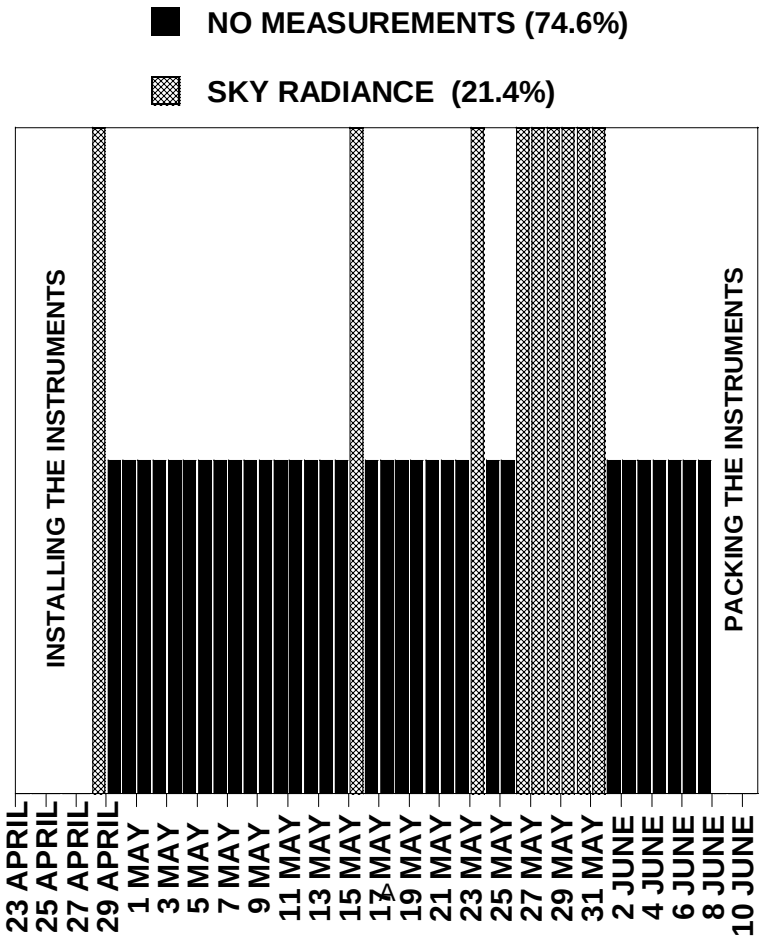

Figure 4.2. Overview of the diffuse sky radiance measurements carried out with the Optronic 754 during the campaign

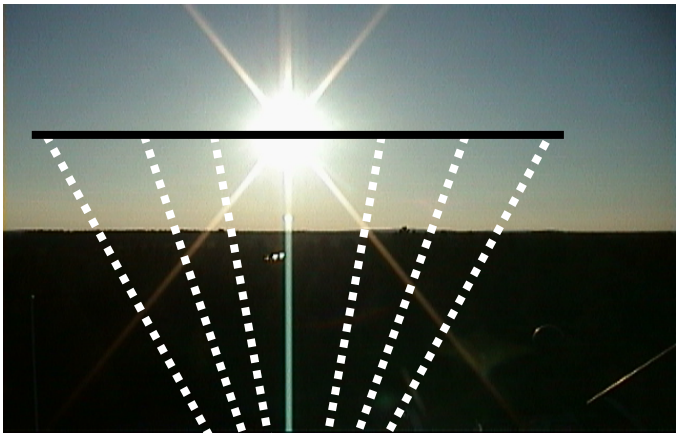

Figure 4.3. Protocol of measurements of the Optronic 754. Azimuth angles {5º, 10º, 20º, 30º, 40º, 50º, 60º} symmetrically chosen in both sides of the almucantar plane of the sun. The measurement at 0º is the direct irradiance

4.1.3 OTHER MEASUREMENTS

During the campaign some other measurements were designed and carried out because of their scientific interest as a complement of the main objectives of the SIFLEX campaign.

4.1.3.1 Transmisivity of the forest.

As the radiation above the canopy was measured with the Li-1800 spectroradiometer, the Optronic 754 was used to measure the spectral irradiance reaching the forest ground after being affected by the system ground + canopy. The measurements took place during two days in the 25x25 m main target. The high spectral accuracy of the instrument, 0.25 nm, allows a good characterisation of the radiation in the oxygen band.

Protocol of measurements:

Range:
[300, 800] nm @ 0.25 nm. Optical entry: quartz dome + integrating sphere.

Measuring time:
- 2 June: 11:15 LT – 16:00 LT every 15 min
17:00 LT – 19:00 LT every hour
-5 June: 12:00 LT – 16:30 LT every 15 min

Weather conditions:
Partly cloudy on both days. Rain on 4 June in the afternoon.

4.1.3.2 Depth of the oxygen band in different directions.

In order to characterise the influence of the architecture of the forest in the radiation in the oxygen band, the depth of the oxygen band was measured in different directions (vertical, north and south). Two altitudes were selected: ground level and on top of the 20 m tower (above the canopy). The measurements took place on a cloudy day (19 May) and on a sunny day (26 May). The instrument used was the Optronic 754 spectroradiometer for its spectral resolution with an optical entrance (quartz dome + integrating sphere) to get the maximum amount of radiation to characterise the scene.

Protocol of measurement

Range:
[652, 657] @ 0.25 nm
[684, 689] @ 0.25 nm
[754, 762] @0.25nm
Measuring time:
Twice a day. Around 13:00 LT and around 16:00 LT for both ground and top of the tower.

4.1.3.3 Depth of the oxygen band in the sky dome

For validation of radiative transfer modelling of fluorescence the diffuse radiation in the sky dome was measured at wavelengths selected for their relevance. Two wavelengths to be related to the PRI and two pairs of wavelengths for the depth of the oxygen band. The instrument used was the Optronic 754 spectroradiometer for its spectral resolution with a telescope in the entrance port in order to have multiangular measurements.

Protocol of measurement

Range:
{530, 531, 685, 687, 758, 760} nm, with 0.25 nm precision, in the almucantar plane of the sun (see figure 2) covering the whole sky dome (360º) at 30º intervals.
The measurement at 0º is the direct irradiance of the sun. The measurements took place only in selected days: 23, 26, 27, 28, 29 and 30 May.

Measuring time:
10:00 – 21:00 every 30 min after the multiple scattering measurement
Required weather conditions:
See multiple scattering measurements.

4.1.3.4 Fluorescence measurements.

Some measurements of the fluorescence at the needle level were carried out using the Optronic spectroradiometer with the telescope as it was possible to measure simultaneously the PRI and the depth of the 685 and 760 nm oxygen bands. The measurements took place only on 6 and 7 June to explore the potential of this kind of measurement

Protocol of mesurement

Range:

{530, 531, 685, 687, 758, 760} nm, with 0.25 nm precision, pointing alternatively at a white reference and at some chosen needles .

Measuring time:

-6 June: 15:00 – 17:15 every 15 min
-7 June: 10:00 – 16:00 every 15 min

4.2 THERMAL MEASUREMENTS WITHIN THE SIFLEX-2002 CAMPAIGN: CANOPY TEMPERATURE RETRIEVAL AND AIR-CANOPY TEMPERATURE DIFFERENCES

Our main purpose in the SIFLEX-2002 campaign was the determination of air-canopy temperature differences, since these differences, together with surface wind speed, are related with the plant energy dissipation by sensible heat flux, which is complementary to other processes, such as fluorescence emission.

Therefore, the first fieldwork was canopy and air temperature measurements, to obtain a continuous thermal database covering the whole of the campaign. Air temperature (AT) was measured around the target with a thermocouple, whereas CT was obtained using a multichannel thermal infrared radiometer. The recovery of CT from thermal infrared data allows us to obtain the effective temperature of the canopy target over which the fluorescence was measured simultaneously.

In this chapter we describe the field thermal measurements strategy during SIFLEX campaign, the CT retrieval methodology, and the final results.

4.2.1 FIELD MEASUREMENTS STRATEGY

4.2.1.1 Canopy temperature measurements

Canopy radiance measurements were performed every 10 minutes by the ***CE 312*** thermal infrared radiometer during the SIFLEX campaign.

This instrument is provided with four channels within the thermal infrared region; three narrow channels and a broad one that covers all this band (from

8 to 14 μm). Their response functions are shown in Figure 1, where the filter transmittance is displayed against wavelength. The performance of the CE312 has been regularly checked against a reference black-body for a wide range of temperatures and field conditions. The CE 312 radiometric temperature accuracy has been determined as a result of these calibration procedures (Table 4.1).

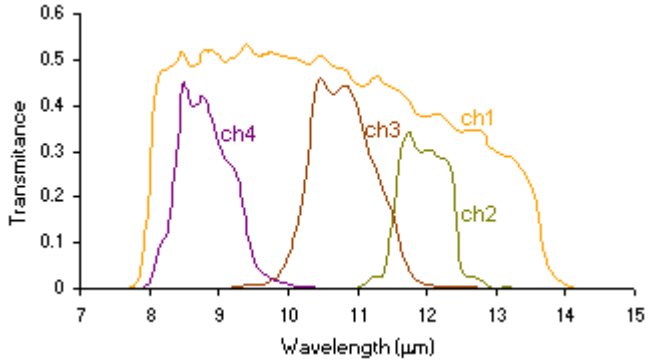

Figure 4.4. CE 312 filter functions.

Table 4.1. Technical specifications of the CE 312 spectral bands.

CE 312 spectral bands				
	Ch 1	*Ch 2*	*Ch 3*	*Ch 4*
Wavelength (μm)	8-14	11.5-12.5	10.5-11.5	8.2-9.2
Resolution(1) (mK)	8	50	50	50
Accuracy (2) (K)	± 0.10	± 0.12	± 0.09	± 0.14

(1) At 20 ºC. (2) Data obtained through sensor calibration processes.

The CE 312 is composed of two major components: (1) the optical head containing the detector (thermopile) and optics, and (2) the electronic unit, which performs the data collection configuration, display and storage. A filter wheel with the four interference filters (one for each channel) is located between the objective lens and a stepper motor that allows the filter selection. Figure 4.4 shows the CE 312 thermal radiometer with its two major components. The radiometer is provided with a concealable, gold-coated mirror, which enables comparisons between target radiation and a reference radiation from inside the optical head. A platinum probe attached to the detector's surface monitors the head's internal temperature and is used to give the reference temperature from which the reference signal is calculated. A second, but external temperature probe can be added by the user into the control unit. It allows collecting the temperature of an external blackbody, usually used for the calibration procedures. The CE 312 has a range of sensed temperature between -80 and +50 ºC, 1 s of response time, and a field of view

of 10º. More details on the technical specifications can be found in Pietras et al. (1994) and Sicard et al. (1999) and at the web site of Cimel Electronique (http://www.cimel.fr/).

During SIFLEX-2002 campaign, the CE 312 radiometer was kept in a shelter to be protected from the environmental conditions and the incoming radiance was observed through a ZnSe window 4 mm thick, which was selected because of its good transmission within the thermal infrared region (Figure 4.5). Moreover, a small bag of silica-gel was placed inside the protective shelter to prevent the formation of condensation drops. For that reason, the calibration of the complete system (protective shelter and sensor) was carried out in the field conditions to cover the observed temperature range (from below zero to about 25ºC), where the window optical properties were taken into account (Niclòs et al., 2002). A portable calibration source Everest Model 1000 was used, and the CE 312 external probe read its temperature. Average radiometric temperature errors of ± 0.15 K, ± 0.19 K, ± 0.13 K, and ± 0.2 K for channels 1-4 respectively were obtained using this calibration procedure on the CE 312 radiometric data taken during SIFLEX-2002 campaign.

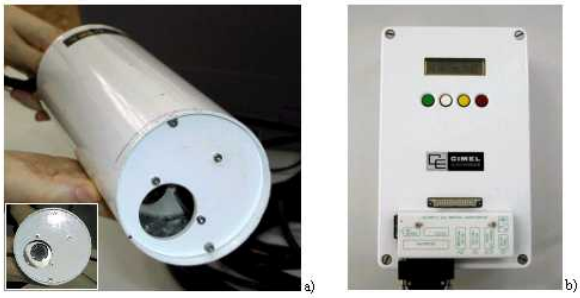

Figure 4.5. Radiometer CE 312 with its major components: a) the optical head and b) the electronic unit.

Figure 4.6. Protective system for the CE 312: optical head inside the protective shelter.

The radiometer was observing the target from a height of 12 m (6th floor of the tower) to assure a homogeneous view of the vegetation (Figure 4.6). It was placed with a fixed zenith angle to ensure the adequate observation of the target over which the fluorescence was measured simultaneously. In addition, we checked the effect of a possible pointing error by changing slightly the observation angle, and the thermal spatial variability around the target was negligible (lower than the radiometric error).

4.2.1.2 Air temperature measurements

Air temperature measurements were carried out every 10 minutes around the target throughout the campaign by a thermocouple. It was located at the top of a tree inside the target area and protected of rain and direct radiation by an opened box (Figure 4.7). The thermocouple was calibrated within the

air temperature range (0 - 33 ºC) in order to obtain a good accuracy (Caselles et al., 2002).

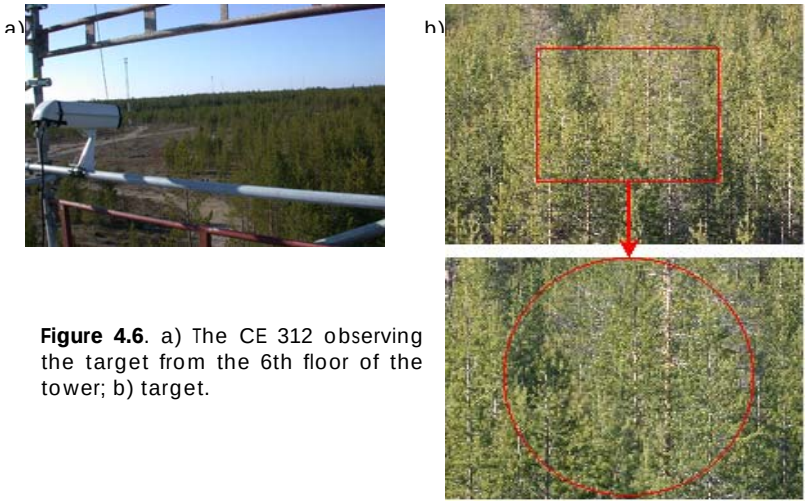

Figure 4.6. a) The CE 312 observing the target from the 6th floor of the tower; b) target.

Figure 4.7. Thermocouple placed at the top of a target tree and protected with an opened box.

4.2.2 TEMPERATURE RETRIEVAL FROM RADIOMETRIC DATA

The radiance reaching the CE 312 radiometer, L_i, is composed of two contributions: (1) canopy direct emission, and (2) reflection of the downwelling sky radiance, so that L_i is defined by the following equation:

$$L_i = \varepsilon_i \, B_i(CT) + (1-\varepsilon_i)L_{Si}^{\downarrow} \qquad (1)$$

where $B_i(CT)$ is the channel i averaged Planck's function for a CT; εi is the surface effective emissivity; and $L_{Si}^{\downarrow}$ is the downwelling sky radiance. The determination of CT requires estimates of both the downwelling sky radiance and the emissivity. This last magnitude needs an accurate determination because of its importance in the radiometric data correction.

4.2.2.1 Emissivity measurements in the laboratory

Several samples were collected to measure their emissivity in the laboratory by means of the box method (Rubio et al., 1997). This consists of measuring the radiance emitted by a sample using an open-based aluminum box and alternating a cold aluminum lid and a hot black lid every measurement. to

perform the emissivity measurements (Figure 4.8).

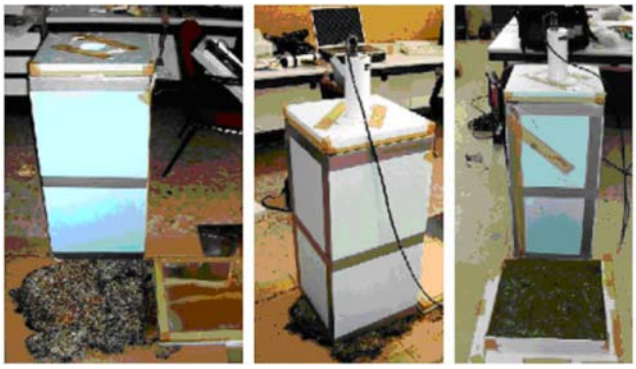

Figure 4.8. Emissivity measurements in the laboratory using the box method.

Figure 4.9 shows the results obtained for the main samples, i.e. the soil below the trees in the target area and the pine branches (Figure 4.10). The most accurate values are obtained for the CE 312 channel 3 (10.5-11.5 μm), with an average error of about ± 0.002 for the pine branches.

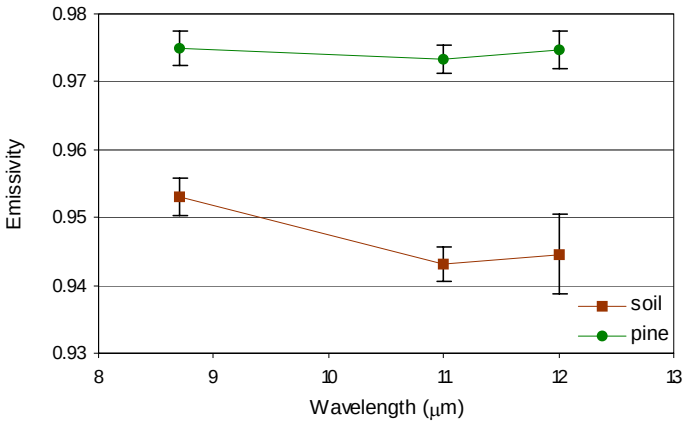

Figure 4.9. Emissivity measurements in laboratory using the box method for the CE 312 narrow channels.

Figure 4.10. Soil and pine branches collected as samples for the emissivity measurement.

4.2.2.2 Downwelling sky radiance determination

The impact of the atmospheric effect in the CT determination was studied. Some radiosoundings launched in the region were selected as representative of two extreme sky conditions: completely clear and cloudy days (0 octas, and 8 octas of cumulus with a cloud base height of 300 m, respectively). They were introduced into the MODTRAN 4 radiative transfer code (Berk et al. 1999) in order to assess the $L_{Si}^{\downarrow}$ contribution for those cases. The results showed that its effect was negligible for clear skies, decreasing the CT only about 0.15 K for the CE 312 channel 3, in which $L_{Si}^{\downarrow}$ is minimum. On the contrary, under cloudy skies with low clouds, a CT decrease higher than 2 K would be possible. Therefore, the downwelling sky radiance was needed to obtain accurate CT measurements.

The main contribution to the $L_{Si}^{\downarrow}$ is due to the cloudiness amount and height. Thus, the variability of the cloudiness conditions was the major factor to be taken into account. We used the downwelling sky radiance from the representative radiosoundings of extreme skies and the Sodankylä's weather database, given by the Finnish Meteorological Institute (FMI), where cloudiness information was available in an almost continuous way. $L_{Si}^{\downarrow}$ was simulated from the consideration of a maximum $L_{Si}^{\downarrow}$ (from the use of the representative radiosounding for the cloudiest sky) and a minimum $L_{Si}^{\downarrow}$ (from the clear-sky representative radiosounding). The $L_{Si}^{\downarrow}$ to correct each CE 312 radiometric measurements was an average value between these minimum and maximum values, where the weight of this average was the cloudiness amount.

4.2.3 RESULTS

Canopy radiometric temperature was obtained with average errors of ± 0.15 K, ± 0.19 K, ± 0.13 K, and ± 0.2 K for CE 312 channels 1-4 respectively after

applying the system calibration correction. A vegetation emissivity of 0.973 ± 0.002 was determined with the *box method* (Rubio et al. 1997) for the CE 312 channel 3, where the emissivity retrieval error is the minimum. Therefore, this spectral band provided us the best radiometric accuracy and the lowest emissivity error. Thus, calibration and emissivity corrections were applied, through (1), using the spectral range 10.5-11.5 μm and taking into account the downwelling sky radiance effect. CT was obtained every 10 minutes from April 26th to June 9th with an average precision of ± 0.4 K (Figure 4.11).

Simultaneously, AT was measured from May 7th to June 9th in the target area by a thermocouple (Figure 4.12). AT accuracy was better than ± 0.1 K in all cases.

Moreover, we have been compared these results with the Photochemical Reflectance Index (PRI), and also global, direct and diffuse radiation, wind speed and energy fluxes, in order to improve our understanding of fluorescence emission processes. The PRI, measured by the LURE-CNRS, is defined as the relative changes in reflectance at 531 nm with respect to those at 570 nm (PRI = R531-R570 / R531+R570). Figure 4.13 shows the CT and PRI evolution for several clear days, where an inverse correlation between CT and PRI appears, with CT maximums and PRI minimums coincidence. Figure 4.14 is a detailed comparison of all these magnitudes for June 1st. A peak in the PRI simultaneous to a CT decrease is observed at about 10:05 UTM. At the same time there are a wind speed reduction and a peak in the diffuse radiation, due to a momentary cover of the sun by a cloud, as the continuous sky photographs taken in the region show. Moreover, a decrease of the sensible heat flux appears simultaneously. This correlation is observed on more days, e.g. for June 9th, when several PRI peaks are shown (see Figure 4.15). Unfortunately, there are not available direct and diffuse radiation data.

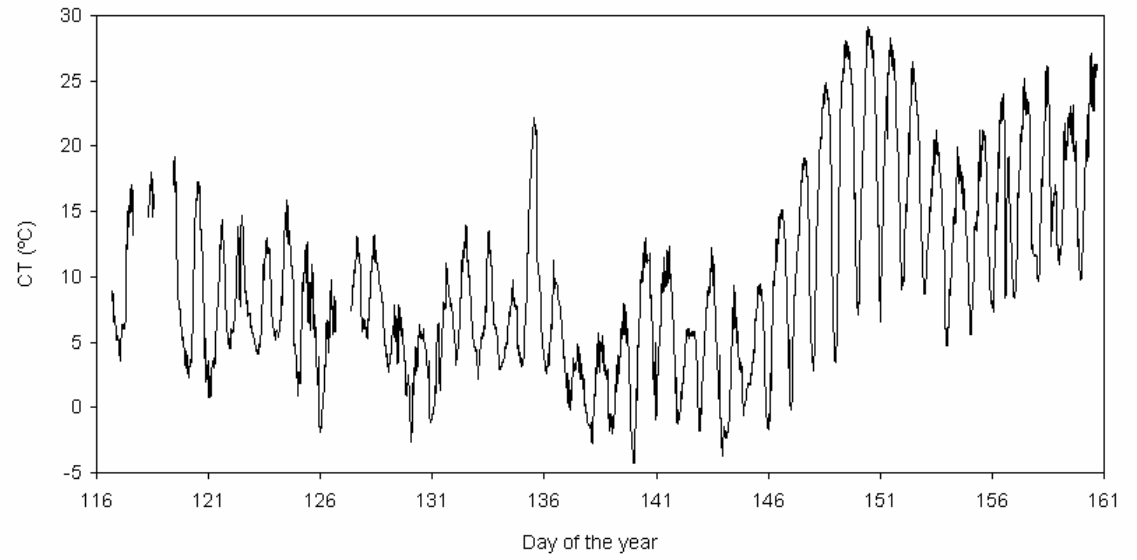

Figure 4.11. Canopy temperature (CT) from April 26th to June 9th.

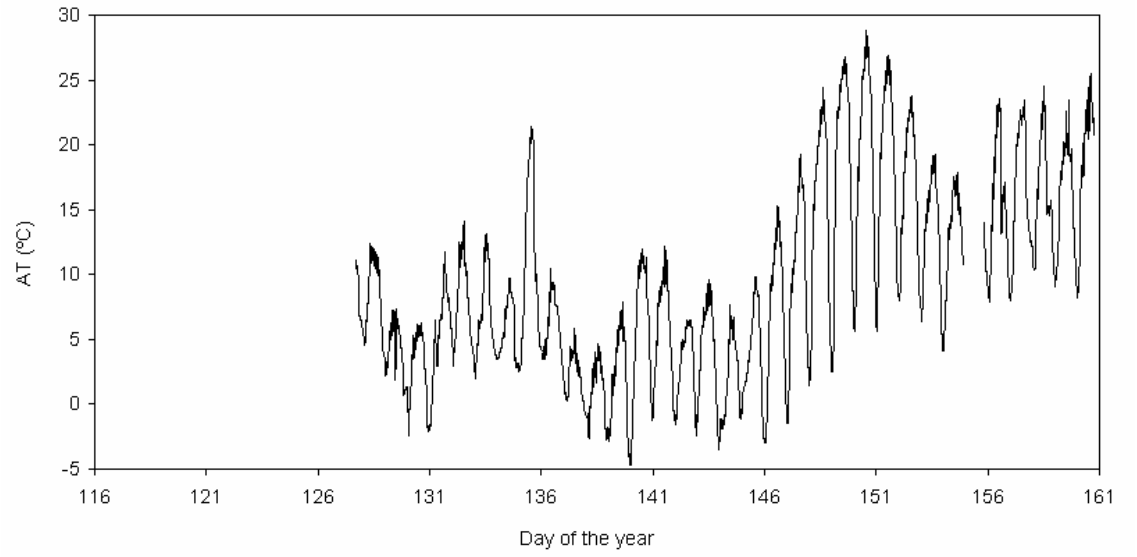

Figure 4.12. Air temperature (AT) from May 7th to June 9th.

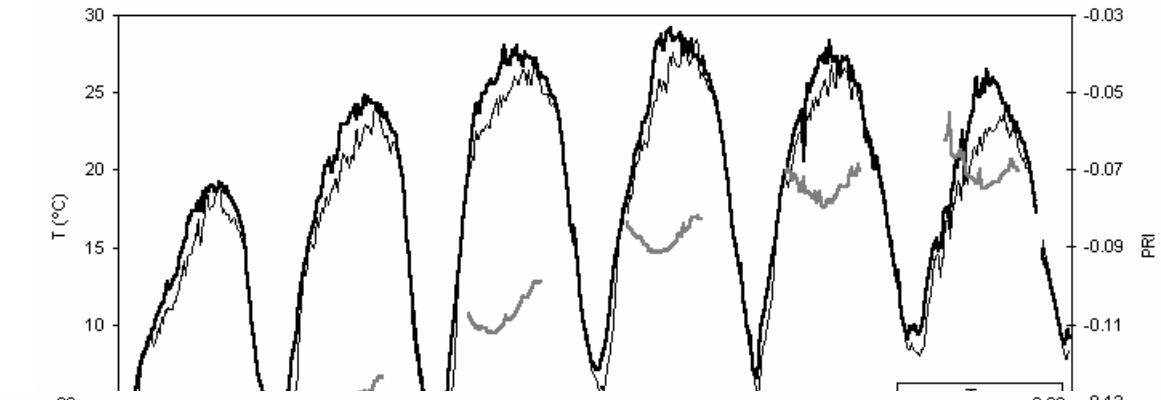
T (°C)
PRI

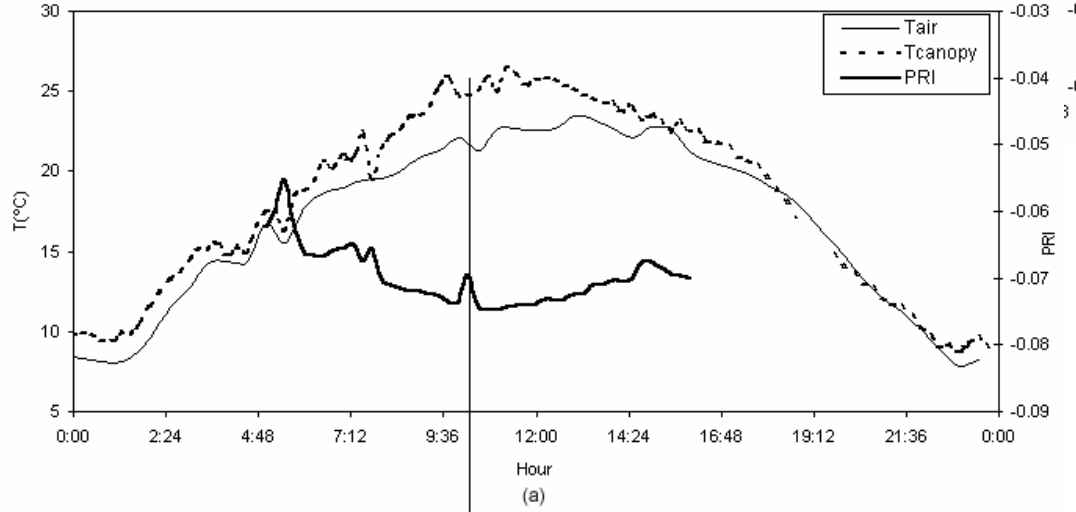
Tair
Tcanopy
PRI
T(°C)
PRI
Hour
(a)

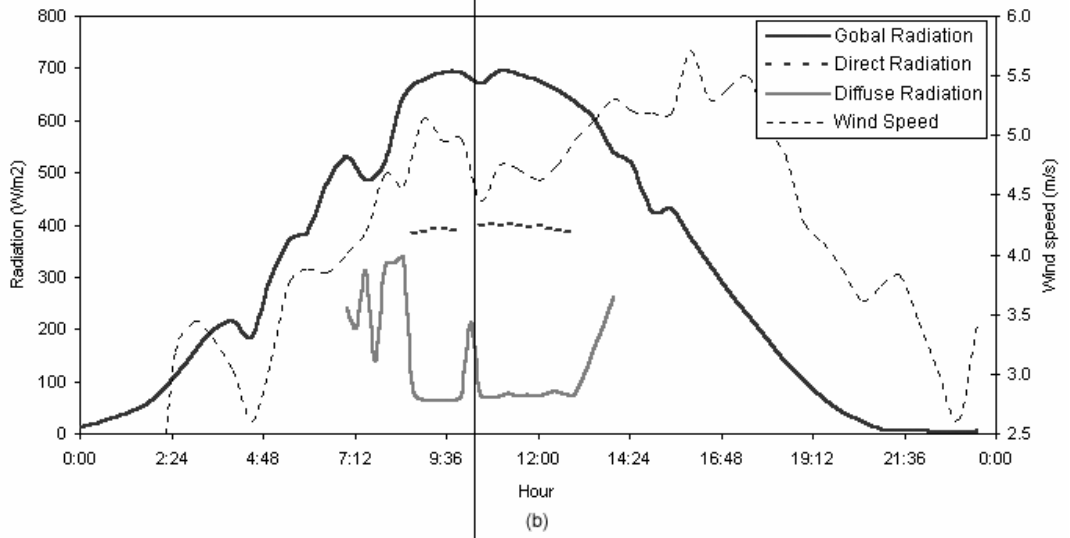
Gobal Radiation
Direct Radiation
Diffuse Radiation
Wind Speed
Radiation (W/m2)
Wind speed (m/s)
Hour
(b)

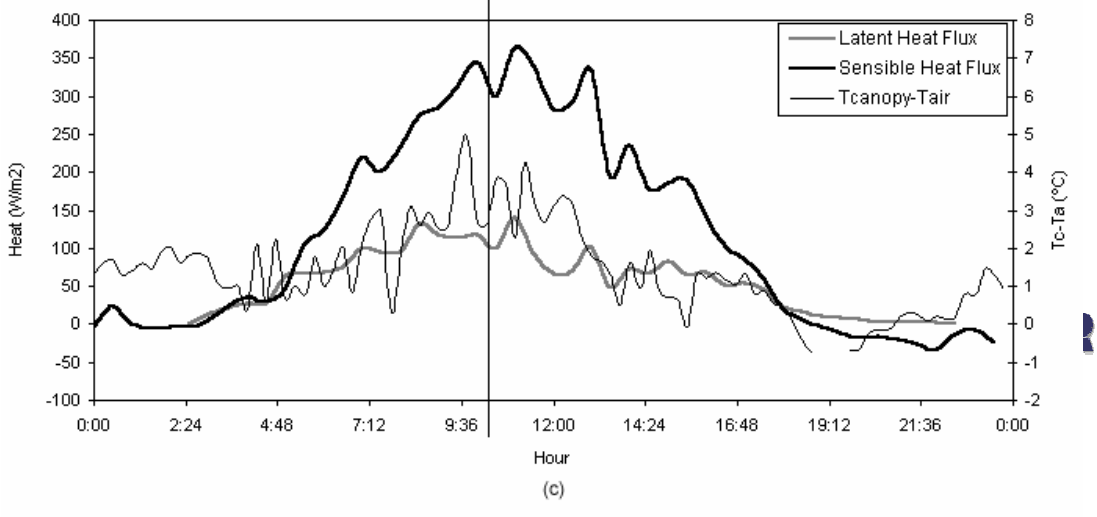
Latent Heat Flux
Sensible Heat Flux
Tcanopy-Tair
Heat (W/m2)
Tc-Ta (°C)
Hour
(c)

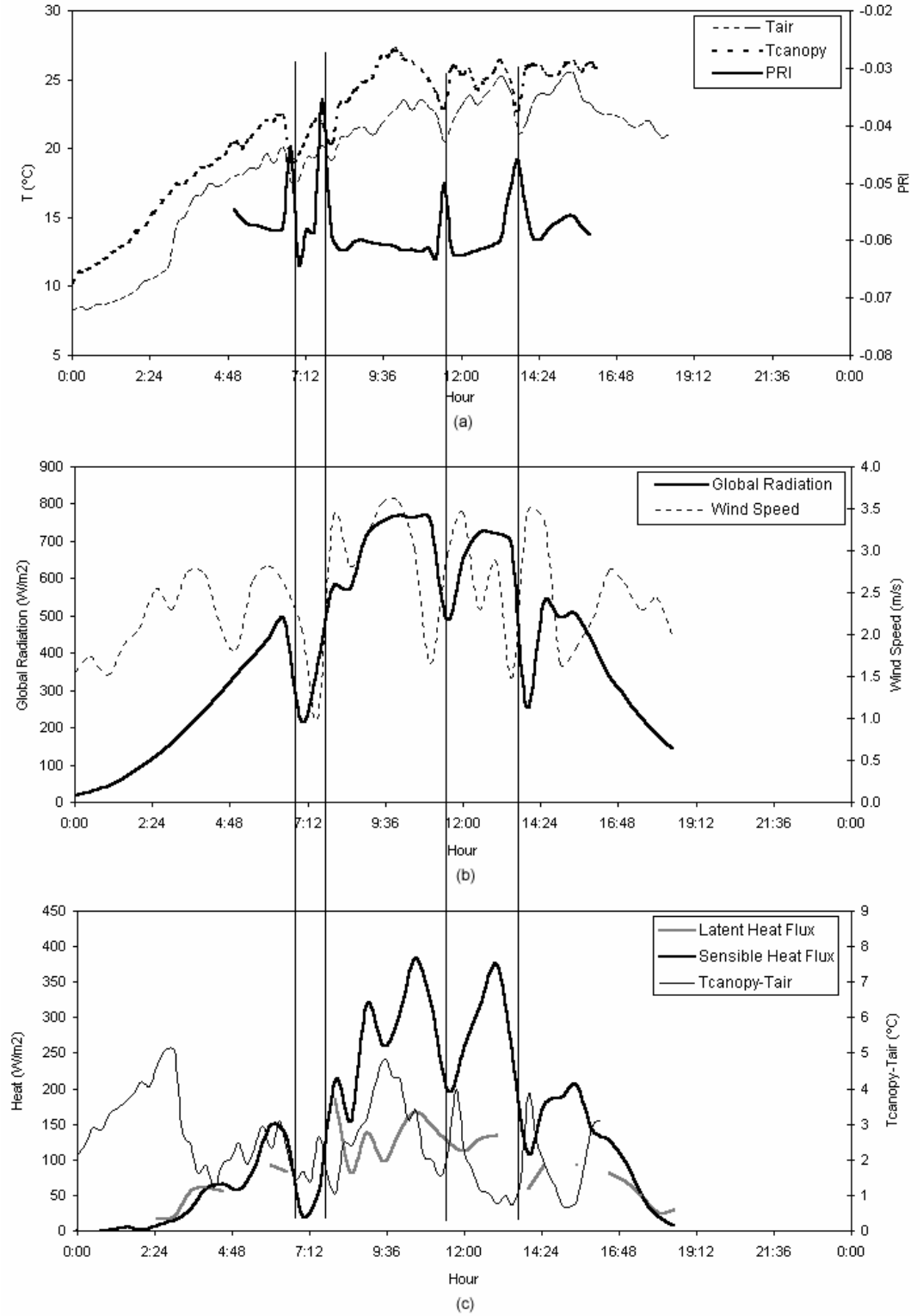

Figure 4.15. Data comparison for June 9th, where (a) shows CT, AT, and PRI; (b) global radiation, and wind speed in the secondary axis; and (c) shows latent and sensible heat fluxes, and canopy-air temperature difference in the secondary axis.

4.2.4 CONCLUSIONS

Radiometric data within 10.5-11.5 μm (CE 312 channel 3) was used to achieve a high accuracy in the CT retrieval. For this end, radiosoundings data and the MODTRAN 4 radiative transfer code were used together in order to estimate the downwelling sky radiance. The emissivity was accurately measured with the box method in laboratory and the average value obtained was 0.973 ± 0.002. CT was determined with an average error of ± 0.4 K introducing the data into (1).

The comparative analysis between temperature and fluorescence magnitudes indicates the possible existence of a relationship that could help to improve the knowledge of the fluorescence processes. There is an inverse correlation between PRI and canopy temperature, solar illumination conditions and sensible heat flux.

4.3 SPECTRORADIOMETRIC MEASUREMENTS IN SUPPORT OF FLUORESCENCE INTERPRETATION IN SIFLEX

4.3.1 OBJECTIVES

The main objective of the reflectance measurements was to support those of the fluorescence measurements, in order to determine different parameters of the vegetation, thus obtaining a broader picture of the status of the trees.

In particular: effects on reflectance values around the red-edge (two peaks of fluorescence) and PRI (xantophyll cycle, role of different pigments, spectral detectability of pigment changes).

Besides, other bio-physiological parameters of the forest can be extracted, and afterwards they can be included in different radiative transfer models. A secondary objective was to measure the dependency of the forest spectra on the observation angle.

To accomplish these objectives, an ASD FieldSpec Pro FR Spectroradiometer was used for these measurements.

4.3.2 STRATEGY

Basically the measurements took place at various times along the day, allowing characterising the daily variation of the spectral signature of the forest, repeating this pattern every day, to follow the fenological evolution of the trees.

All the reflectance measurements were always linked to those of fluorescence. The spectroradiometer was always pointing to the same target than the fluorescence sensor.

During the last week of the campaign, a pair of digital cameras was mounted on the same support of the radiometer to reconstruct the three-dimensional structure of the forest below by means of stereovision.

4.3.3 DESCRIPTION OF THE INSTRUMENT

The FieldSpec Pro is a highly portable, general-purpose spectroradiometer. A fiber optic bundle is used for light collection. Inside the instrument, light is projected from the fiber optics onto a holographic diffraction grating where the wavelength components are separated and reflected for independent measurement by the detectors. The response of each detector is digitized to 16-bit precision.

The Visible/Near Infrared (VNIR) portion of the spectrum, the 350-1050 nanometer wavelength domain, is measured by a 512-channel silicon photodiode array. Each channel is geometrically positioned to receive light within a narrow (1.4 nm) bandwidth. The VNIR spectrometer has a spectral resolution (FWHM of a single emission line) of approximately 3 nm at around 700 nm.

The Short-Wave Infrared (SWIR) portion of the spectrum is acquired with two scanning spectrometers. These differ from the array used in the VNIR in that they measure wavelengths sequentially, rather than simultaneously. Each spectrometer consists of a concave holographic grating and a single thermoelectrically cooled indium gallium arsenide (InGaAs) detector. The gratings are mounted about a common shaft, which oscillates with a period of about 200 milliseconds (100 ms/scan). Unlike the VNIR, each SWIR spectrometer has only one detector, which is exposed to different wavelengths of light as the grating oscillates. The first spectrometer (SWIR1) measures light between about 900 – 1850 nm; the second (SWIR2) covers the region between about 1700 – 2500 nm. The sampling interval for each SWIR region is about 2 nm, and the spectral resolution varies between 10 nm and 12 nm, depending on the scan angle at that wavelength.

Light may be collected with a bare fiber optic, with a field of view (FOV) of

25º, or with the use of fore-optic devices, that provide FOV of 8º or 1º, and Remote Cosine Receptors (RCR) for full-hemisphere albedo measurements.

4.3.4 MAIN SUPPORT MEASUREMENTS

At the measurement coordination meeting that took place on site at the beginning of the campaign, a core time for measurements was set, from 10am to 4pm at which all instruments should be measuring. For automatic instruments the measurements should go as long as the meteorological conditions made it possible. Also, it was decided to try to extend the measurements whenever possible. In the case of the ASD, it was manually operated, and measurements went nominally from 10am to 4pm, although the measurements were subjected to weather conditions and manpower availability.

During the first week a series of test measurements were conducted on site to set the best measurement protocol. The conclusion was to use the 1º fore-optic, as it is the closest to the 4º FOV of the fluorescence instrument. The radiometric measurements were to be taken every 15 minutes during core time. Each acquisition consisted on alternate radiometric measurements of the white reference (Spectralon) and the target (forest), starting and ending with the reference, as well as in between of the three target measurements; in order to make sure that any changes in the illumination conditions between target acquisitions were registered.

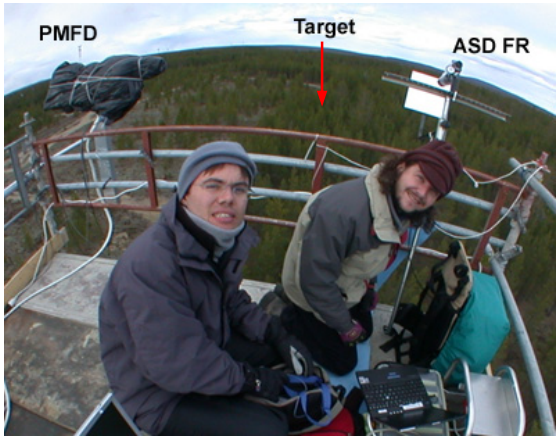

Figure 4.16. Instrument setup at top of the main tower (bottom), and detail of the target measured (top).

Thus, we end up with the radiance of four references and three targets every 15 minutes during 6 hours, every day. The reflectance of the target will be calculated from these measurements during post-processing.

For the secondary objective, angular measurements were taken several times, under clear sky at different times of the day. The 1º and the 8º FOV fore-optics were used. The angular interval ranged from 70º below the horizon, up to 90º above the horizon (zenith), using 5º increments. The measurements were taken in the 15 minutes interval between the main measurements, when the conditions were appropiate, and lasted about 10 minutes. The lack of an optimum setup for these measurements restricted the measurements to be taken always in the same azimuthal plane, the need of a clear sky to avoid illumination variations during the measurement period and the fact that the fore-optics needed to be interchanged made these measurements difficult to carry out, thus they were not performed as often as desired. In any case, the main angular measurements were taken, including measurements in the solar principal plane.

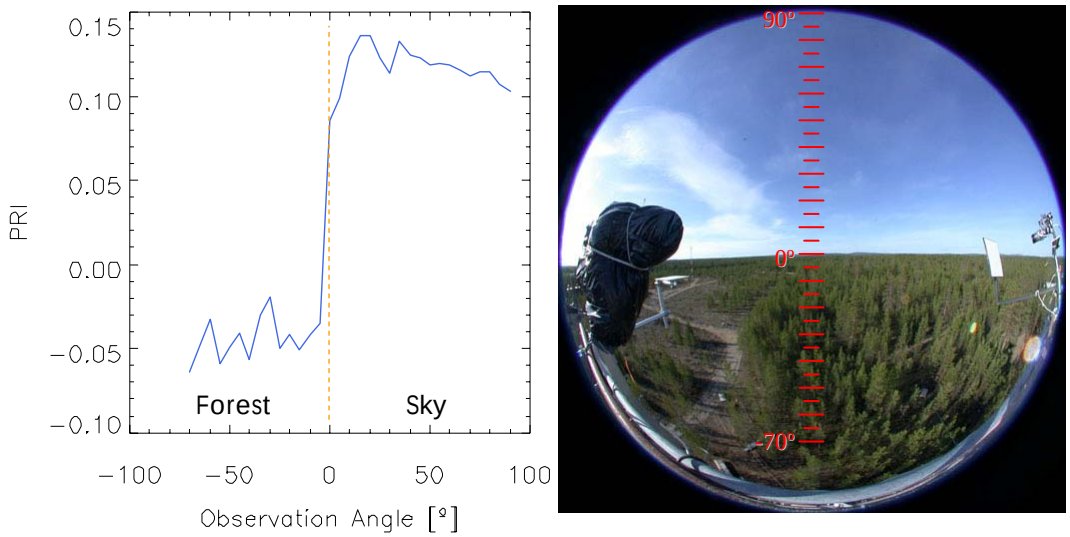

Figure 4.17. Angular measurements from the tower, corresponding to the 31st of May. PRI derived from the reflectance measurements (left). A hemispherical picture (right) helps to interpret the results, in this case, the saw-like form of the PRI is related to the sun/shadow portions of the forest canopy.

4.3.5 COMPLEMENTARY MEASUREMENTS

Besides the main experiment, some other measurements were designed during the campaign to answer some questions that arose as the team discussed on preliminary results.
These issues were:

- The orientation of the Spectralon was in an almost vertical position, similar to the apparent surface of the forest canopy, whereas the white reference used for the PMFD was placed horizontally. Some measurements were carried out to try to estimate the difference on the measurements using both vertical and horizontal orientations of the reference.

- The white reference used for the PMFD was not standard and it was measured against the Spectralon in order to know its spectral response. It was found that the reflectance of the panel in the spectral region of interest was about 80% and almost constant.

- The FIPAM was measuring fluorescence at shoot level, and the ASD was used in two occasions to measure simultaneously the same shoot. Trees surrounded the target and the shadows prevented the measurements during long runs. Thus the measurements took place at 4 seconds intervals during sets of about 20 minutes.

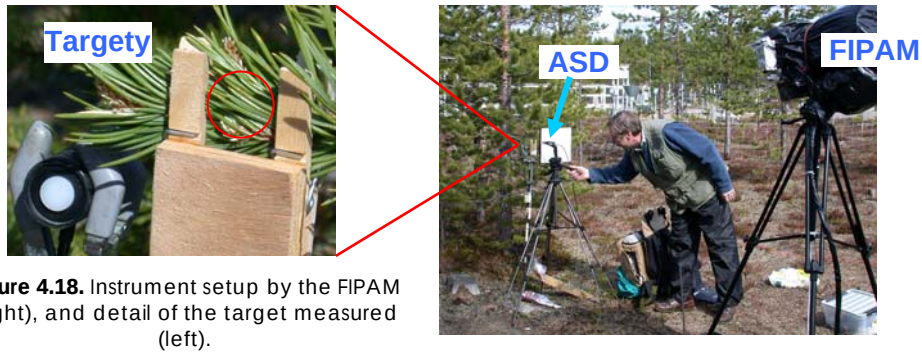

Figure 4.18. Instrument setup by the FIPAM (right), and detail of the target measured (left).

- A comparison of the global irradiance measured using the Licor 1800 and the ASD FS-FR with the RCR fore optic was done. The results show good agreement of the measurements. Global irradiance measurements were made sporadically from the top of the main tower, using the RCR foreoptics in between takes of the main experiment as complement to the standard global irradiance measurement being taken with the Licor 1800 from the 17m tower.

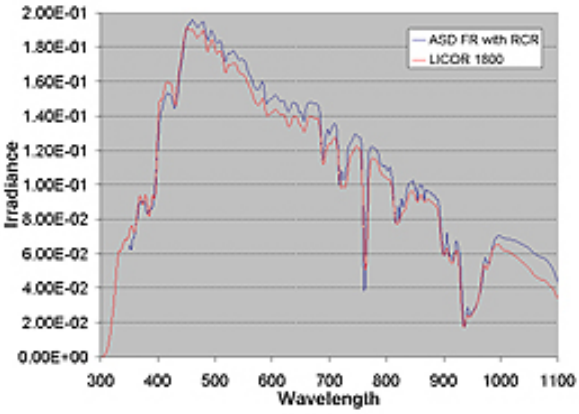

Figure 4.19. Comparison of global irradiance measurements using the LICOR 1800 and the ASD FS-FR in the VIS/NIR spectral range.

- The forest structure is very complex, and the contribution of the light reflected within the forest to the illumination of the target could be non-negligible. In order to characterise the light within the forest a set of measurements were conducted: at each platform of the main tower, measurements were taken of the global irradiance, pointing the RCR

fore-optic towards west, south and east; and at ground level, level 6 and top level also towards north; also at the top, sky global irradiance was measured.

It was conducted several times, at different times of the day and under different sky conditions.

This experiment was conducted once in coordination with the Solar Radiation Group.

Later, a similar experiment was conducted several times under different illumination conditions climbing to a ladder attached to one of the target trees, at different heights. Also, once in coordination with the Solar Radiation Group.

Figure 4.20. Global Irradiance measurements inside the forest at different heights.

- Measurements of the ground and the understorey at the test area were taken. These measurements were performed regularly by the FMI team, but as their instrument's spectral range is limited to the VNIR measurement, with the ASD FR were taken exceptionally. A comparison of instruments with FMI's ASD PSII and U.V. ASD FR was carried out.

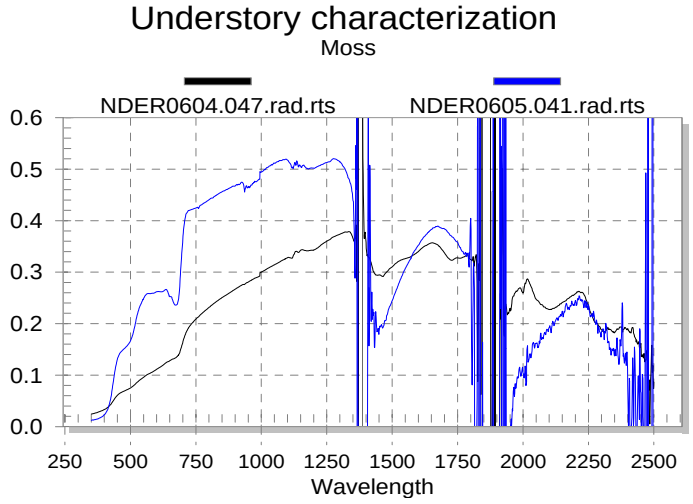

Figure 4.21. Understory reflectance measurements. Comparison of moss reflectance: under dry (black line) and wet (blue) conditions.

- The Solar Radiation Group requested measurements of the forest's albedo. For that purpose we used the RCR fore-optic, covered with a cap that limited the light being collected to half a hemisphere (instead of the standard full hemisphere). This way, pointing straight down from the tower top we were able to collect juts light coming from the forest and avoiding the light coming from the tower. The acquisitions from the north side, together with the one from the south side, make an albedo

measurement of a complete hemisphere. To check the validity of the method we carried out the same time of measurement pointing to the sky, and right after we took a measurement of the complete sky hemisphere taking off the cap from the RCR optic. The addition of the irradiance of both half hemispheres gave almost exactly the same

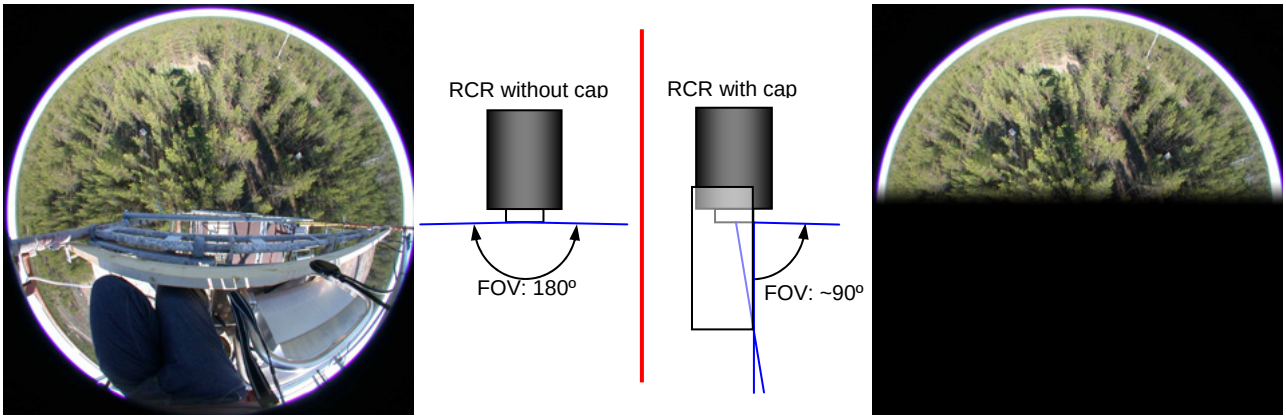

Figure 4.22. Diagram of the RCR fore-optic for the albedo measurements. The pictures show the area viewed by the sensor without (left) and with the cap on (right). The cap was painted jet-black, with a very low reflectance in all the spectral range of the ASD FS-FR.

values as the measured global irradiance.

- Under the request of Ismael Moya, the ASD spectroradiometer was setup and used to measure induced fluorescence of pine needles taken from the same branches as the samples taken for chemical analysis. The setup was located indoors, in a dark room. The bare fiberoptic was placed at 2cm of the samples. The samples were exited using a HeNe laser, and a filter placed before the fiberoptic in order to remove the laser from the signal being measured. The samples had been kept in darkness so at the moment of the measurement they were already dark-adapted. Measurements of this kind were performed once a week, during the last three weeks.

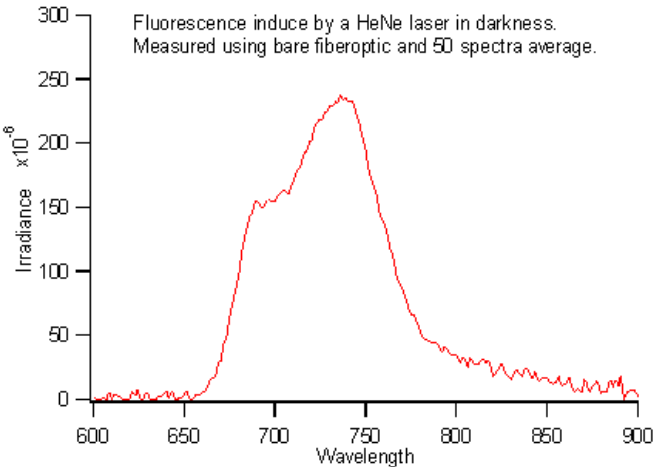

Figure 4.23. Fluorescence emission measured with the ASD FS-FR set up as fluorimeter.

4.3.6 ADDITIONAL MEASUREMENTS

During the main experiment, sky photos were taken using a fish-eye lens attached to a digital camera lends for that purpose by the LURE team. The camera was setup at the top of the main tower on a tripod. Pictures were taken every 5 minutes if the sky conditions were variable, and every 15 minutes (simultaneous to the spectroradiometric measurement) if the sky was evolving slowly.

Besides, for the characterisation of the illumination within the forest, pictures were taken using the fish-eye lens pointing in the same direction as the RCR fore-optic.

The fish-eye lens with the digital camera was also used to take pictures of the forest partial cover. The camera was placed on the ground pointing to zenith, oriented so the bottom of the picture corresponds always to the north direction. These images were taken at the test area (shown in the diagram below), from the stations (12) designed for sampling. Measurements took place under clear sky and under overcast sky. These pictures will be processed later to estimate fractional cover, clumping and LAI.

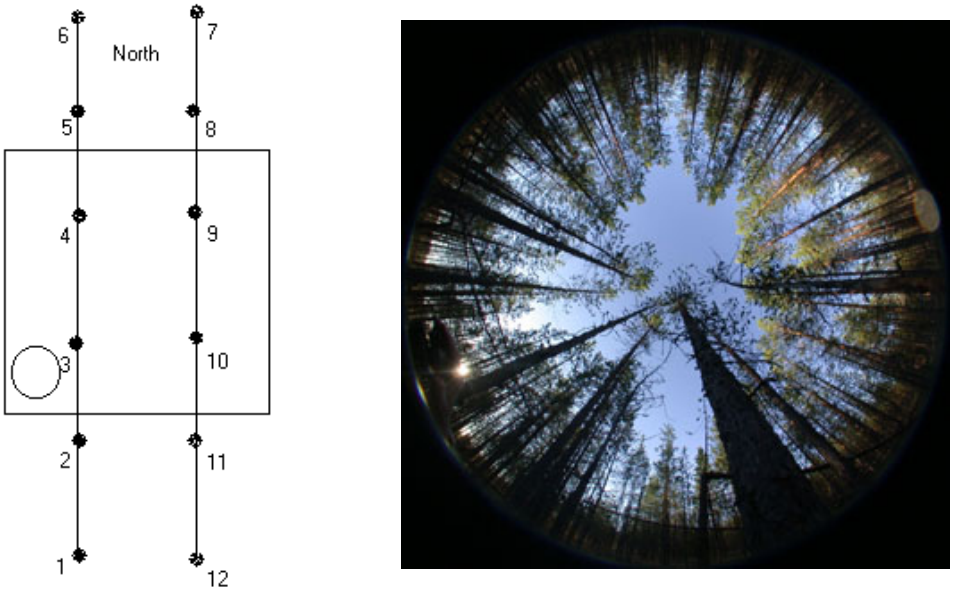

Figure 4.24. Sampling points for the characterization of the test area (left). Hemispherical pictures were taken from these points to measure LAI and clumping.

A more detailed description of the measurements is available in the Data Base together with the corresponding measurements.

Table 4.2. Measurements with the ASD spectroradiometer

Date	Time span of Main measurements	Weather conditions	Additional measurements
04/30	11:05-18:00		
05/01	11:45-12:00	Rainy	
05/02	10:15-16:16	Cloudy, some showers	
05/03	10:35-18:00	Overcast	
05/04	10:20-18:15	Partly clouded	
05/05	10:05-12:30	Partly clouded	
05/06	10:20-18:30	Cloudy	Global Irr. test
05/07	10:00-15:00	Rain	
05/08	10:00-18:15		
05/09			
05/10	10:15-17:00	Overcast	Spectralon test
05/11			Understory
05/12	11:05-12:00	Partly clouded	With FIPAM
05/13			
05/14	10:05-18:45 (5min)	Very cloudy	
05/15			FIPAM
05/16			Fluorimeter Test
05/17		Overcast	Heights Spectralon test
05/18			Fluorimeter Test
05/19	11:15-16:15	Overcast to partly clouded	Heights Glob Irr at test site
05/20	10:30-16:45	Partly clouded	
05/21	10:40-16:00.	Partly clouded	Angular
05/22			Fluorimeter
05/23	10:35-16:15	Sunny	Heights (only three heights). Albedo.
05/24			
05/25	13:00-15:15	Cloudy	
05/26			
05/27	13:00-16:00	Sunny	
05/28	10:35-17:45	Sunny	Albedo and Global Irr. (tower) Heights.
05/30	10:55-18:00	Sunny	Global Irr. (tower)
05/31	11:10-18:00	Sunny	Global Irr. (tower)
06/01	11:15-18:00	Sunny	Global Irr. (tower) Tree Test
06/02		Mainly sunny	Tree Test Understory Global Irr at test site.
06/03		Rainy	
06/04			Understory
06/05			Tree test Understory
06/06	13:05-16:00	Sunny	Angular
06/07	10:50-16:00	Sunny	Angular
06/08			
06/09			Tree test (sun/shadow) Fluorimeter

4.4 ADDITIONAL THERMAL MEASUREMENTS IN SUPPORT OF SIFLEX-2002

4.4.1. INSTRUMENTATION DESCRIPTION

Our objective during the SIFLEX-2002 campaign was the measurement of thermal parameters simultaneously with the measurement of fluorescence instrument. To this end, radiometric measurements were carried out in the thermal infrared region with various instruments that include fixed FOV and single band or multi bands radiometers. In addition, a thermocouple for thermometric temperatures measurements and a black body (calibration source) for calibration purposes were used.

A1) CIMEL 312 radiometer.

The CIMEL 321 description can be seen at 4.2.1.1.

A2) Infrared temperature transducer EVEREST 3000.4ZLC

The Everest thermometer, model 3000.4ZLC single band 8-14 µm collect the infrared radiation from the sample converting it into electrical signal (Figure 4.25). With the suitable calibration process, the electrical signal is converted to a signal in terms of temperature. It is scaled from -40ºC to 100ºC with a resolution of 0.1 K, an accuracy of ±0.5 K and a repeatibility of ±0.1K. The Field of View -FOV- is 4º. With adjustable emissivity equal to unity. The output signal is in mV (10 mV/º), and the power requirements is 5V to 26V DC. Power supply was provided by an auxiliary Einhell power station.

Table 4.3. EVEREST 3000.4ZLC transducer specifications.

Spectral pass-band:	Single band: 8-14 µm
Operating range	from -40º C to 100º C
Accuracy	0.2 K
Field of view	4º
Resolution	±0.5 K
Repeatibility	±0.1 K
Other characteristics	Adjustable emissivity equal to unity (ε=1). Readout Data: Local display and transferable on PC by a Dataloger.

Figure 4.25. EVEREST 3000.4ZLC transducer

Figure 4.26. Rytek model ST8

A3) Infrared radiometer RAYTEK ST8

A portable RAYTEK, model ST8 (Figure 4.26), single band 8-14 µm, with a FOV of 8 degrees, and with adjustable emissivity operation mode was used. It ranges up to 100ºC with a sensitivity of 0.1 K and an accuracy of 0.5K. It has a laser beam that helps to locate the target for the measurements.

A4) Thermocouple Type K.

The temperature measurement of the air surrounding the canopy target is relevant in the study of fluorescence processes and was measured with a thermocouple. This was located at 10 meters high in a tree in the target area and its error is lower than 0.1 ºC.

A5) Calibration source EVEREST 1000

A calibration source EVEREST model 1000 (Figure 4.27) was used to calibrate the radiometers. Its operating range is from 0ºC to 60ºC, with a resolution of 0.1 K, with an absolute accuracy of 0.3 K over entire range. Details of the instruments are given in Table 4.5.

Figure 4.27. Everest model 1000

Table 4.4. Thermal Infrared instrument settings.

MODEL	SPECTRAL BANDS	RANGE OF TEMPERATURE	ACCURACY	FOV
Cimel CE 312	8-13 μm 8.2-9.2 μm 10.3-11.3 μm 11.5-12.5 μm	-80 To 60º C	0.1º C	10º
Everest 3000.4ZLC	8-14 μm	-40 to 100º C	0.5º C	4º
Raytek ST8	8-14 μm	-30 to 100º C	0.5º C	8º
Calibration Source: EVEREST 1000		0 to 60 ºC	0.3º C	

4.4.2. MEASUREMENT PROTOCOLS

Prior to the radiometric measurements, a calibration process was carried out to compare each instrument with the reference blackbody source and the thermocouple (Figure 4.28).

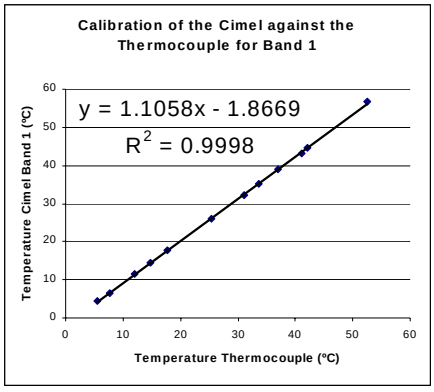

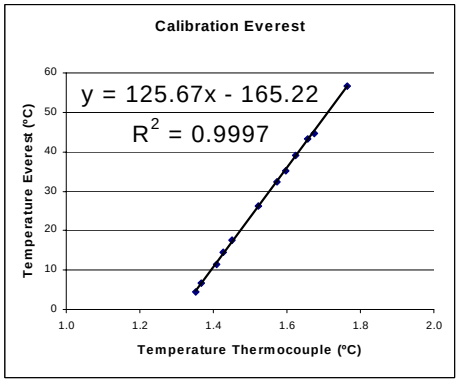

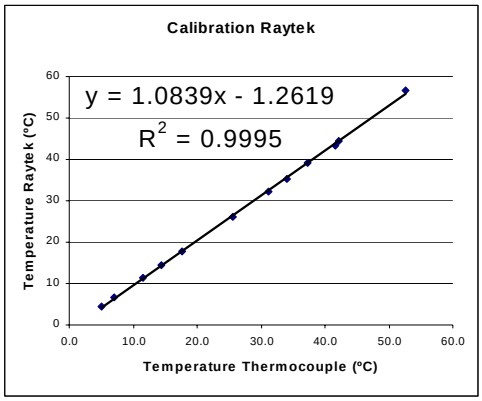

Figure 4.28. Calibration of the different instruments.

4.4.3. EXPERIMENTAL CAMPAIGN DESCRIPTION

The experimental work of the Global Change Unit of the University of Valencia was the measurement of thermal radiometric temperatures, emissivities, atmospheric radiances, air temperature, temperature transects and angular measurements within the Tähtelä area (see Table 4.6). File *Cimel-2_Readme.txt* indicate the different types of files on the Cimel-2 Database. All these data are available in the SIFLEX database (SIFLEX-2002 CD-ROM).

Table 4.5. Field work developed by Global Change Unit during SIFLEX-2002 with the CIMEL 312, EVEREST radiometers and the thermocouple.

Date	Sample	Work	Instrument
28/04/2002 to 06/05/2002	Pine (pine branches, trunk, soil)	-Brightness temperature at 15º -Sky temperature at nadir	A1, A2, A5
07/05/2002 to 19/05/2002	Pine (pine branches, trunk, soil)	Angular measurements	A1, A2, A4, A5
20/05/2002 to 27/05/2002	Target	Simultaneous with passive fluorescence measurements	A1, A2, A4, A5

28/05/2002 to 31/05/2002	Various samples River, grass, asphalt, sand	Transects Angular emissivity	A1, A2, A3, A4, A5
01/06/2002 to 09/06/2002	Target	Simultaneous with passive fluorescence measurements	A1, A2, A4, A5

4.4.3.1 Radiometric temperature measurements simultaneously with passive fluorescence

The CIMEL CE312 four-bands radiometer was used for continuous recording of the surface brightness temperature as a function of time. Temperature measurements were carried out every 10 minutes. The CIMEL was placed at

(a)

(b) (c)

the top of the main tower (20 meters) with a view angle direction of 70º and pointing to the same target as the PMFD (Passive Multiwavelength Fluorescence Detector) instrument (Figure 4.29). During this period of measurement, the EVEREST radiometer was located at the top of the main tower to measure downwelling sky radiance. The effects of cloud periods are evident in the temperature measurements (Figure 4.30).

Figure 4.29. (a) CIMEL 312 radiometer location at the top of the main tower with simultaneous PMFD measurements, (b) target observed by the CIMEL 312, and (c) experimental location of EVEREST.

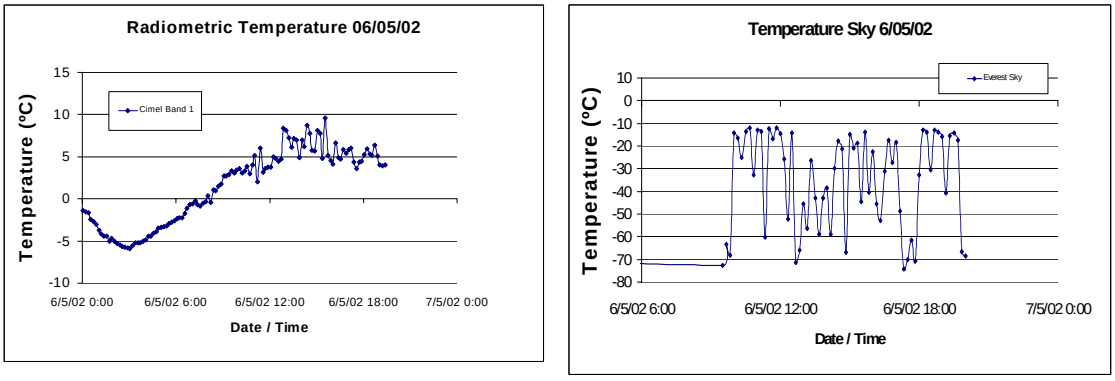

(a) (b)

Figure 4.30. Temporal evolution of the radiometric surface temperature measured with (a) the CIMEL (channel 1) on 6 May 2002 and (b) the corresponding sky temperatures measured at nadir with the EVEREST.

4.4.3.2 Radiometric temperatures for a mixed target

The CIMEL CE312 radiometer radiometer was also located at the 12 meters level of the main tower (20 meters) with a view direction near to nadir (15º) and pointing to a mixed target (pine branches, trunk and soil) (Figure 4.31). Temperature measurements were also carried out every 10 minutes. During this period of measurement, the EVEREST radiometer was located at the top of the main tower to measure downwelling sky radiance.

(a)

(b)

Figure 4.31. Experimental location of (a) CIMEL, and (b) observed target.

Figure 4.32 shows respectively, as an example, the temporal evolution of the radiometric temperature measured in this location during the campaign. It should be noticed that all these data can be find in the database of the SIFLEX campaign.

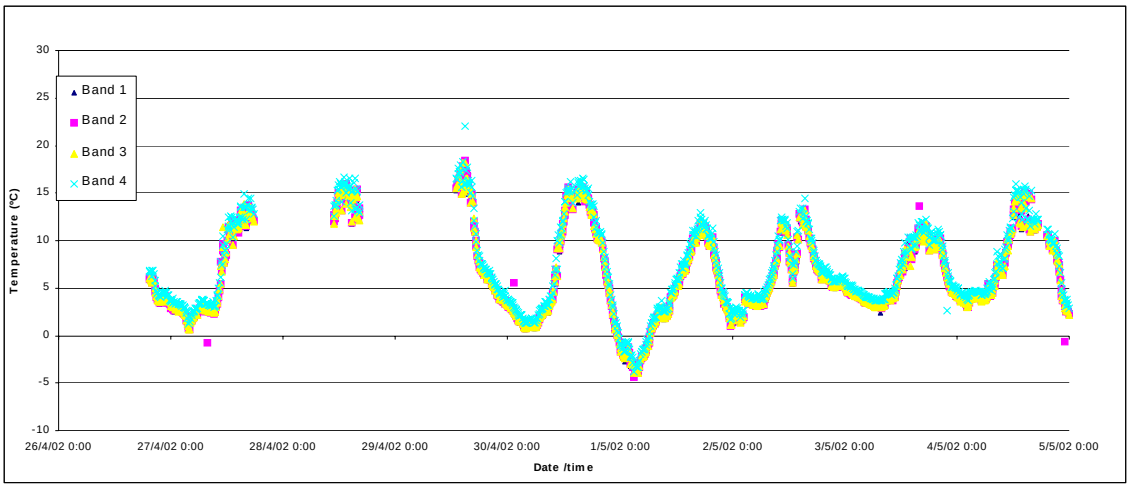

Figure 4.32. Plot of the radiometric temperatures measured with the CIMEL radiometer during the period 27 April to 5 May 2002. The values in the four bands of CIMEL are given.

4.4.3.3 Angular Measurements

Measurements with simultaneous viewing in two directions were also taken. For this purpose, the CIMEL radiometer was placed as before, and the EVEREST radiometer was placed at 10 meters level with a view angle direction of 55º

(see Figure 4.33).

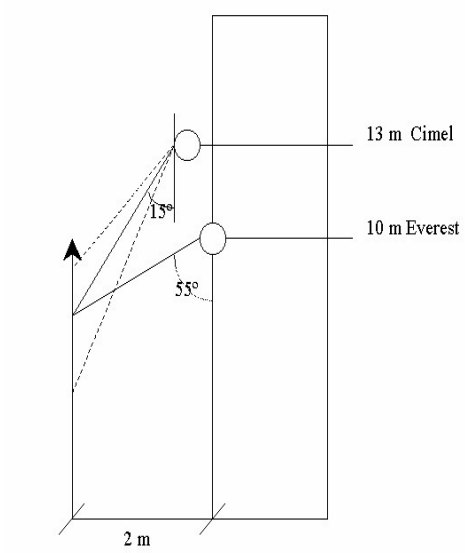

Figure 4.33. Graphical representation of the observation geometry with the CIMEL and EVEREST radiometers.

An example of the comparison between the radiometric temperatures measured at (15º) and 55º are given in Figures 11 and 12.

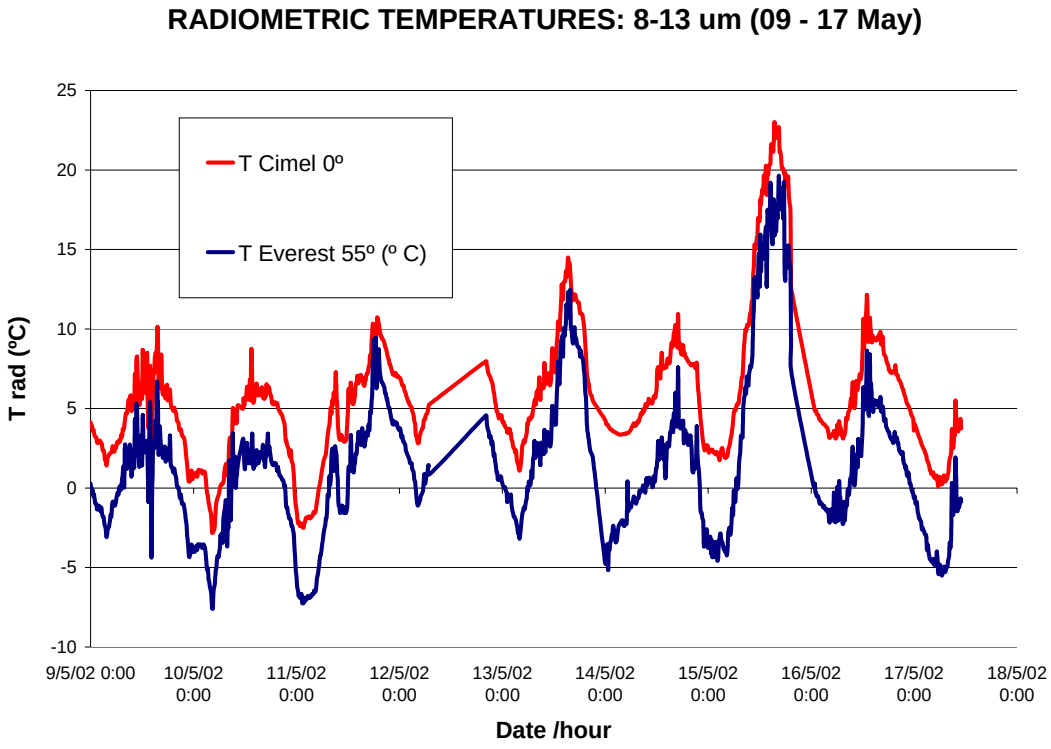

Figure 4.34. Plot of the radiometric temperatures measured at 15º (CIMEL-Channel 1) and at 55º (EVEREST) for 9 to 18 May 2002.

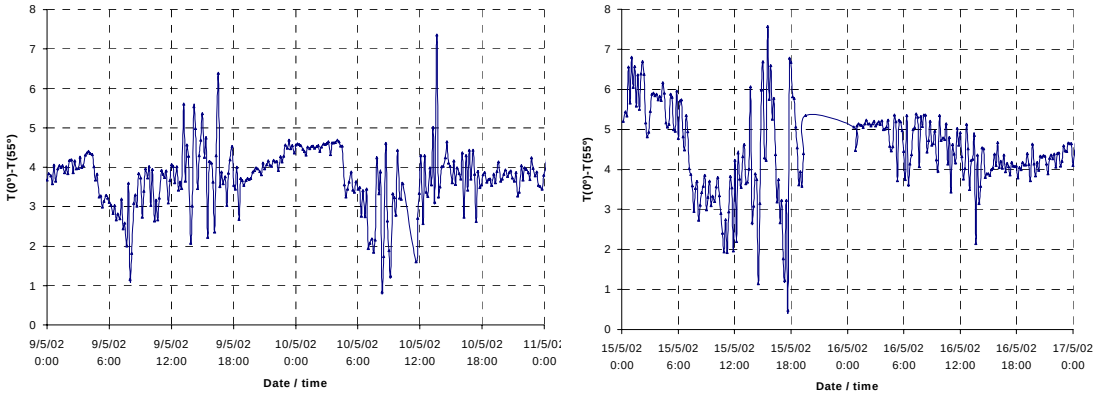

Figure 4.35. Difference between at both radiometric temperatures at 12º and at 55º.

4.4.3.4 Angular variation of relative emissivity

Emissivity has a high impact in the determination of the surface temperature from radiometric measurements. Emissivity measurements were carried out in situ, during the campaing. Due to the high view-angle of the radiometers and its influence on temperature measurements, angular variation of emissivity was also studied. To this end angular radiometric measurements were carried out with the CIMEL and EVEREST radiometers, and a 2 meters bar fixed onto the studied sample, changing the observation angle from 0º to 60º by intervals of 10º. Different surfaces were considered: sand, green grass, gravel, moss and water (Figure 4.36).

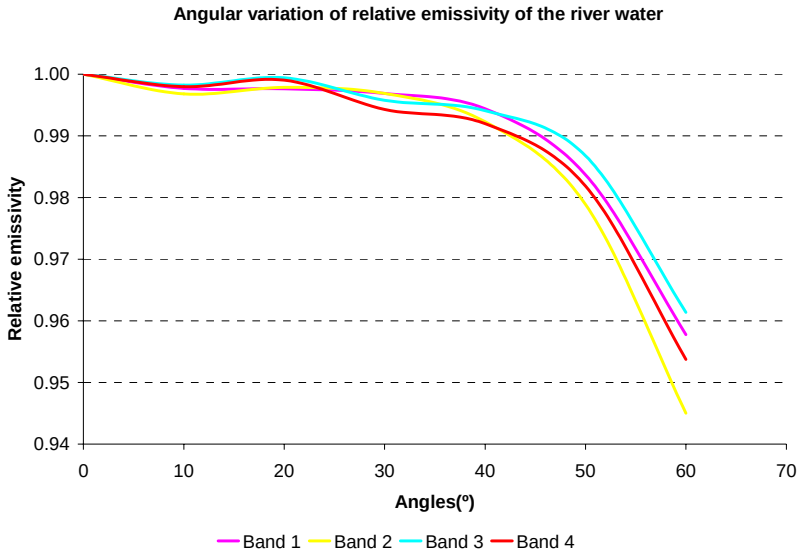

Figure 4.36. Angular variation of relative emissivity measured with the CIMEL. The four CIMEL bands are included.

4.4.3.5 Transects

Temperature transects were performed concurrently to the ENVISAT flights over the Tähtelä region. The transects were carried out taking temperatures measurements with three field radiometers (CIMEL, RYTEK and EVEREST), at regular steps (3 meters) along a walk performed within a well defined area. Different sites were selected for the transects: the river, green grass, dry grass, bushes, asphalt and sand (see Figure 4.37 and 4.38).

Figure 4.37. Temperature transects performed in the field.

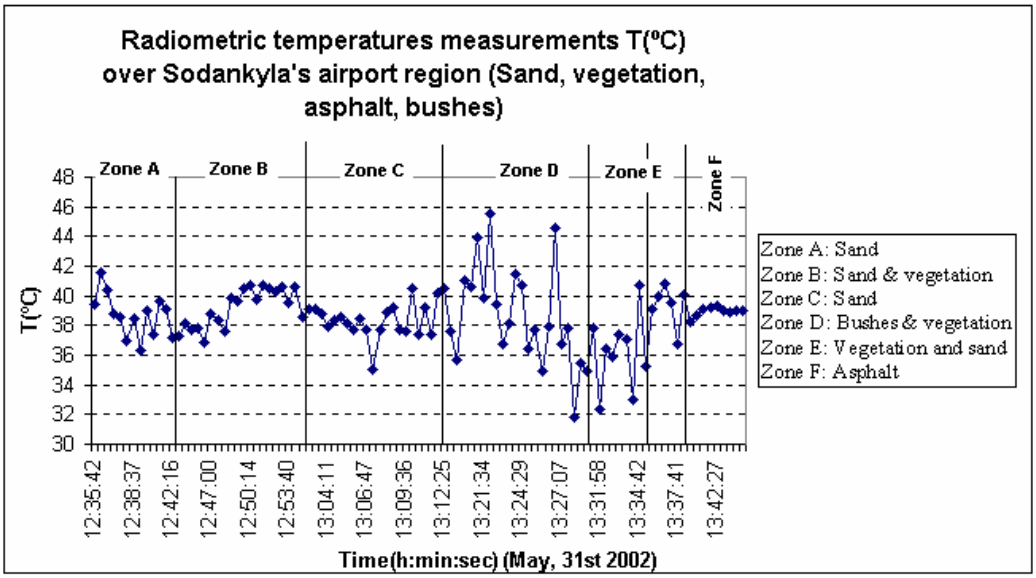

Figure 4.38. Radiometric temperatures for transects over different areas.

4.5 3D-RECONSTRUCTION OF THE FOREST TEST SITE

A detailed three-dimensional reconstruction of the forest structure around the main tower site (25 x 25 m area) was made during the campaign. Different 3D techniques were used in order to obtain the better description of the canopy at the study site:

- Stereo-vision reconstruction.
- Detailed 3D description of the 25 x 25 m study area.
- Sample tree measurements.
- Detailed 3D description of the BDILP tree.

Next we will carry out a detailed description of each one of these points.

4.5.1. STEREO–VISION RECONSTRUCTION

A stereo–vision system was used from the top of the tower to obtain a 3D reconstruction of the field of view of the instruments.

To obtain these pictures two digital cameras were used with a resolution of 1792 x 1200 pixels.

The measurement procedure consisted on the acquisition of some photos from the top of the tower, in order to obtain a 3D reconstruction. More photos were acquired using the zoom of the cameras to see the target tree with more detail. The couples of pictures were taken exactly at the same time, because the two cameras can be shot with the same remote control. Figure 4.39 shows a photo that covers the 25 x 25 m area.

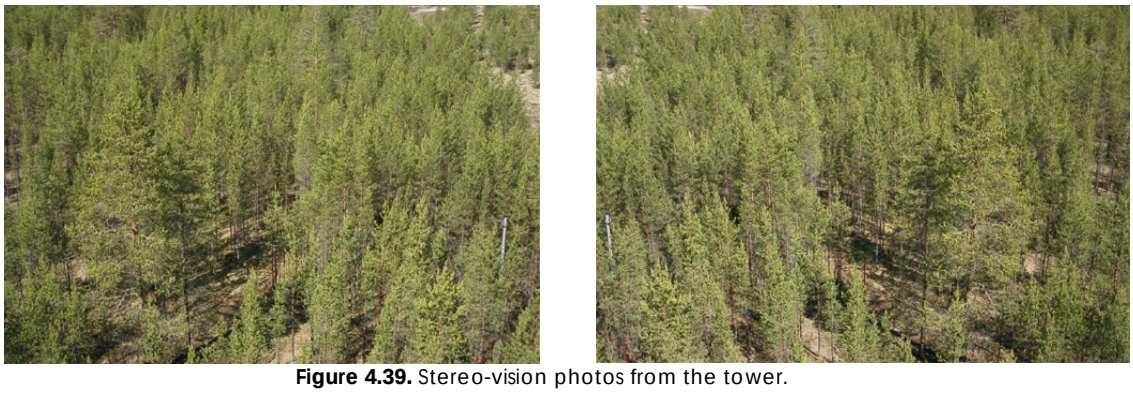

Figure 4.39. Stereo-vision photos from the tower.

The processing of the images neccesary to obtain the digital elevation model of the distances measured from the tower consist in the following steps (Pérez , 1999):

- To calibrate the cameras: determination of the relation between the 2D images and the 3D information of the scene.
- To correlate the images to obtain the correspondences between the two images.
- 3D reconstruction: using the calibration of the cameras and the positions of each point in both images, the 3D co-ordinates in the reference system can be calculated.
- Interpolation: necessary to assign a value to the points that have not any elevation data in the digital elevation model.

4.5.2. DETAILED 3D DESCRIPTION OF THE 25 x 25 M STUDY AREA

These measurements consisted in the elaboration of a map with the positions

of the trees inside the study area (25 x 25m). Moreover, the perimeter of the trunk, the height of the top and the height where the green stems starts (the lower stems usually are dry) was measured for each tree.

To do the measurements the following instruments were used:

- A digital camera RICOH RCD 5300.
- Hand-held laser distance meter DISTO™.

Inside the study area there are more than 600 trees. For this reason we measured the height of about 400 trees, to have sufficient information to estimate statistically the height from the perimeter of the trunk for all the trees.

Using as reference the map with the positions of the trunks, we did a map of the vegetation understory and the soil under the trees. We found 4 different classes that are shown in the map of the figure 4.40.

Inside the areas with moss and bush the density of the plants is multiplied by a factor 10. We suppose liken appears in all the area with the same density. The information can be found in the database and is divided in 8 columns as shown in table 4.6:

Table 4.6. Database of the trees properties.

Column	Description
1	Number of the tree.
2 and 3	Coordinates inside the 25x25m area (referred to the position of the tower).
4	Diameter of the trunk (m).
5	Height (m).
6	Height of the fist green branch (m).
7	Indicates the trees that have been used to make statistics in the calculation of the heights that were not measured.
8	Indicates the trees where the height value has been calculated from the diameter.

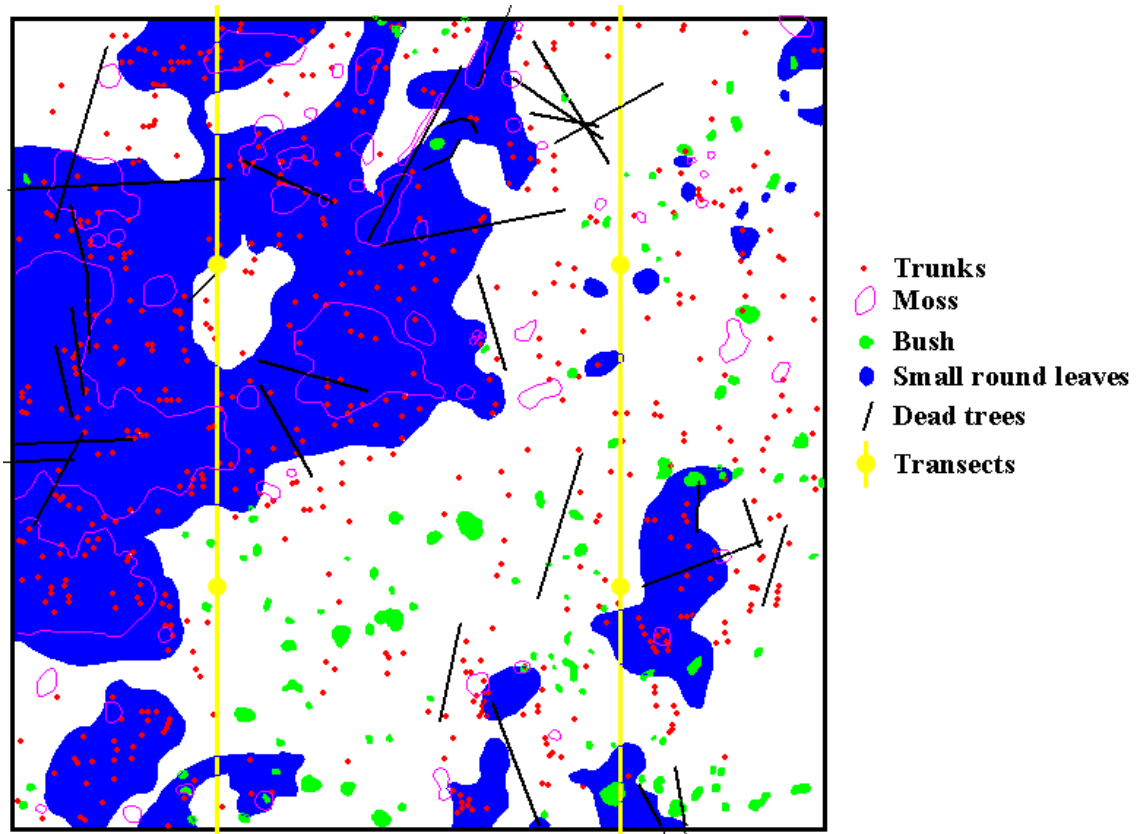

Together with this information, we took photographs that describe the structure of the trees as we can see in figure 4.41. The black folder was used in the pictures like a reference, to do a geometric correction and to be able to measure distances.

4.5.3. SAMPLE TREE MEASUREMENTS.

Moreover, trees 10, 13, and 577 were felled on June 25-27 by FMI, and more properties were measured with detail, in order to have a better description of the trees of the area. Detailed biomass calculations and growth parameters of these sample trees are shown at 2.8.2 (see chapter 2).

4.5.4. DETAILED 3D DESCRIPTION OF THE BDILP TREE

4.5.4.1 Measurement procedure

The BDILP tree is small and isolated, perfect to do a 3D reconstruction with photographs acquired from different angles. Figure 4.42 shows the three views of this tree that will be used to generate the model.

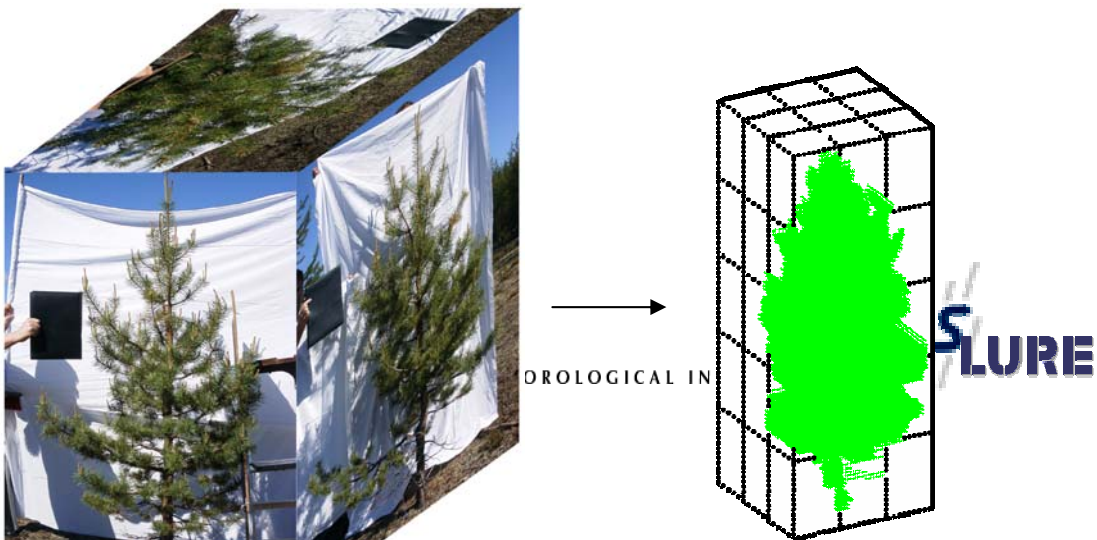

After the acquisition of the photos, they have to be processed before doing the 3D reconstruction (García, 2001).

- The first step is a geometric correction of each image to compensate the distortions and to measure distances directly in the image.
- The second step consists in the classification of the plants and the background. We classify as 1 the pixels corresponding to the plant material and as 0 the background.
- Then we use our software to generate a three dimensional matrix that describes the tree.

With the 3D matrix (shown in figure 4.42), we have measured for this tree a LAI = 1.257. We also have measured the vegetation density distribution in the x, y and z directions. Figure 4.43 shows this result. The integration of each one of these LAI distributions gives the total LAI of the tree. The same procedure can be used to calculate the LAI and distributions of the 25 x 25m study area.

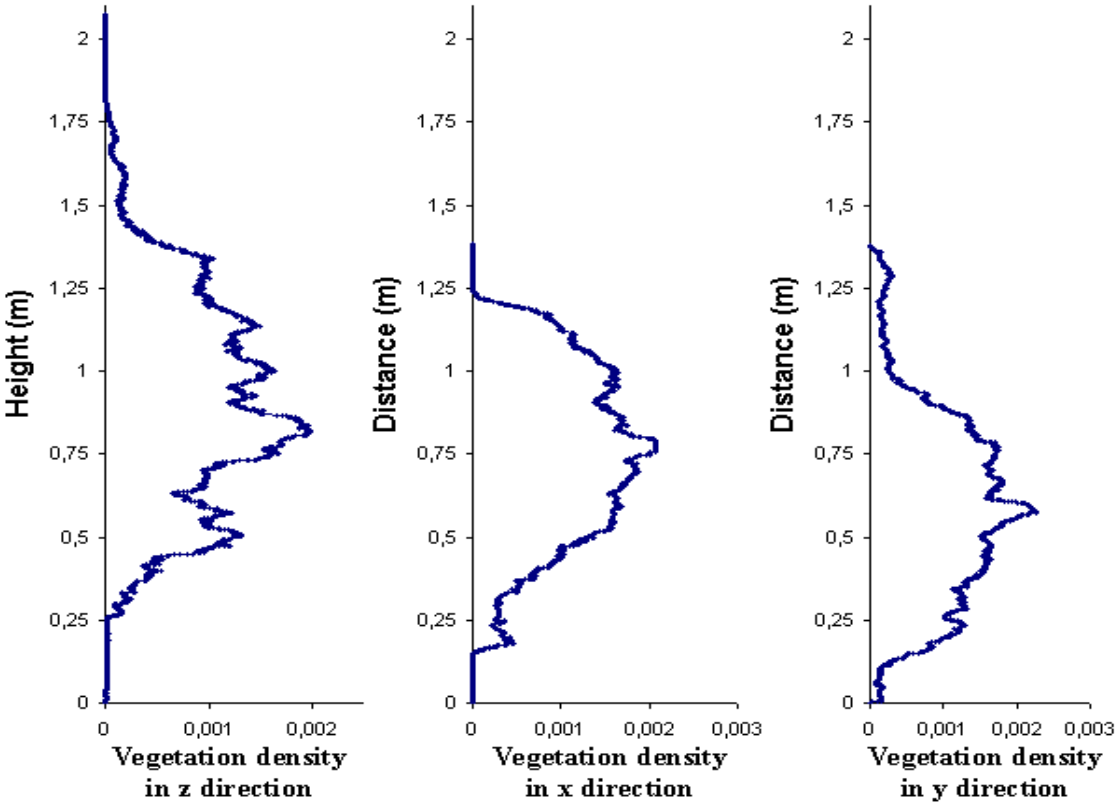

Figure 4.43. Vegetation density distribution in x, y and z directions.

Moreover, stereo-vision photographs (shown in figure 4.44) were acquired for a better description of the tree.

Figure 4.44. Stereo-vision photos of the BDILP tree.

We used two identical digital cameras separated 35 centimetres. The distance from the cameras to the tree was two meters, the same that the distance from the BD instrument to the tree.

From these two images obtained from different angles, we can obtain a three-dimensional model of the tree from the point of view of the BD instrument. With this stereo-vision system we can obtain a digital elevation model with 1mm spatial resolution in the x and y axis, with erros of +/- 10 mm near the centre of the image. Far of the center of the image, appear some distortions due to the lens of the conventional cameras.

4.5.4.2 Conclusions

Using all this information, it will be possible to model the trees with detail and to obtain a 3D scene of the site. Polygons will be used to describe each tree inside the study area, using statistical information extracted from the measurements described before.

Figure 4.45 shows a three dimensional model of the trees obtained using the information that we measured in the field for each tree. This is a first approximation that describes each tree with two cones: one for the trunk and another one for the leaves.

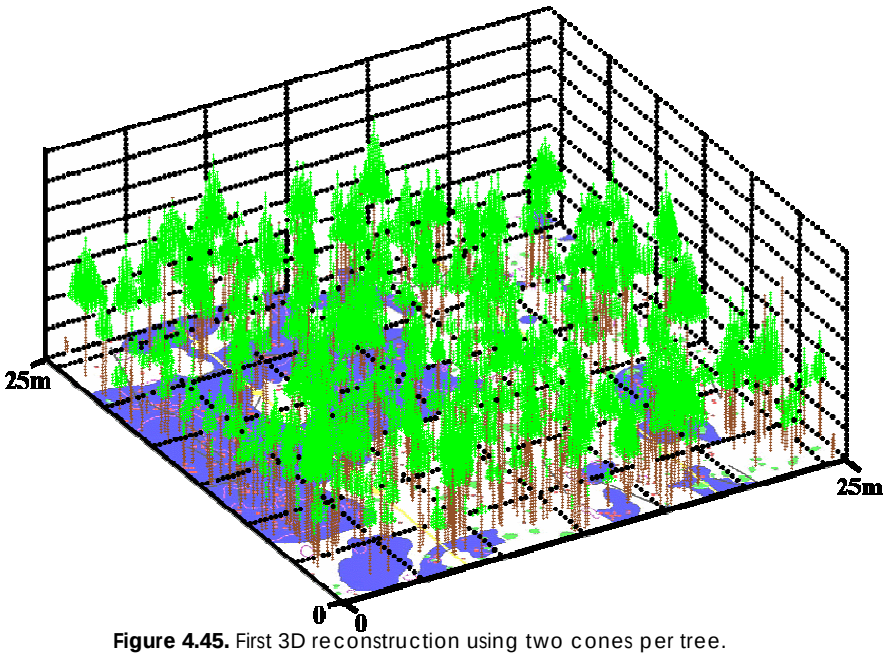

Figure 4.45. First 3D reconstruction using two cones per tree.

With the model we will be able to measure different vegetation properties as Leaf Area Index (LAI), cover percentage, etc. and to study the light propagation through the canopy, studying canopy structural effects with the variation of shadows and solar illumination changes. Althoug still more work is needed for a detailed 3D reconstruction, the current data allow to run canopy reflectance models.

5. Data analysis and integration of results

This chapter presents a preliminary comparison of some conspicuous results obtained during the SIFLEX campaign and intends to discuss it in the frame of the current biophysical and physiological knowledge of the functioning of boreal forest.

- Measured signals with the PMFD from the 20 m tower:
  Irradiance: horizontal spectralon panel (Reference)
  Channels: 760.5, 758.5, 687, 685, 570, 531 nm
  Radiance from the target
  Channels: 760.5, 758.5, 687, 685, 570, 531 nm

- Calculated parameters
  Reflectance at 687 and 760 nm,
  Fluorescence flux at 687 and 760 nm,
  Photosynthetical Reflectance Index (PRI).
  Relative fluorescence "yield" (Fluorescence Flux/reflectance flux at 531 nm)

- Target composed of two individual trees
  Distance of the reference ~ 1 m
  Distance of target ~50 m, zenithal angle 107° azimutal angle ~ 15°
  Temporal resolution 2 s
  Useful measuring period 8:00 to 19:00

- Other measurements
  Pigments (Chls, Carotenoids, Xanthophylls)
  Active fluorescence measurements,
  - Maximal photochemical yield (Fv/Fm = (Fm-Fo)/Fm)
  - Actual photochemical yield ($\Delta F/Fm' = (Fm'-Fs)/Fm'$)
  - Non-photochemical quenching (NPQ = (Fm-Fm')/Fm')
  - Air-needles difference temperature,
  Main CO2 tower
  Meteorological data
  CO2 uptake

5.1 INTRODUCTION

Conifers are the most common evergreen plants in the temperate and sub-arctic northern hemisphere, where freezing temperatures occur regularly and cold acclimation processes are essential to enable plants to withstand periods of very low temperature. Conifers retain their needles for several years and so their photosynthetic apparatus must survive severe freezing periods, often combined with high light, while retaining the capacity for photosynthesis when warmer periods return.

Earlier studies have documented that evergreen conifers of cold climates experience great seasonal changes in photosynthetic activities, exhibiting a gradual decline during late summer and autumn, a strong inhibition during winter and a rapid recovery in early spring. These seasonally induced changes in the rate of net photosynthesis are well correlated with electron transport studies performed in isolated thylakoids isolated from Scots pine (*Pinus sylvestris* L.) and Norway spruce. The autumn and winter induced inhibition of PS2 photochemistry of Scots pine in vivo has been reported to be due to low temperature induced photoinhibition of PS2 accompanied by a loss of the reaction centre D1 protein (Ottender et al. 1995). Plastoquinone (PQ) has also been recognised as a primary site of winter-induced inhibition of electron transport (Oquist and Martin, 1980).

A significant increase of the relative proportion of lipids as well as in the degree of unsaturation of the fatty acids of the lipids has been observed in the thylakoid membranes of conifers chloroplasts (Oquist 1982, plant Physiol, 69: 869-875). Such changes indicate an increase in the membrane fluidity and, as a consequence in the membrane stability at low temperatures in particular.

5.2 PIGMENT ANALYSIS

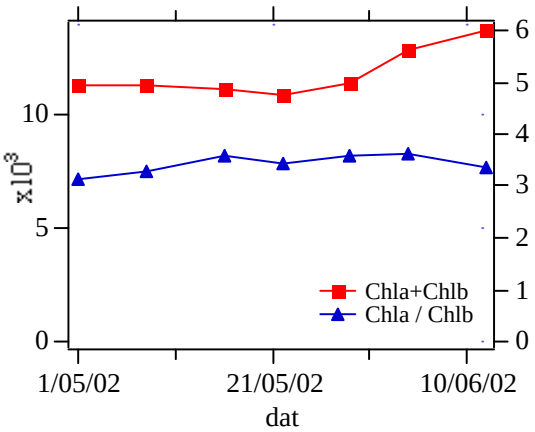

Figure 5.1. Squares: Variation of the total Chl content (Chla+ Chlb) during the measuring period (µg/gFW); Triangles: variation of Chla/Chlb ratio.

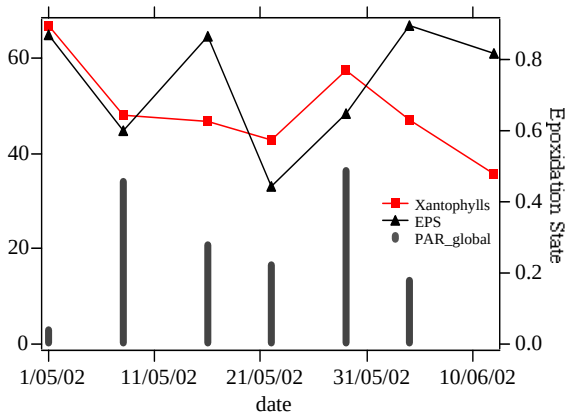

Figure 5. 2. Squares: Variation of the total pool of Xantophylls (Z+V+A) during the measuring period (µg/gFW). Triangles: epoxydation state(EPS=[0.5A+V]/[A+V+Z]). Vertical Bars: averaged PAR

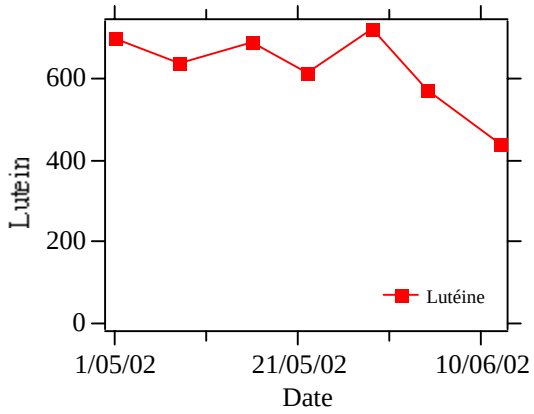

Figure 5.3. Variation of the lutein content during the measuring period (µg/gFW).

The pigment analysis was done on needles collected weekly since 30 April at 10:00 local time in several defined sites. Figure 5.1 shows that the total [Chl] maintains almost constant except a slight increase at the end of the period, whereas the a/b ratio stays stable. This indicates that no major Chl reorganisation takes place during the observation period. Figure 5.2 shows a decrease of the carotenoid pool, more pronounced for the lutein pigment (Figure 5.3). The EPS seems markedly influenced by the illumination before collecting the samples. The illumination effect may be particularly important due to the unusual length of the light period at this high latitude. These findings are in good agreement with data reported in the literature for the boreal forest (Ottender et al.

5.3 ACTIVE FLUORESCENCE MEASUREMENTS

The figures shown bellow summarise the evolution of the chlorophyll fluorescence and temperature parameters under two extreme light conditions, under high light conditions (see Figure 5.4 and Figure 5.5) and under low light conditions (see Figure 5.6 and also Figure 5.7). More details related to these data are presented in legends and also in chapter 3.



FINNISH METEOROLOGICAL INSTITUTE

LURE

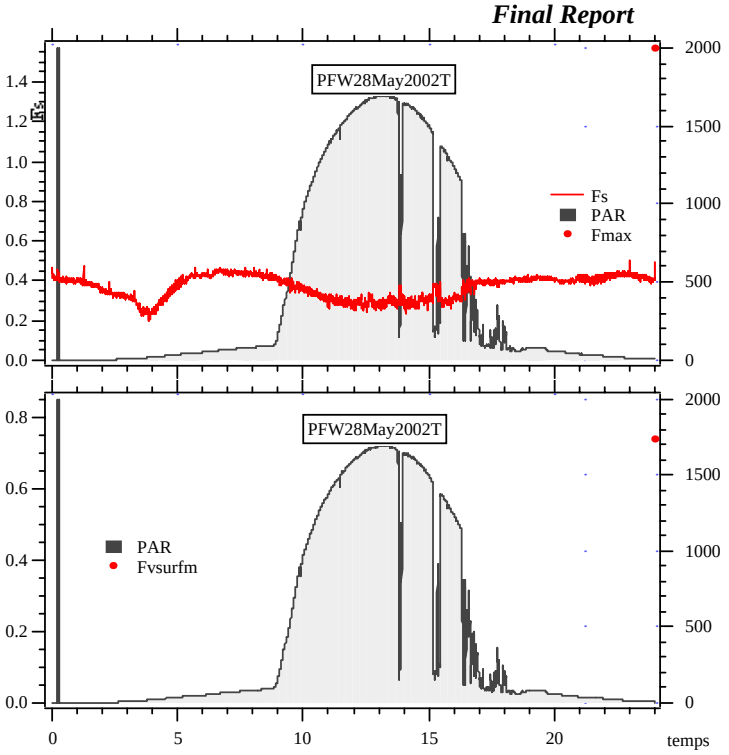

Figure 5.4. High light conditions (May 28th 2002). Diurnal cycle of the Chl fluorescence parameters measured with the FIPAM microlidar. Top.:Stationary (Fs) and maximum (after a saturating pulse, Fmax) fluorescence signal. Incoming irradiance (PAR) is superimposed. Observe the pronounced decrease of both parameters at noon. Bottom: Diurnal evolution of ΔF/Fm' (quantum yield of PS2, allowing to calculate Electron Transfert Rate (ETR), Genty et al. (1989), derived from the same data.

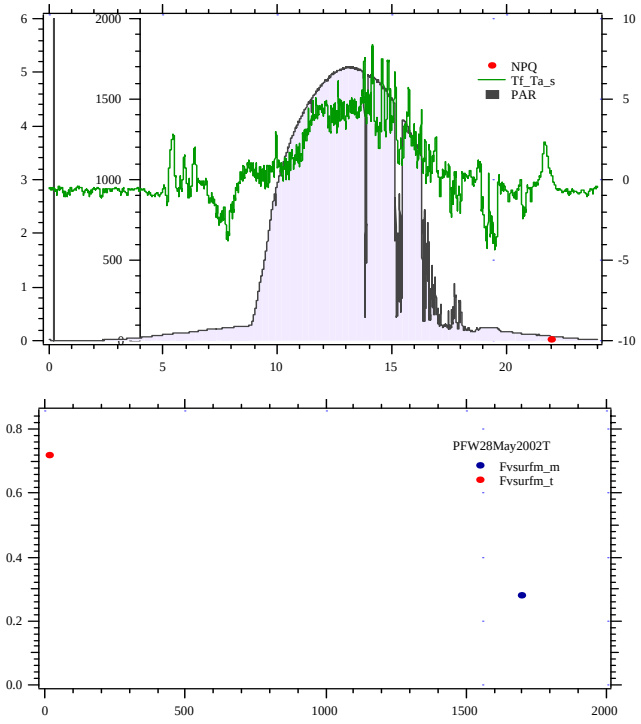

Figure 5.5. High light conditions (May 28th 2002). Diurnal cycle of the Chl fluorescence parameters measured with the FIPAM microlidar.
Top. Squares:NPQ = [(Fm-Fm')/Fm']. Continuous line: difference between needle and air temperatures measured with thermocouples in the same place as fluorescence measurements are done. Note the good correlation with NPQ.
Bottom : Φ(PS2) versus PAR. Red dots correspond to after-noon data. Observe the reduced Φ(PS2) after noon due to the accumulation of NPQ.

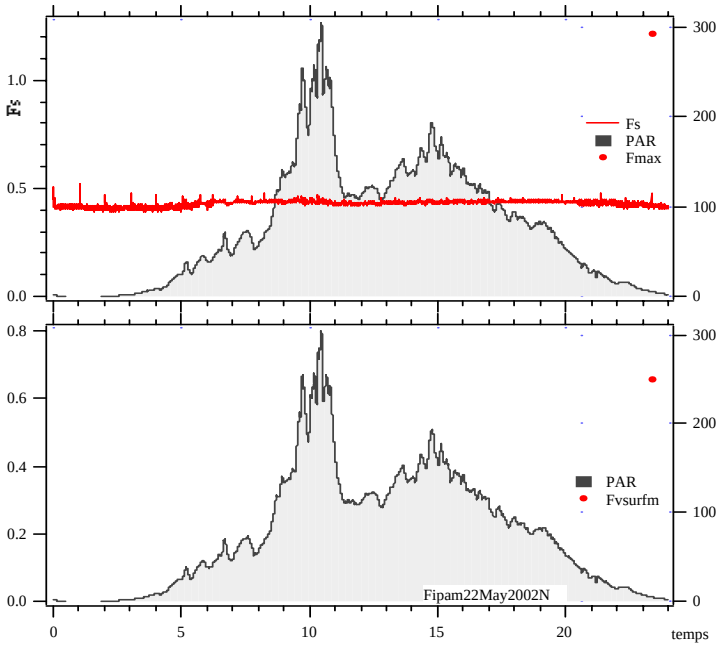

Figure 5.6. Low light conditions (May 22th 2002). Diurnal cycle of the Chl fluorescence parameters measured with the FIPAM microlidar. Top. Stationary (Fs) and maximum (after a saturating pulse, Fmax) fluorescence signal. Incoming irradiance (PAR) is superimposed. Both Fs and Fmax did not decrease at noon due to the low NPQ level.
Bottom. Diurnal evolution of ΔF/Fm' = Φ(PS2), Genty et al. (1989), derived from the same data.

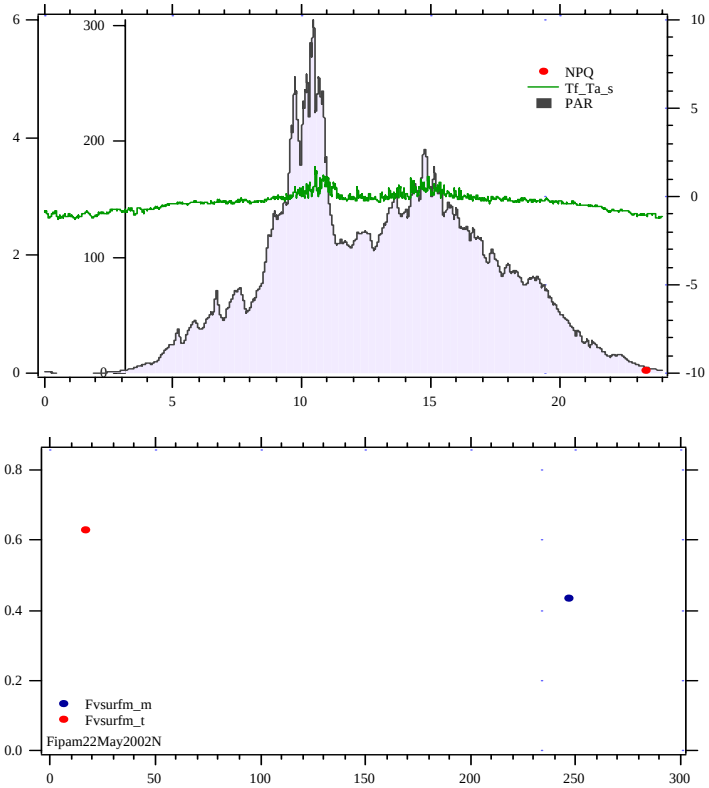

Figure 5.7. Low light conditions (May 22th 2002). Diurnal cycle of the Chl fluorescence parameters measured with the FIPAM microlidar. Top. Squares: NPQ = [(Fm-Fm')/Fm']. Continuous line: difference between needle and air temperatures measured with thermocouples in the same place as fluorescence measurements are done. Note the good correlation with NPQ.
Bottom : PS2 ETR versus PAR. Red dots correspond to after-noon data. No difference is observed between morning and afternoon data in the absence of light constraint.

The measurements performed with the FIPAM in the boreal forest during SIFLEX campaign showed an increasing level of the maximal photochemical yield (Fv/Fm) after the snow melting period, from 0.60 to 0.80 (Figure 5.8A), and hence an increase of the photosynthetic activity. These measurements showed also that the effective photochemical yield (ΔF/Fm') is strongly modulated by the absorbed PAR, and also by the maximal photochemical yield. Indeed, for the same PAR (see circles in Figure 5.8-A), one can see that ΔF/Fm' is increasing as Fv/Fm increases, for both high and low levels of the PAR.

In Figure 5.8-B, the temperature difference between the needles and the air, and the Non-Photochemical Quenching (NPQ) are strongly correlated, as expected, due to the dissipative processes of needles. These variations are also well correlated with PAR variations (see Figure 5.8-A). The NPQ was relatively high during sunny days. Indeed, during these days, the temperature can reach up to 32 °C (see chapter 3).

As shown in Figure 5.8-C, the photosynthetic electrons flux of PSII (Photosystem II) is following the variation of the PAR, and hence is also well correlated with NPQ and the temperature difference between the needles and the air.

In Figure 5.8-D, the stationary fluorescence (Fs) recorded both with the FIPAM and the Laser-PAM showed a good correlation even if the measurements were performed at two different places in the experiment site, on two different trees and two different scale levels of measurement. When comparing the variation of PAR (Figure 5.8-A) and the variation of Fs (Figure 5.8-D), one can see that any increase of the PAR was followed with a decrease of Fs. This negative correlation between Fs and PAR is mainly due to the NPQ (see Figure 5.8-B).


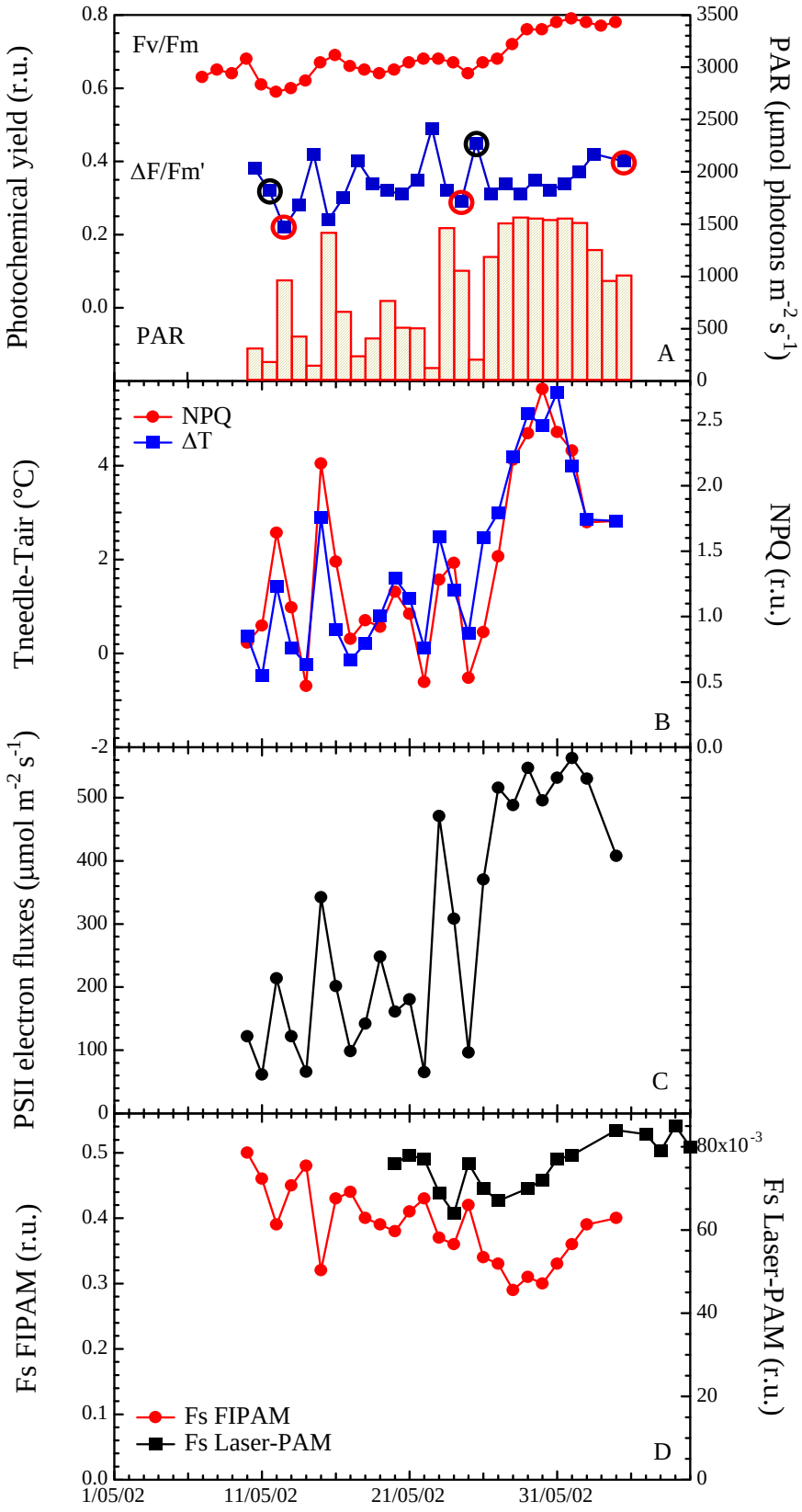

Figure 5.8 : Time series of ChlF parameters and temperature recorded with the FIPAM in the boreal forest, during SIFLEX campaign. The measurements were performed daily on Scots pine needles and averaged between 11h and 15h (UT + 3), except Fv/Fm measured at night.

(A) Evolution of the maximal and actual photochemical yield (Fv/Fm and ΔF/Fm') and the PAR. Red circles correspond to a PAR of about 1000 μmol photons m^{-2} s^{-1} and black circles correspond to a PAR of about 200 μmol photons m^{-2} s^{-1}.

(B) difference of temperature between the needles and the air, and the Non-Photochemical Quenching.

(C) The photosynthetic electrons flux of PSII calculated as the product of ΔF/Fm' and the PAR.

(D) Stationary ChlF yield (Fs) recorded with the FIPAM and compared to the one recorded with the Laser-PAM. The measurements carried out with the Laser-PAM were performed at a scale of a tree. Only measurements performed on the ground (near the 20-m high tower) with the Laser-PAM are presented.

5.4 PASSIVE FLUORESCENCE MEASUREMENTS FROM THE 20 M TOWER WITH THE PMFD INSTRUMENT

5.4.1 Radiance signals

The comparison during a daily cycle of the radiance signals from the target and the horizontal reference panel shows huge differences. Figure 5.9 compares these two signals at 685 nm with the PAR measured with a quantum-meter placed in the vicinity of the PMFD, on the top of the tower.

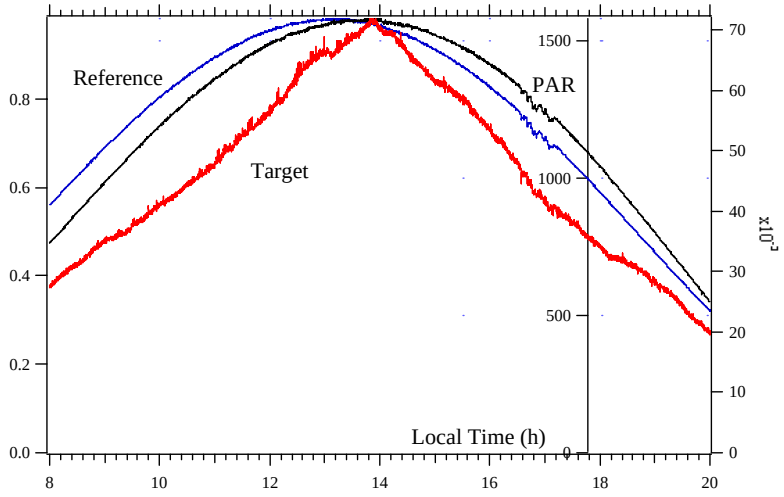

Figure 5.9. Comparison of the radiance fluxes from the target and the reference measured at 685 nm (border of the O_2 B band), with the PAR.

The shape of the Reference curve is in agreement with the Modtran modelling. One can observe a very similar shape for PAR and Reference signals. The shift of the maxima of the two curves is attributed to small differences in the horizontality between the quantum-meter and the reference panel.
The shape of the target signal is strongly influenced by the structure of the Scots pine forest. The peak around 14:00 is probably ascribable to a Hot Spot effect, whereas the other undulations could be due to the variation of the shadows within the target depending on the variation of the direction of the illumination during the day. It has been checked that these effects are independent of the fluorescence contribution.

Wavelength effects

In figure 5.10 are compared the four radiance signals from the target. The general shape is very similar excepted for the 758 nm channel, which exhibits a much less pronounced peak at 14:00 local time. This effect is explained by the lower reabsorption and the higher transmission of the vegetation at 758 nm, compared to the more absorbed wavelengths, including 531 nm. These

differences in target radiance almost disappeared under diffuse illumination conditions (Figure 5.11).

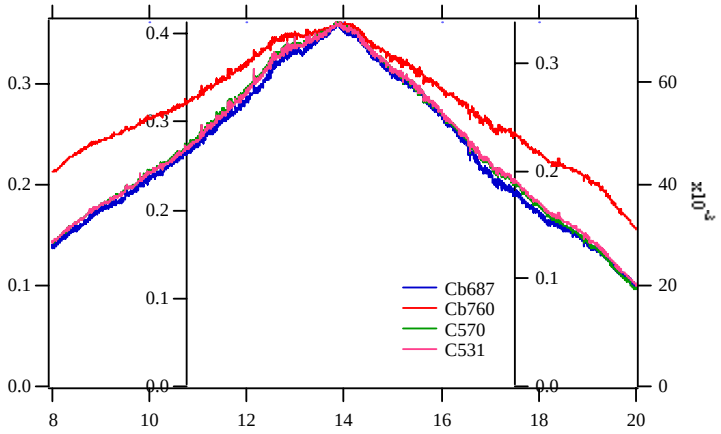

Figure 5.10. High light conditions. Comparison of the radiance fluxes from the target for the different wavelengths of the PMFD. Note the special behaviour of the target radiance at 758 nm.

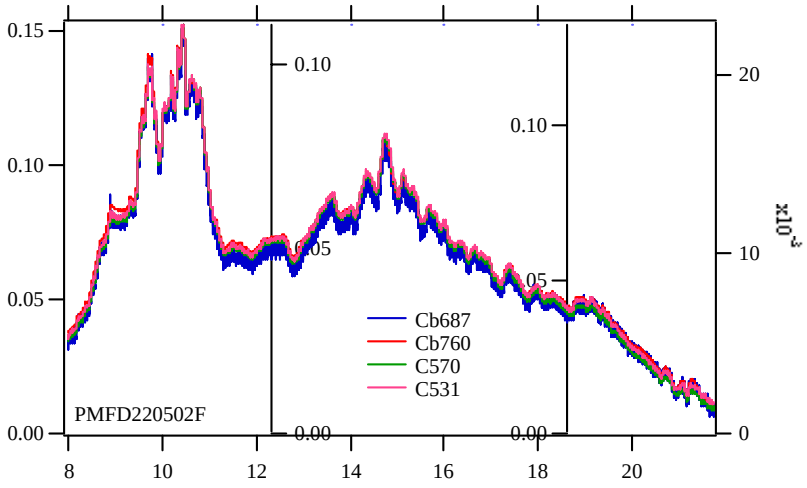

Figure 5.11. Low light conditions. Comparison of the radiance fluxes from the target for the different wavelengths of the PMFD.

5.4.2 ATMOSPHERIC CORRECTION

Due to the strong atmospheric absorption at 760 nm, a correction should be applied to the radiance fluxes to account for the attenuation due to the distance between the target and the reference panel (50 m). This attenuation has been considered negligible for all the target radiance's except for the bottom of the absorption band (760.5 nm) and introduced as a multiplying factor = 1.07. This correction is important to retrieve a positive value for the fluorescence flux at 760 nm in all data measured from the 20m tower.

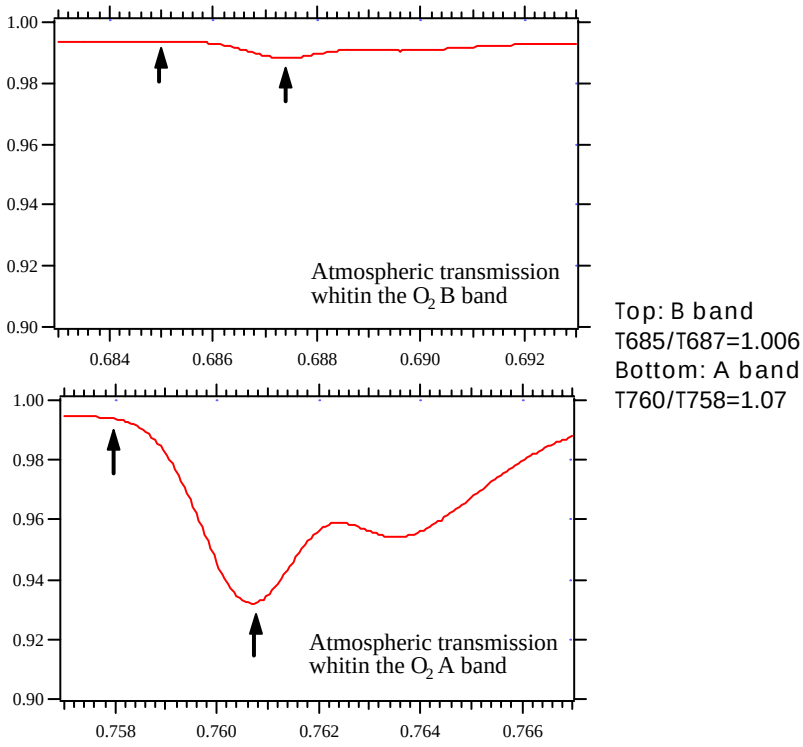

Figure 5.12. Atmospheric transmission, determined with MODTRAN 4, for a horizontal pathlength of 50 m at ground level.

5.4.3 Fluorescence fluxes

Fluorescence fluxes have been determined from Target and Reference radiance data according to Moya et al. 1998.

5.4.3.1 Sunny day

Fluorescence flux at 687 nm (F687) exhibits a similar dependence against time to that observed for the radiance signal at the same wavelength (Figure 5.13 A). This is attributed to the target structure effect already evoked to explain target radiance curves. The same remark holds for F760, which also exhibits a less prominent pick at 14:00, local time, as target radiance at 760 nm does. In contrast with active fluorescence methods, in which the excitation energy can be known, the exact excitation of sunlight-induced fluorescence depends on the radiation intercepted by the target, which is difficult to estimate.
At the leaf level, the problem can be solved using a quantum-meter or using the light reflected by the reference panel. In most cases, also the leaf

radiance may be an acceptable estimation of the incoming light.

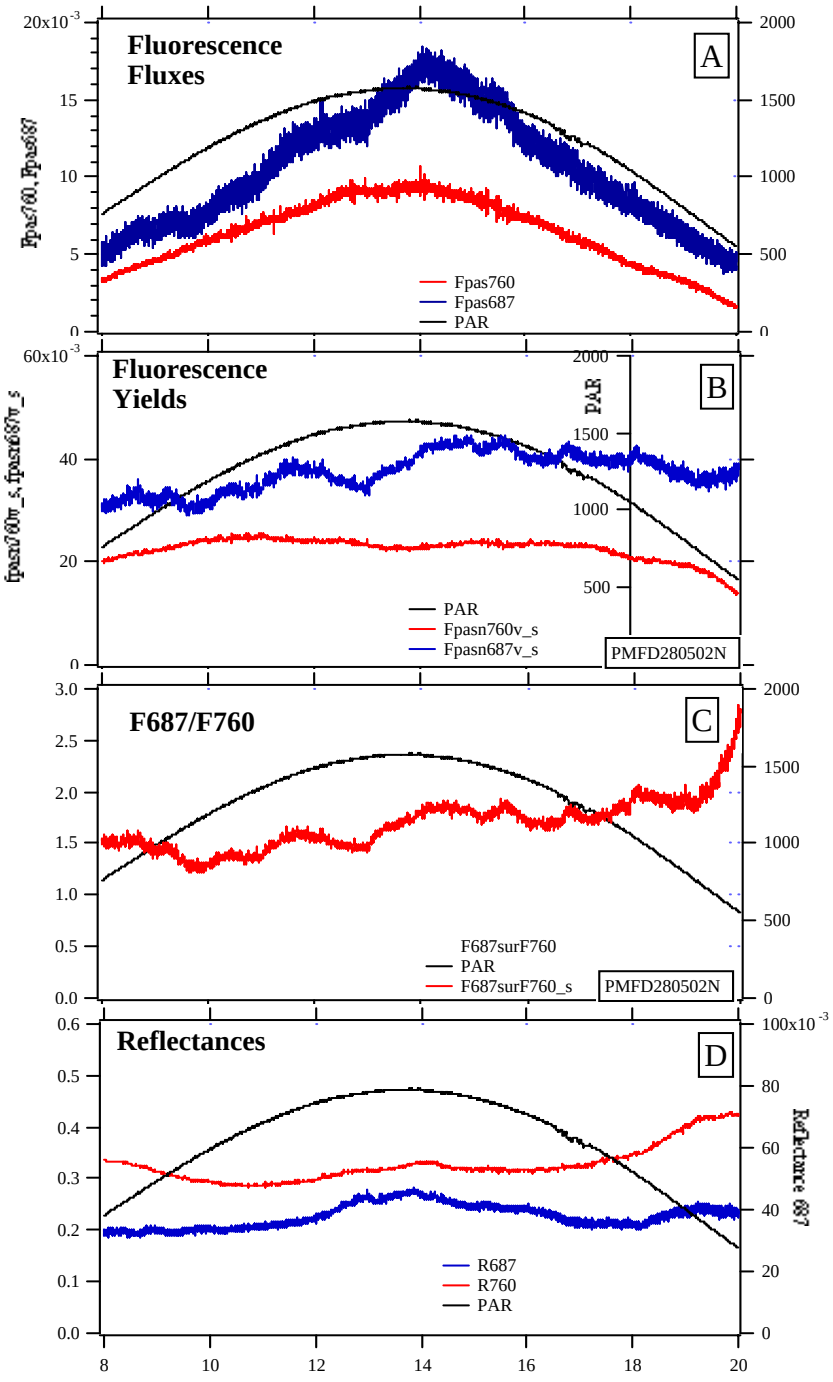

Figure 5.13. High light conditions (May 28th 2002)
A: Diurnal cycle variations of the fluorescence fluxes at 687, 760 nm and PAR.
B: Relative fluorescence "yield" obtain by dividing the fluorescence flux by the target radiance signal at 531 nm. C: Fluorescence ratio. D: Reflectances

Obviously this is not the case when measuring at the population level, in the special case of the boreal forest. Both PAR and radiance of the reference panel are measured from bidimensional surfaces, which hardly reflect the complexity of a three-dimensional canopy structure. After trying several possibilities we found that the radiance reflected by the target at 570 nm was the more appropriate to define a relative fluorescence yield. However target structure effects probably remain after dividing fluorescence fluxes by the radiance of the target at 570 nm.

Figure 5.13-B shows that ϕF687 increases continuously from 8:00 to 20:00 local time, with a step transition after 14:00. This variation has not been observed in the measurements reported in the preceding section, for the same day, using active instruments (see Figure 5.8). In the same conditions ϕF760 seems to be less sensitive to these effects, although the noon depression expected under high light conditions is hardly visible (I. Moya, unpublished results).

Figure 5.13-C shows the variation of F687/F760 ratio during the day. This ratio is supposed to depend on three parameters: i) [Chl] (Lichtenthaler et al 1986), ii) contribution of the PS1 fluorescence (Agati et al. 2000) and iii) State transitions (Allen 1992). The first parameter cannot play any role as the [Chl] is constant at the day scale. *The second parameter may influence the F687/F760 ratio as the PS1 emission is constant and contributes mainly in the long wavelength part of the spectrum.* A direct contribution of the PS1 fluorescence to the whole emission is difficult to assess especially under field conditions. When fluorescence emitted by PS2 increases markedly the F687/F760 ratio also increases. Conversely, the effect of a strong NPQ tends to decrease the F687/F760 ratio. In the present case, after several hours under full sun light one can suppose that the PS2 fluorescence stays almost constant. So we don't expect important variations of this ratio due to the variation of the PS2 photochemistry. The third mechanism is poorly known. Although state transitions play an important role as a regulating mechanism in algae, very little is known on the possible contribution of state transitions in the modulation of the fluorescence yield of Scots pine trees under natural condition, but it is generally assumed that it acts under low or moderated light conditions. In the present case it seems more realistic to assign the variations of the F687/F760 ratio to a different response of the target to the reflection, diffusion or transmission of the light at 687 and 760 nm.

This is confirmed by the variation of the reflectance at 687 and 760 nm during the day (Figure 5.13-D). One can observe that the bidirectional reflectance (radiance of the target divided by the radiance of the reference) increases at midday, possibly as a consequence of a hot spot effect. This effect is more pronounced at 687 nm.

5.4.3.2 Overcast day

During days where diffuse light dominates, F687 and F760 closely follows light variations (Figure 5.15-A). The diurnal variation of the fluorescence yields, ϕF687 and ϕF760, are perfectly parallel and almost constant. When the PAR increases above 400 μmol.m^{-2}.s^{-1}(at approximately 9:50 local time), a slight increase of both yields is observed (Figure 5.14 middle). Interestingly an oscillation of the F687/F760 ratio occurs when the PAR increases. As the increase of PAR trends to preferentially increase F687, the observed decrease of the F687/F760 ratio may be due to State2-State 1 transitions. However this question deserves further investigation. The observed increase of Fs is well correlated with a decrease of PRI (see Chapter III) as already observed (Moya et al. 2000).

5.4.3.3 Kinetic of passive fluorescence measurements

On cloudy days huge light variations take place, allowing a dynamic study of the response of the vegetation. This is the case, for example, on May 24th 2002 (Figure 5.14).

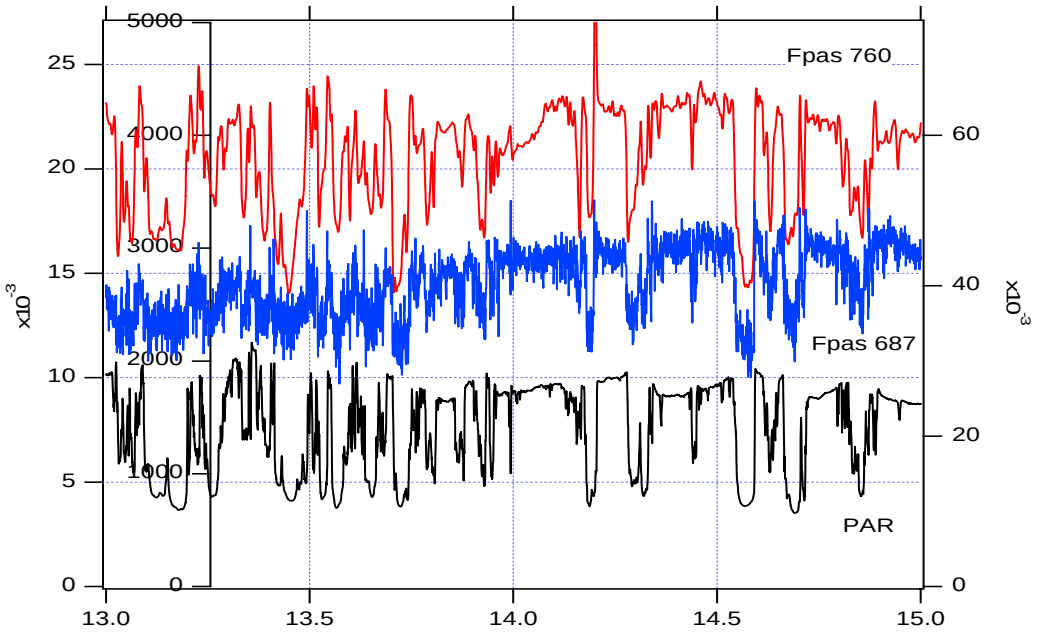

Figure 5.14. Rapid fluorescence flux changes produced by clouds on May 24th 2002

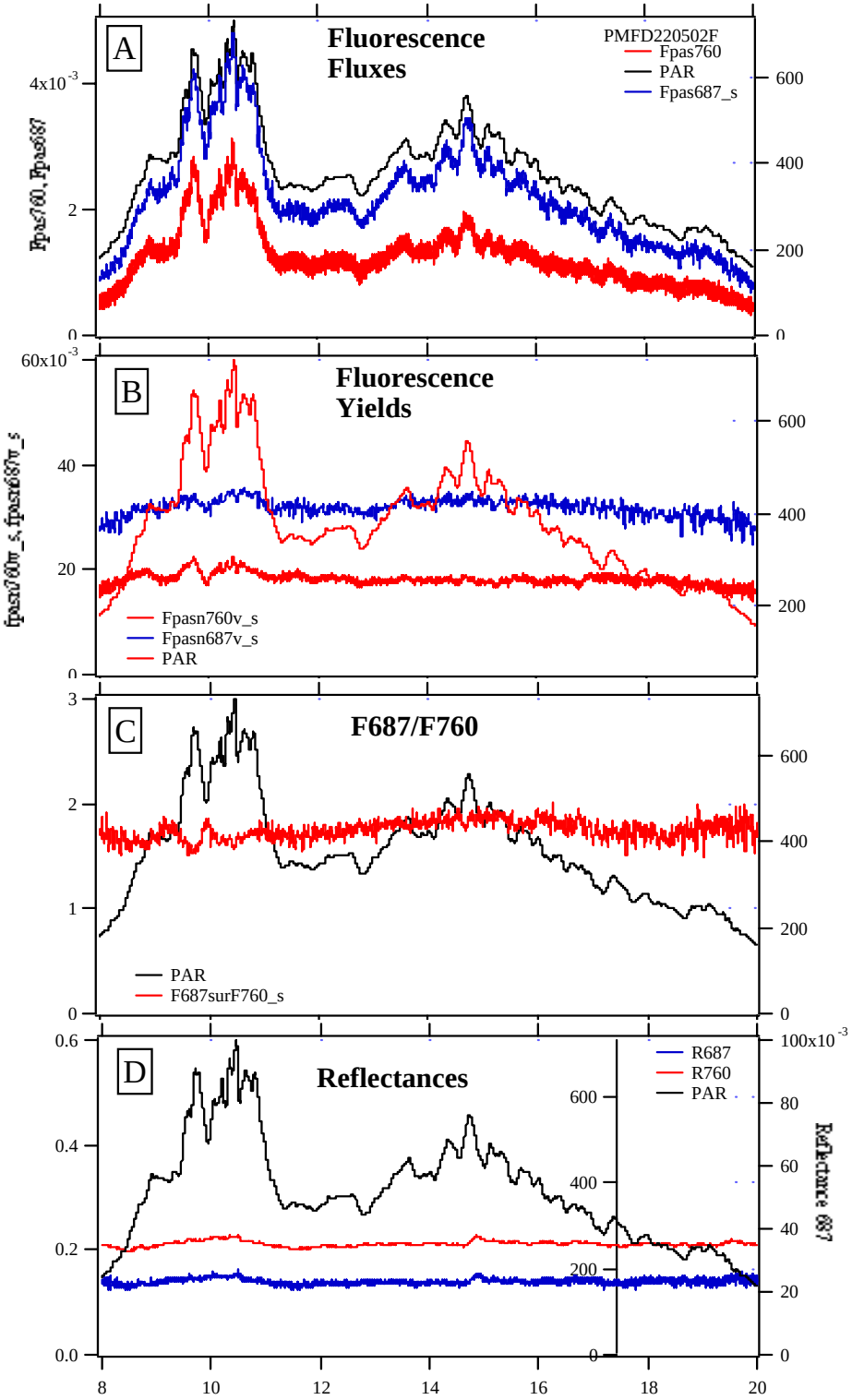
A
Fluorescence Fluxes
PMFD220502F
Fpas760
PAR
Fpas687_s
4x10-3
Fpas760, Fpas687
B
Fluorescence Yields
Fpasn760v_s
Fpasn687v_s
PAR
C
F687/F760
PAR
F687surF760_s
D
Reflectances
R687
R760
PAR
100x10-3
Reflectance 687
8
10
12
14
16
18
20

Figure. 5.15. Low light conditions (May 22th 2002)
A: Diurnal cycle variations of fluorescence fluxes at 687, 760 nm and PAR.
B: Relative fluorescence "yield" obtain by dividing the fluorescence flux by the target radiance signal at 531 nm .C: Fluorescence ratio. D: Reflectance.

Under favourable conditions (cloud producing a sharp transition) a Kautsky fluorescence transient can be recorded, as on June 9th 2002 (Figure 5.16)

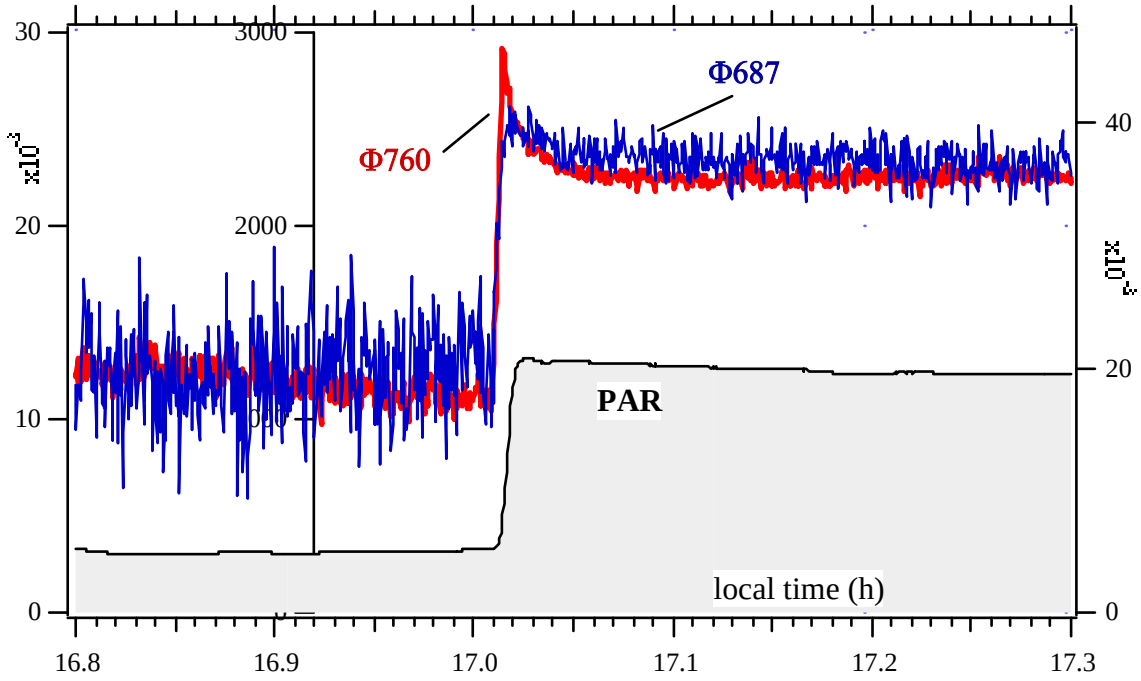

Figure 5.16. Passive fluorescence induction produced by a cloud on June 9th 2002. Notice the smaller amplitude of the kinetics at 687 nm

5.4.3.4 Evolution of the passive fluorescence signals during the campaign

The target radiance signal at 570 nm (C570) has been used as a relative measurement of the incoming PAR, instead of the signal of the quantum meter situated at the top of the 20 m tower. This minimised the structure effects as they affected both the radiance and the fluorescence signals. We also obtain a better time correlation during light transitions. Relative fluorescence yields have been defined:

$$\Phi 687 = F687 / C570$$

$$\Phi 760 = F760 / C570$$

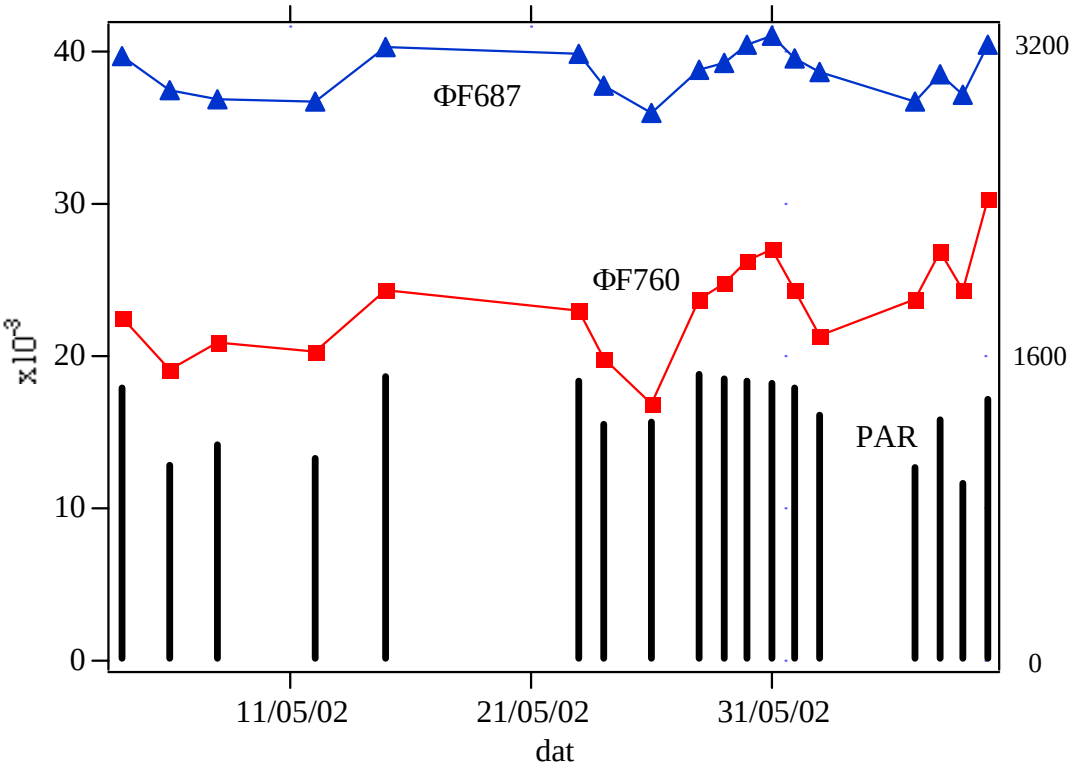

Figure 5.17. Time series of fluorescence yields and PAR integrated over 4 hours around solar noon.

To compare the evolution of the principal parameters, time-series have been generated by integrating the data between 11:00 and 15:00 local time, (i.e. over 4 hours centred on the solar noon). Very cloudy days have been discarded. The time-series of the two fluorescence yields are plotted on the same scale in Figure 5.18. One can observe that the daily-integrated value of both Φ687 and Φ760 are well correlated with the integrated PAR. This type of response is usually observed under low light conditions (Flexas et al. 2000) and is at variance of the observations made using active fluorescence methods (see Figure 5.8-D). In fact for the same days we observe a huge decrease of stationary fluorescence in the FIPAM experiment, a lower decrease on measurements using Laser-PAM, while passive measurements using the PMFD instrument showed an almost constant value for Φ687 or a slightly increasing value for Φ760 (Figure 5.17).

One possible explanation of these apparently contradictory results may be the inhomogeneity of the illumination due to the nature of the target. In the case of the FIPAM the needles are fixed and homogeneously illuminated. They responded all together in the same way: as a result the quenching effect due to the high light is very pronounced. In the case of the Laser-PAM, the target,

which extends over 300 x 300 mm, is constituted of several stems with shadowed parts. The response is less homogeneous but still the Fs decreases when high light conditions dominate. In the case of the PMFD target the heterogeneity is still higher.

Needles were not illuminated during a sufficiently long period, due to light changes and shadowing on the target, to evidence the quenching effects.
Only Φ760 shows an increase at the end of the campaign, which parallels the modest total chlorophyll concentration increase, while Φ687 stays constant (Fig. 5.1). Changes on the apparent fluorescence yield could result of an increase of the absorbed PAR as a consequence of the higher [Chl]. The fluorescence yield at 760 nm (Φ760), which is measured at a wavelength not affected by reabsorption, would increase, but Φ687, which is a strongly affected by reabsorption would not.
Besides the possible [Chl] effect, one may invoke a modification on the PS2 photochemical efficiency. Fs data obtained with the laser-PAM (Figure 5.8-C) also showed a slight increase at the end of the measuring period. Due to the differences in the light climate discussed above, the comparison with the FIPAM data seems less relevant.

5.4.3.5 Dynamic passive fluorescence analysis

In order to evidence possible changes in the photochemical response of the Scots pine forest during the campaign, fluorescence yield variations at 687 and 760 nm during cloudy days exhibiting rapid light changes have been examined. The kinetics from the beginning and from the end of the campaign has been compared (Figure 5.18).

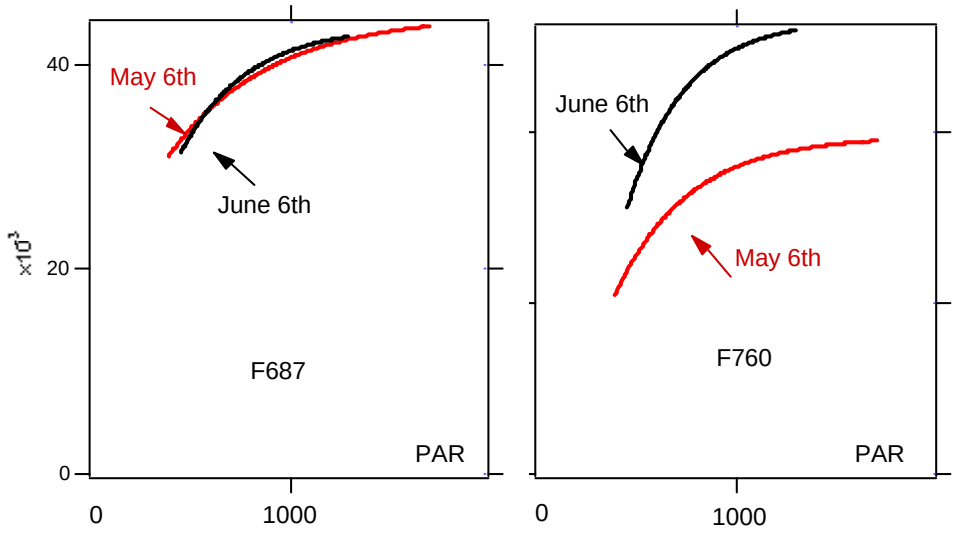

Figure 5.18. Comparison of the slopes of the fluorescence versus PAR curves during light transients. Observe the faster fluorescence yield increase at the end of the campaign (June)

Figure 5.18 shows the fits of the relations between fluorescence yield and PAR. For clarity, the clouds of points have been omitted. It can be seen that fluorescence variations respond positively to PAR variations, as already stated. The response is faster for the measurements done in June for any wavelength. In addition F760 shows larger variations. This result was already observed in the kinetics from Figure 5.17.

5.5 PRI MEASUREMENTS

Under conditions where light is in excess of the amount that can be used for photosynthesis, ΔpH and the de-epoxydation state of xanthophylls both increase, and are involved in a photoprotective mechanism that dissipates excess light as heat (Demmig-Adams & Adams, 1992; Niyogi, 1999). This photoprotective mechanism varies along the diurnal time-course, as well as in response to temperature, water and nutrient stresses (Demmig-Adams & Adams, 1992). This mechanism is supposed to involve zeaxanthin-induced changes in the conformation state of PSII light harvesting complexes (Ruban et al., 1993; Moya et al., 2002). Dynamic changes in the de-epoxidation state of the xanthophyll cycle were known to be accompanied by absorbance changes at 505-515 nm (Bilger et al., 1989; Heber, 1969; Heber et al., 1986; Krause, 1973; Yamamoto & Kamite, 1972). It seems that the accumulation of zeaxanthin allows rapid changes in the aggregation state of antenna chlorophyll-protein complexes, which are reflected by absorbance changes centred near 531 nm (Bilger et al., 1989; Ruban et al., 1993).
Gamon et al. (1990) were the first to show that rapid reflectance changes around 531 nm, occurring upon sudden changes in incident light, could be sensed remotely and passively from leaves and canopies, using a portable radiometer. These changes were related to the above-described chloroplast conformational changes associated with increased pH and de-epoxidation state of the xanthophyll cycle (Gamon et al., 1990). Therefore, passive remote sensing of reflectance changes at 531 nm has been proposed as a useful tool for nutrient and water stress detection, although the latter is not always possible, especially in water-stressed canopies undergoing severe wilting (Gamon et al., 1992; Peñuelas et al., 1994; Gamon et al., 1997). The PRI index, defined as the relative changes in reflectance at 531 nm with respect to those at 570 nm (PRI = R531-R570 / R531+R570), correlates with xanthophyll-related dynamic changes of non-photochemical quenching of chlorophyll fluorescence. In a recent work (Evain et al., submitted), we strengthened the robustness of this relationship by simultaneous remote sensing of PRI and

chlorophyll fluorescence. Overall, the PRI is better correlated with the non-photochemical quenching of chlorophyll fluorescence (NPQ) than with any other measured parameter, including the photochemical efficiency of PSII. However at the leaf level we observed the existence of two kinetically distinct components of PRI. A fast (within seconds) component is partly attributed to ΔpH-induced chloroplast shrinkage, and a slow (within minutes) major component is related to xanthophyll de-epoxidation, as demonstrated by its abolition by DTT.

It has been suggested that the mechanism of photoprotection mediated by carotenoids is involved in preserving conifers from winter injury (Adams and Demmig-Adams, 1994). This has been confirmed by Ottender et al (1995) which showed that the carotenoid content of Scot pine needles is subject to important accumulation during the cold season followed by a decrease when the full photosynthetic capacity is recovered in June. These changes are also accompanied by a decrease during winter of the carotenoid epoxidation state. Owing to the link between the PRI index, the xanthophyll cycle and NPQ in general, it appeared important to monitor the PRI index in parallel to passive fluorescence parameters during the spring recovery of vegetation.

5.5.1 Daily cycle results of PRI

Figure 5.19 shows a typical diurnal cycle of the PRI index together with PAR. One can observe an almost symmetric variation from the morning to the evening with a minimum around local noon. A decrease at noon of the PRI index has already been reported (Moya et al. 2000, Evain et al. 2003) and has been explained by the accumulation of NPQ depending on the light constraint with the subsequent relaxation in the afternoon and during the night. During sudden changes of PAR the decrease of the PRI index can be observed followed by its subsequent relaxation when returning under low PAR conditions (Figure 5.20).

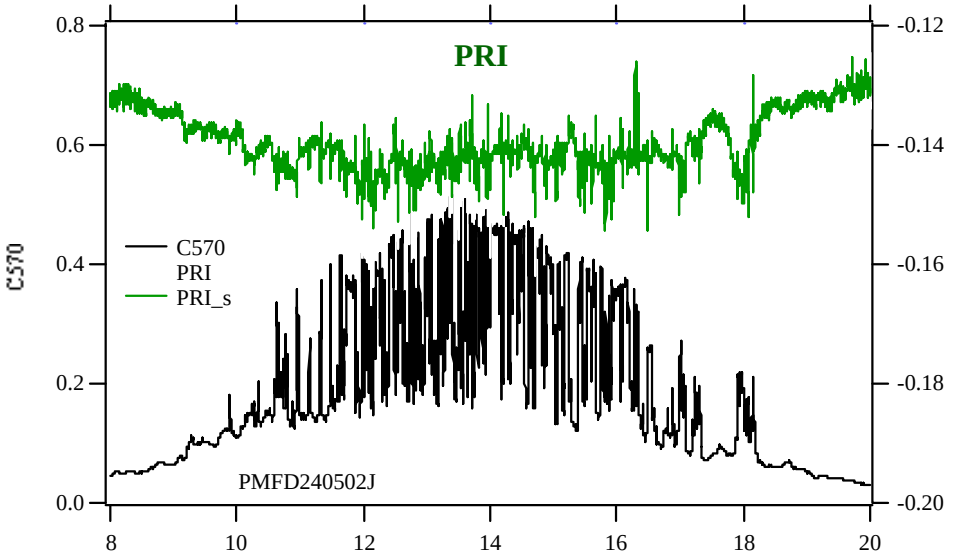

Figure 5.19. Typical diurnal cycle of the PRI index together with PAR. Data from May 24th 2002. Due to rapid alternation of sun and shade, PRI variations are not clearly resolved excepted at 18:00 when the transition is longer.

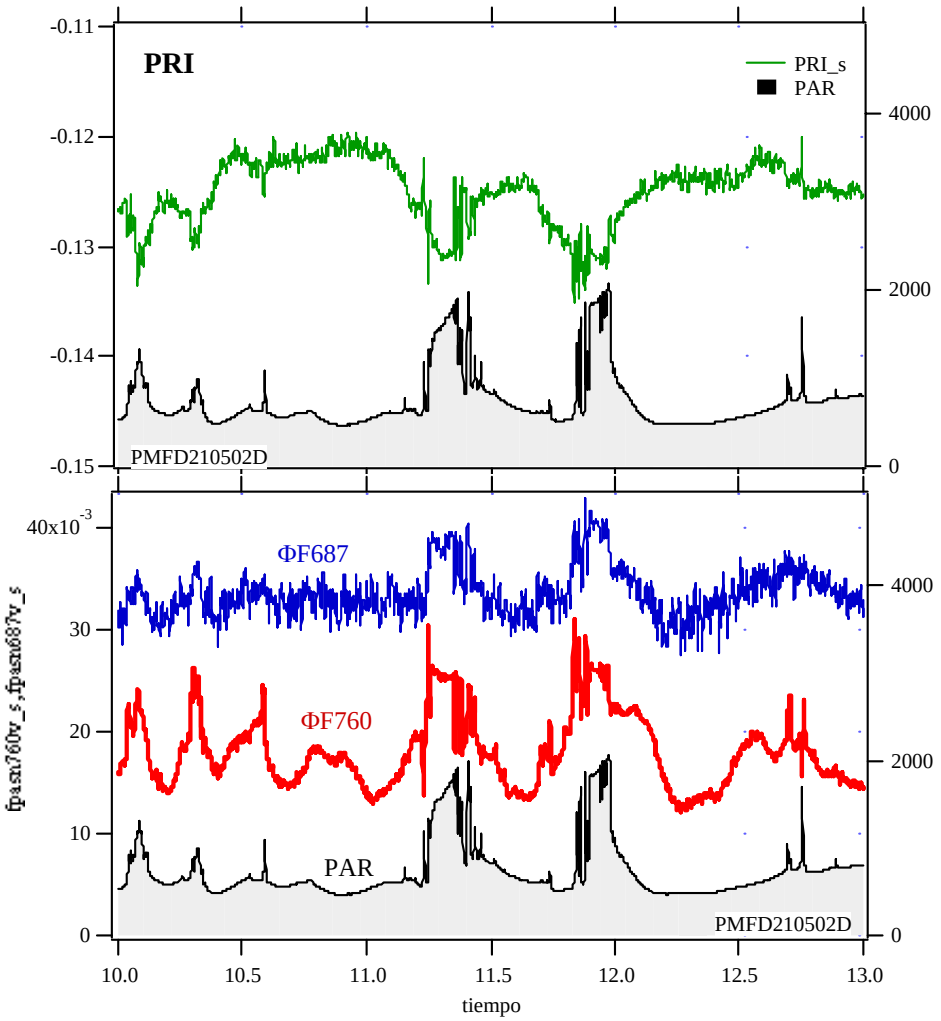

Figure 5.20. A. Decreases of the PRI index occuring after a sudden transition lasting several minutes from overcast to full sunlight. B. Simultaneous measurement of the fluorescence yields. Notice the ΦF760 increase resulting from the PAR increase, followed by decay under high light due to the development of NPQ. Data from May 21th 2002

5.5.2 Time-series of the PRI index during the campaign

The averaged value of the PRI index has been calculated after integration between 11:00 and 15:00 as for the other parameters (Figure 5.21). The PRI stays almost constant until the end of May and rises continuously up to the end of the campaign. This striking result is similar to the rise observed in Figure 5.8.

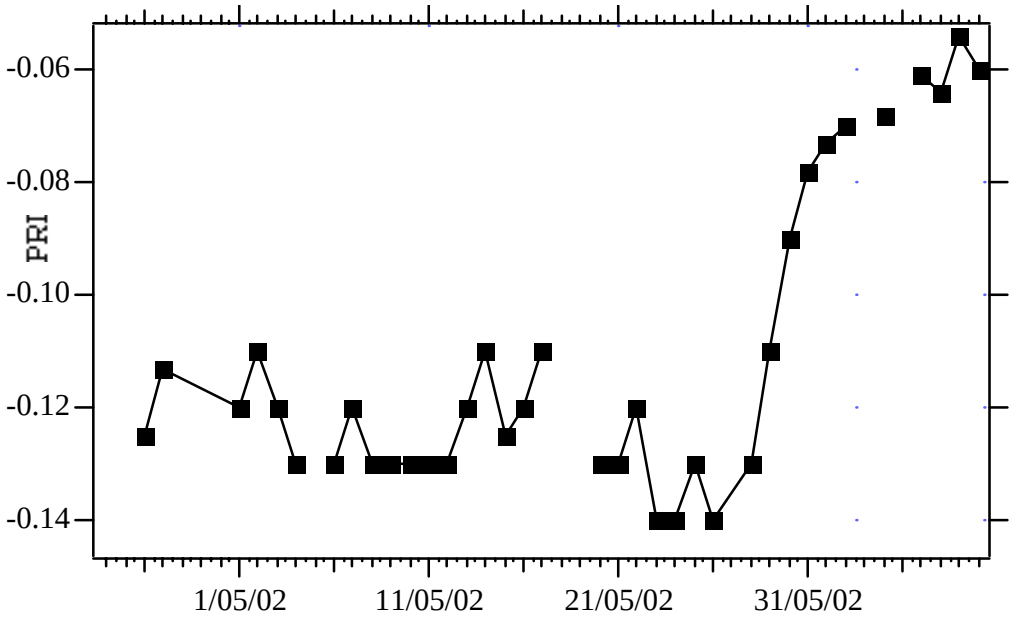

Figure 5.21. Evolution of the averaged PRI index during the campaign

5.5.3 PRI data from the group of Valencia

In addition to the PMFD, an ASD FR/FS spectroradiometer has been used for the measurement of target spectral reflectance in the range from 350 nm to 2500 nm with 1nm spectral resolution in the VIS/NIR region. This instrument was able to derive the Double-Peak Ratio as well as PRI. The spectral resolution of this instrument is not narrow enough to use the oxygen absorption bands for fluorescence measurements.

The ASD instrument provided by the group of Valencia was placed at the top of a 20-m high tower, besides the PMFD instrument. The target was the same portion of the canopy located at a horizontal distance of 55 m northwards from the tower, and at a height of about 10 m. The reference panels were located at the tower for practical reasons. Both instruments were pointing to the same spot, with a FoV (field of view) of approximately 4º (the FoV of the ASD was slightly smaller). The measurements took place from 10:00 to 16:00 in 15 minutes intervals with the ASD, and continuously with the PMFD. They were repeated on a daily basis, whenever the weather allowed it, from the 29th of April to the 6th of June. Figure 5.22 compares the values of the ASD spectro-radiometer with the similar data measured by the FIPAM, in the case of PRI. One can see that both measurements agree fairly well, the differences are considered mainly due to the differences in the FoV and the spectral resolution.

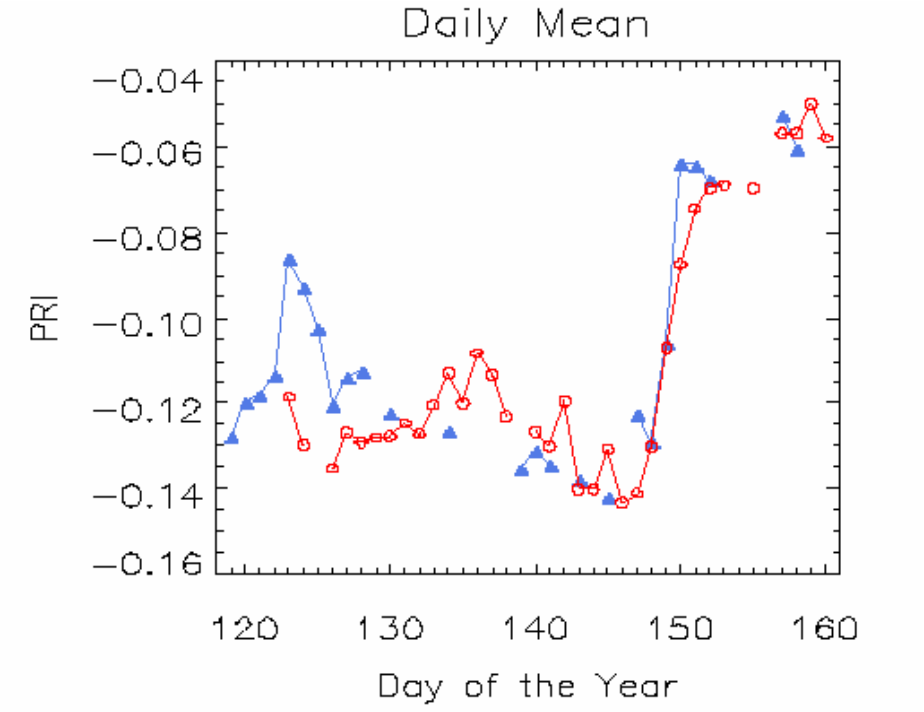

Figure 5.22. Comparison of the PRI index along the SIFLEX campaign, as measured with PMFD (circles) and ASD (triangles).

5.6 MAIN FINDINGS AND CONCLUSIONS

In the beginning of the campaign on April 23–24, when there was still a continuous snow cover, negative net CO_2 fluxes of about -0.05 mg $m^{-2}s^{-1}$ at noon were observed. Already then, the CO_2 uptake by the canopy exceeded the total respiration. The warm weather advanced the development of Scots pines, and in the end of April, the net CO_2 fluxes at noon reached the -0.3 mg $m^{-2}s^{-1}$ level. During the cool period in May, when temperatures at noon varied between 3 ºC and 12 ºC and were below or around 0 ºC at night, the net CO_2 fluxes at noon were only -0.15 mg $m^{-2}s^{-1}$.

The light response curve (Figure 2.1) illustrates the relatively high net CO2 uptake in the end of April, considering the fact that there was still snow on the ground. This warm period was followed by uptake periods of alternating intensity. Net uptake was high in the middle of May, after which it decreased during the colder period that followed (Figure 6 of the FMI Report). The nocturnal freezing temperatures were over on May 27 (Figure 2.2). Despite the very warm weather in the end of May, the net CO_2 uptake remained low. After June 2, the net CO_2 fluxes at noon increased to -0.4 mg $m^{-2}s^{-1}$, which is a typical value in summer.

The maximum photochemical efficiency (Fv/Fm) of the Scots pine was around 0.2 in winter and above 0.8 in summer (Ottender et al. 1995, but see also FMI

Report).

At the beginning of May, Fv/Fm was about 0.6 so most of the transition from winter to summer condition was done. Nevertheless, CO2 uptake was only 30-40 % to the summer values. In figure 5.23, CO2 uptake was plot in the same time-scale than PRI. It is striking to observe that the two curves exhibited a steep increase for the same days and varied in a parallel way. We may hypothesise that both parameters are indicative of the same change of photosynthetic capacity of the Scots pine forest.

FIPAM measurements during this period shows a continuous increase of the effective PS2 electron transfer rate (ΔF/Fm') both under low or high light conditions (Figure 5.8-A) which confirms the progressive recovery of the full photosynthetic capacity. Interestingly these changes are also observed using passive fluorescence measurements. This is clearly shown in Figure 5.19 in which the faster fluorescence response against PAR during light transitions can be interpreted as a reduced amount of NPQ. The observed decreased amount of xanthophylls and lutein in June (see Figures 5.2 and 5.3) is also in line with this interpretation.

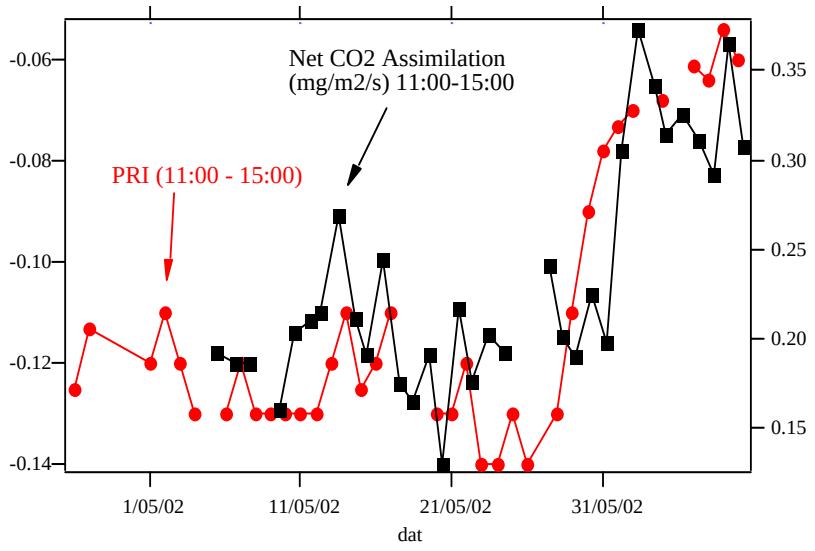

Figure 5.23. Parallel plot of the PRI index and CO2 uptake measured at the meteorological tower, averaged from 11:00 to 15:00 local time



FINNISH METEOROLOGICAL INSTITUTE

6. CONCLUSIONS AND RECOMMENDATIONS

The main objective of the SIFLEX experiment was to determine weather passive solar-induced vegetation fluorescence can be remotely measured and, in case it can be measured, to quantify the variations through diurnal cycle and seasonal (winter to summer) evolution. The selected target was from the very beginning considered a challenge, because boreal forests have a small dynamic range of variation in canopy conditions, plus illumination conditions are quite low at such high latitudes. Moreover, the structural properties of the canopy are extremely complex, thus making difficult the interpretation of the signal. From the very beginning it was also clear that to interpret fluorescence measurements one needs to measure a number of complementary variables, related to actual instantaneous illumination conditions, canopy properties and background meteorological conditions, including air and canopy temperatures. All these complementary variables were measured in SIFLEX, so that the resulting dataset represents an important source of information for future dedicated studies.

In general, SIFLEX has been a highly successful experiment, because not only it has demonstrated the possibility to measure fluorescence even in the case of difficult targets, but it has also provided new ideas for future developments.

In particular, the main conclusions derived from the analysis of SIFLEX data can be summarised as follows:

(a) Magnitude of the fluorescence signal from a boreal forest

One of the objectives of the SIFLEX experiment was to quantitatively determine the fluorescence levels in the case of a boreal forest, in order to compute the amount of signal to be detectable —in the case of a boreal forest— for a potential satellite mission.

The amount of fluorescence signal emitted by a boreal forest should be determined in units of radiance or in terms of relative reflectance. Although both formulations are equivalent, the radiance computations provide a direct indication of the detectability from a satellite, because radiance is the ultimately magnitude which is measured by the detectors.

In order to recover the radiance values, we need to go back to the way in which fluorescence was passively measured in the SIFLEX experiment, by using the standard absorption-line filling approach for the retrieval of fluorescence from measured radiances.

In the standard approach, fluorescence in retrieved from four radiance measurements, two for the canopy and two for a non-fluorescent reference, and with one measurement inside the O2 absorption band and another close outside the absorption band, for both targets. Then, in this case fluorescence is usually computed as

$$F_{target} = R^{(2)}_{target} - R^{(2)}_{reference} \frac{R^{(1)}_{target} - R^{(2)}_{target}}{R^{(1)}_{reference} - R^{(2)}_{reference}} \quad [1]$$

where (1) means a spectral band outside the absorption line and (2) means a spectral band inside the absorption line.

However, in the case of the geometrical configuration used for the SIFLEX experiment, the distance from the detector and the canopy target was significantly different than the distance from the detector to the reference target (a panel located at the top of the tower). The difference in the atmospheric transmission from the canopy to the detector and from the reference to the detector must be accounted for, and the resulting equation to derive fluorescence in the case of SIFLEX measurements is of the form

$$F_{target} = \frac{R^{(2)}_{target}}{\tau^{(2)}_{target}} - \frac{R^{(2)}_{reference}}{\tau^{(2)}_{reference}} \frac{\frac{R^{(1)}_{target}}{\tau^{(1)}_{target}} - \frac{R^{(2)}_{target}}{\tau^{(2)}_{target}}}{\frac{R^{(1)}_{reference}}{\tau^{(1)}_{reference}} - \frac{R^{(2)}_{reference}}{\tau^{(2)}_{reference}}} \quad [2]$$

The transmittances τ are the critical terms that must be accounted for. Such transmittances are shown in Figure 6.1, for both target-detector and reference-detector, for the geometrical conditions of SIFLEX, and one can see clearly the important effects of the reduced atmopsheric transmittance through the path inside the oxygen absorption band, an effect usually neglected in laboratory or near-field conditions, but that is relevant as the distance from the detectors and the target becomes more significant.

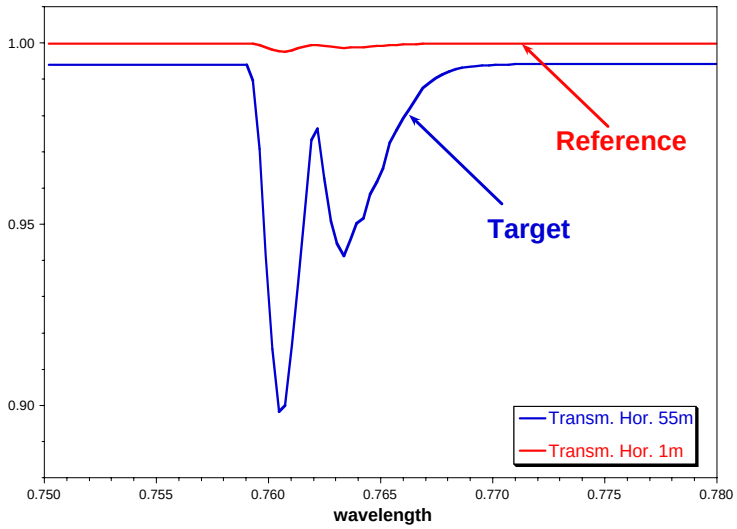

Figure 6.1. Target-tower atmospheric transmittance

Such transmittances are also a function of surface pressure, and then actual surface pressure changes during SIFLEX must be taken into account:

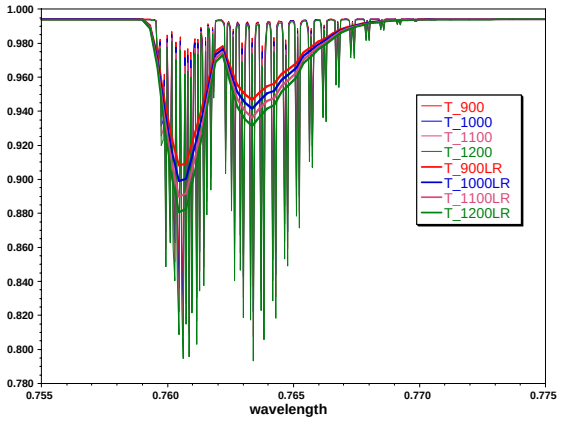

Figure 6.2. Dependence of target-tower atmospheric transmittance on surface pressure

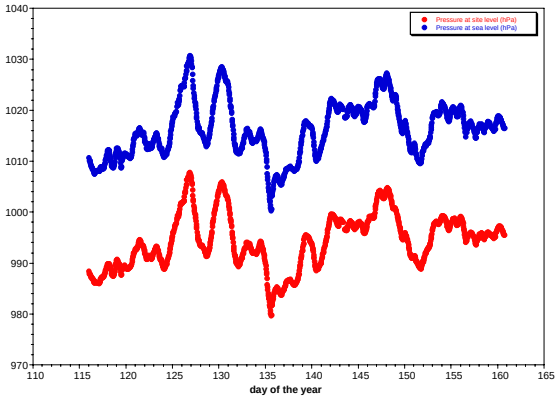

Figure 6.3. Actual surface pressure values as measured in SIFLEX

Figure 6.4 shows the fluorescence levels derived from Eq. 1 and Figure 6.5 shows the fluorescence levels derived from Eq. 2. As expected, the effects is rather small in the case of 687 nm absorption band, but they are quite significant in the case of the 760 nm band.

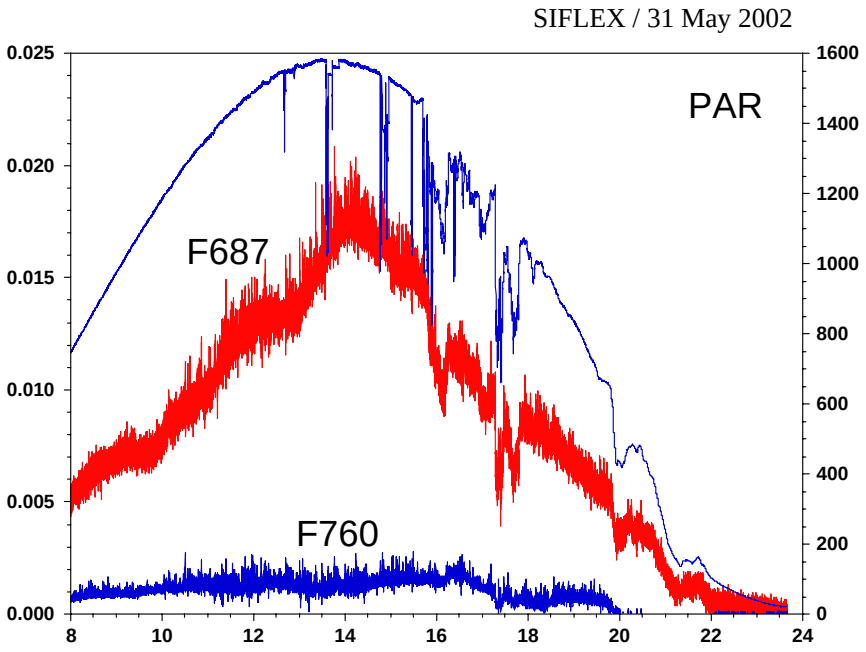

Figure 6.4. Fluorescence computation without accounting for O2 differential absorption

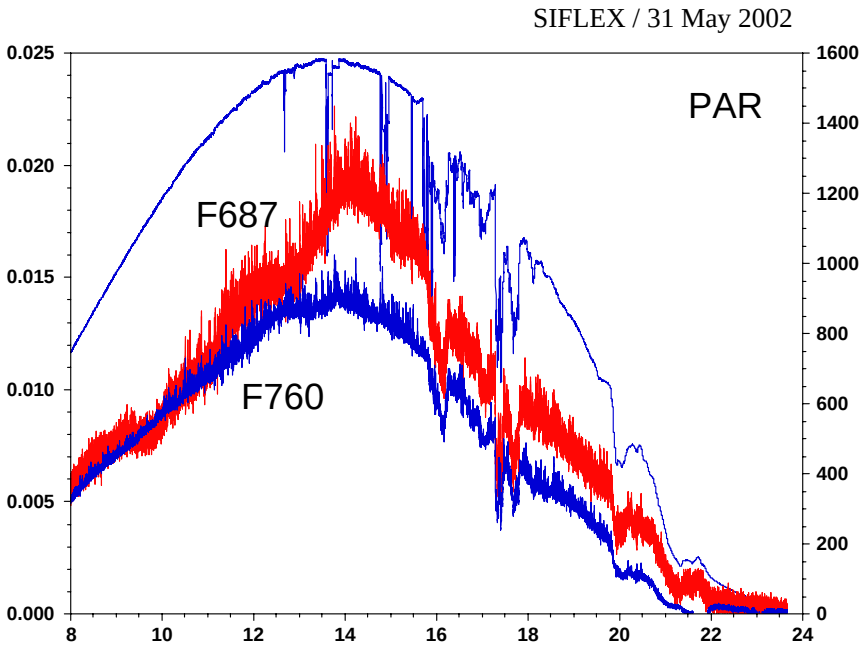

Figure 6.5. Fluorescence computation by accounting for O2 differential absorption

The absorption factors to compensate the different paths in the measured signals are derived from MODTRAN 4, by reproducing the geometric configuration in SIFLEX observations and accounting for the atmospheric status at the time of the experiment.

We have learn significantly from the SIFLEX experiment on how to handle remote measurements within the O2 absorption band, taking into account the role played by the intrinsic atmospheric absorption in the signal. Applying the appropriate correction factors we are confident that the resulting values are representative of the actual fluorescence levels. These corrections are essential when we move to airborne or satellite sensors, where there is a clear need for accurate compensation of differential atmospheric absorption effects among the different spectral bands.

However, in order to avoid problems coming from the need to compensate atmospheric effects, it would be important in future experiments to test fluorescence measurements by using the Hα band, where atmospheric variability is less significant than in the case of techniques based on oxygen absorption bands, to compare absolute fluorescence levels measured by different methods, particularly with methods less sensitive to atmospheric effects.

(b) Diurnal cycle of fluorescence changes

The determination of the diurnal variation of fluorescence levels was a main objective in SIFLEX, because the diurnal cycle provides a key in the interpretation of the fluorescence signal as driven by illumination changes over a fixed target. Moreover the analysis of diurnal cycles provides information about the expected levels (minimum and maximum) and on how the diurnal changes can mask secular changes along seasonal evolution, that are usually more interesting from a remote sensing perspective.

The main problem is to refer the diurnal cycle to a reference reflectance, because fluorescence changes mostly track the diurnal illumination cycle. In this case we have normalised the fluorescence levels to the measured reflectance at the same wavelength. The result for a typical day is illustrated in Figure 6.6: PAR variations are shown along with F687 and F760 levels. As it can be seen, F687 is more sensitive to BRDF effects (structural effects) while F760 is less sensitive to structural effects (F760 is less directional) due to the more diffuse component.

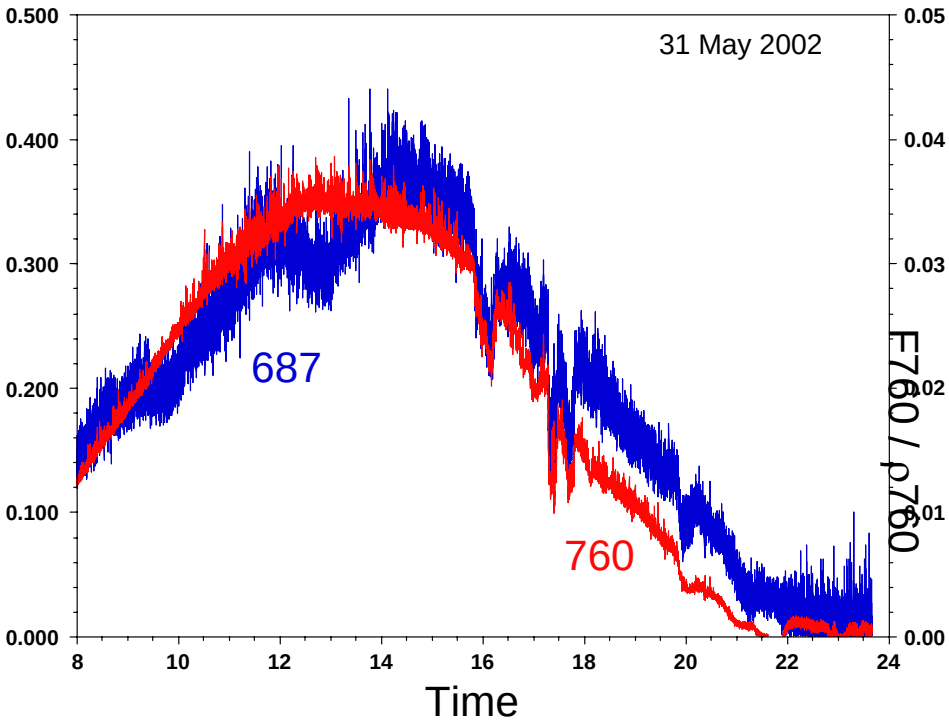

Figure 6.6. Fluorescence levels expressed as reflectance ratios

As we can see in the figure, fluorescence levels (as expressed as ratio to reflectance) change by a factor 4 along the day. There is enough dynamic range to detect changed versus the background noise. Moreover, the observed diurnal cycle can be understood as a function of illumination conditions, vegetation response to environmental conditions, and dependence on canopy structural effects, which are more significant at 687 nm than at 760 nm.

(c) Long-term dynamical behaviour: Secular evolution of fluorescence changes following forest spring recovery

Apart from information about typical behaviour of the diurnal cycle of canopy fluorescence, SIFLEX has provided also information about the long-term secular evolution of vegetation recovery from spring to summer Arctic conditions.

A key issue in the analysis of such long-term changes was to determine how fluorescence is related to environmental conditions, and in particular with the also varying CO2 flux between the canopy and the atmosphere. If fluorescence changes track changes in CO2 fluxes, then we can use fluorescence as inputs in models describing the CO2 exchanges between vegetation and the atmosphere.

In order to compare fluorescence changes with other potential photosynthetic indicators, two other indicators were measured in SIFLEX:

(a) The Photosynthetic Reflectance Index (PRI), defined as the ratio PRI = (ρ531 - ρ570)/(ρ531 + ρ570), that is related to photochemical changes ocurring at the leaf level (xanthophyll cycle, conformational changes, etc.) that are directly or indirectly associated to photosynthesis

(b) Changes in the spectral reflectance along the red-edge, in particular changes in the position and amplitude of the maxima of the derivative of the spectral reflectance, defined as the ratio of the two peaks observed in such spectral reflectance derivative.

Then, we will compare the CO2 fluxes with three potential indicators that were measured in SIFLEX:

- passive fluorescence
- red-edge peeks ratio
- PRI

Figure 6.7 shows the variation of fluorescence levels along the SIFLEX campaign, as compared to the variation of CO2 flux measured at the same site and for the same period. As we can see, fluorescence changes somehow track changes in CO2 flux, but the diurnal cycle is quite large as compared to the secular evolution. Then, diurnal changes can mask the measurement of long-term seasonal variations.

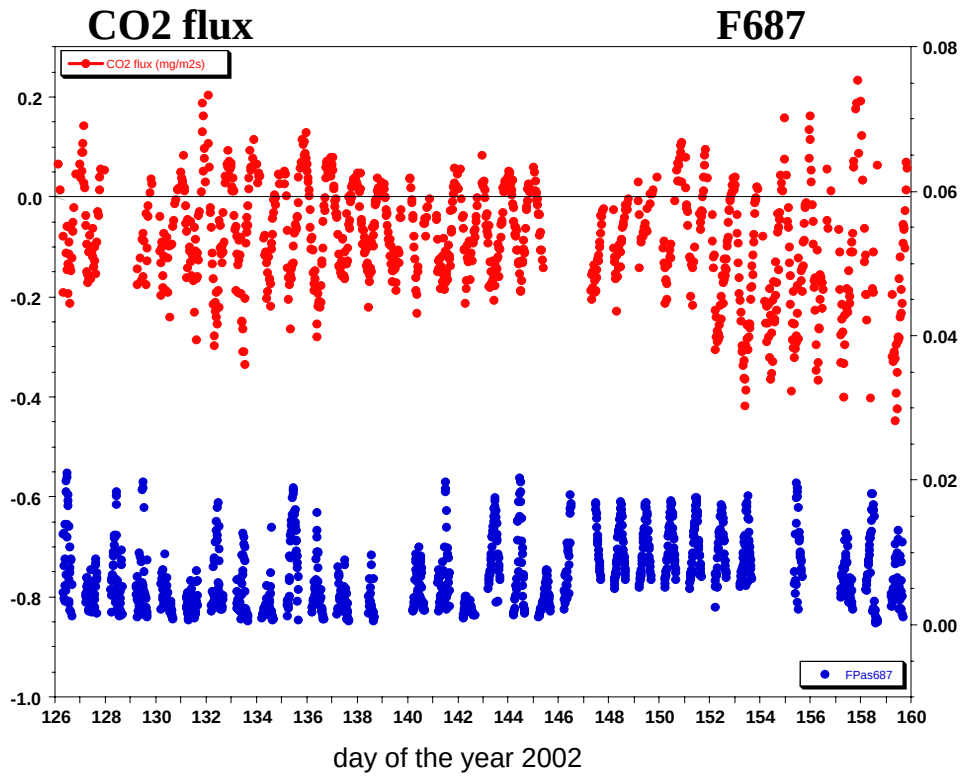

Figure 6.7 Variation of fluorescence levels along the SIFLEX campaign, as compared to the variation of CO2 flux measured at the same site and for the same period.

Figure 6.8 shows the same CO2 flux data for the same period but in this case compared to the "peaks ratio" (red-edge derivative reflectance indicator). This indicator seems to track the secular changes somehow better than fluorescence, but date are somehow influenced by strong diurnal changes. It seems that the peaks ratio not just follow fluorescence changes, but provide alternative different information, and the peaks ratio index can be used together with fluorescence for vegetation photosynthesis monitoring.

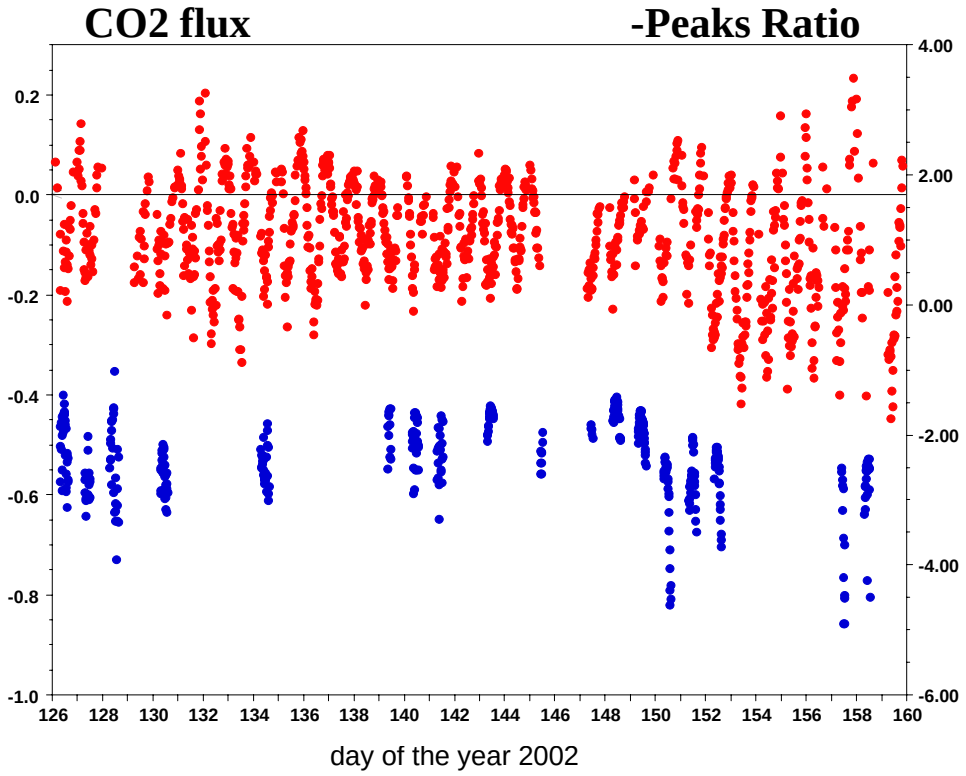

Figure 6.8. Variation of reflectance shape along the red-edge (derivative peaks ratio) along the SIFLEX campaign, as compared to the variation of CO2 flux measured at the same site and for the same period.

Figure 6.9 shows also the same CO2 flux data for the same period, but in this case using the PRI index as photosynthesis indicator. It is clear from the figure that seasonal variations of PRI are quite dominant over the typical diurnal charges, what is quite positive to measure changes in photosynthetic activity of vegetation without the disturbances caused by the strong diurnal variations occurring with fluorescence.

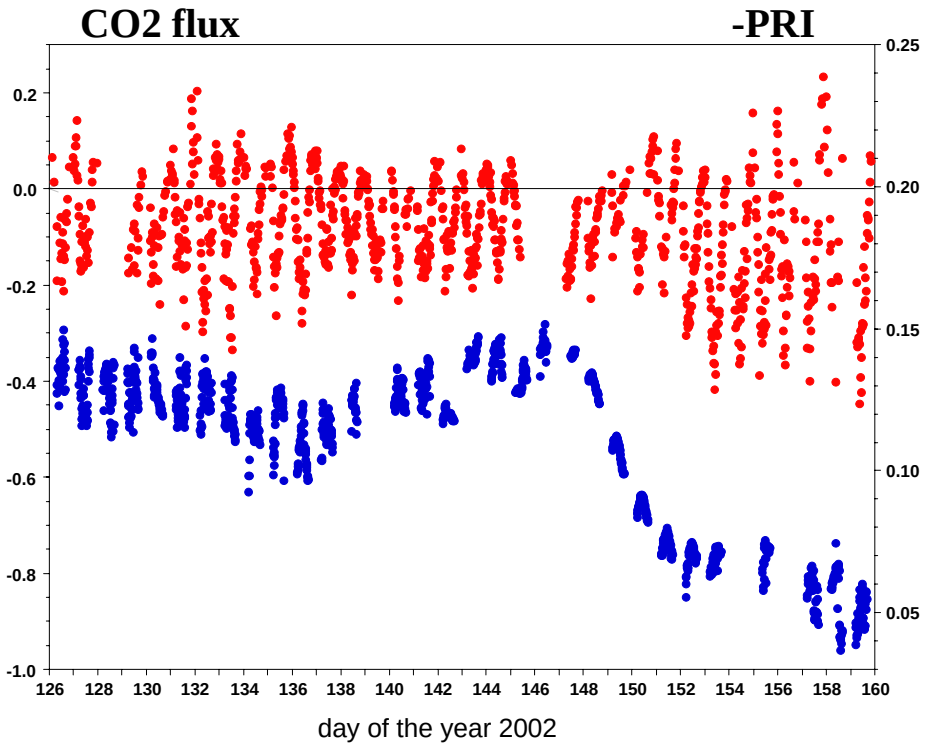

Figure 6.9. Variation of the spectral reflectance index PRI along the SIFLEX campaign, as compared to the variation of CO2 flux measured at the same site and for the same period.

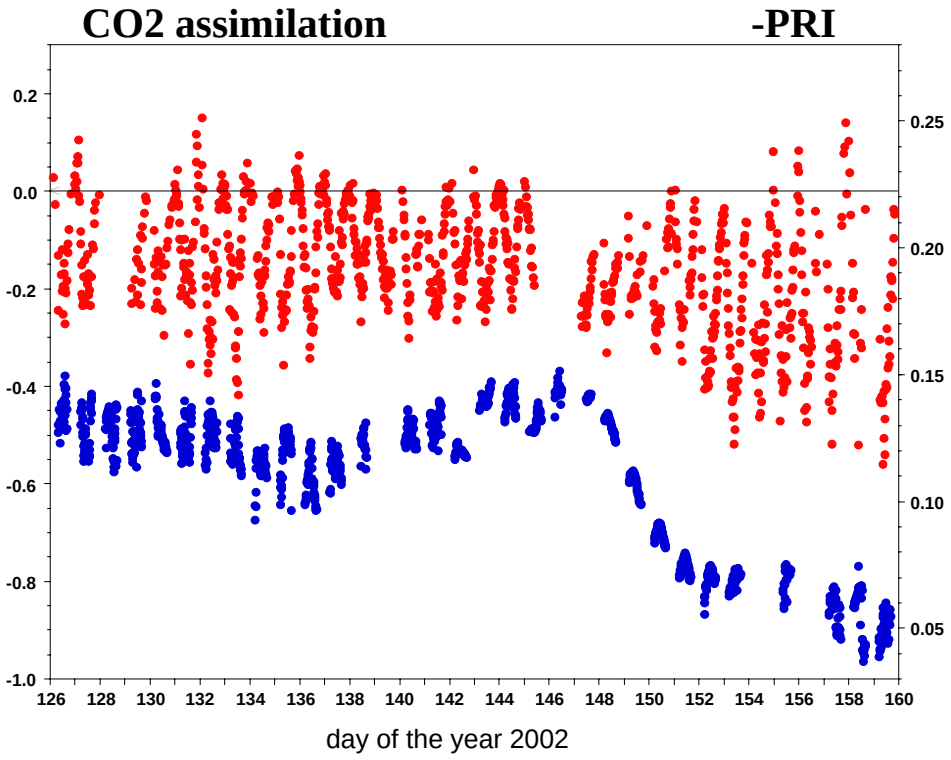

Figure 6.10. Variation of the spectral reflectance index PRI along the SIFLEX campaign, as compared to the variation of CO2 assimilation as modelled for the same period.

As we can see from these figures, to complement the fluorescence measurements for the monitoring of seasonal changes it is very important to have also some other spectral indicators (particularly PRI), to better understand the dynamical behaviour of vegetation changes.

In particular, PRI is a very good indicator of photosynthetic activity, as it has been demonstrated in SIFLEX, and then future campaigns and activities related to fluorescence measurements should consider PRI as a candidate variable to be simultaneously measured together with canopy fluorescence.

(d) Extrapolation to airborne/satellite measurements

A final step in the analysis of SIFLEX data has been a first attempt to simulate the signal at the top of atmosphere with the perspective of a possible future satellite mission with the goal of measuring fluorescence from the space.

Taking as starting point the signal levels at the top of the canopy as measured in SIFLEX, and for the typical solar illumination and atmospheric conditions of Sodankyla in summer, Figure 6.11 shows the measured (simulated) spectral radiance at the top of the atmosphere for a fluorescent target and for a non-fluorescent target. The difference between the two radiance levels determines the required sensitivity to detect fluorescence from the space.

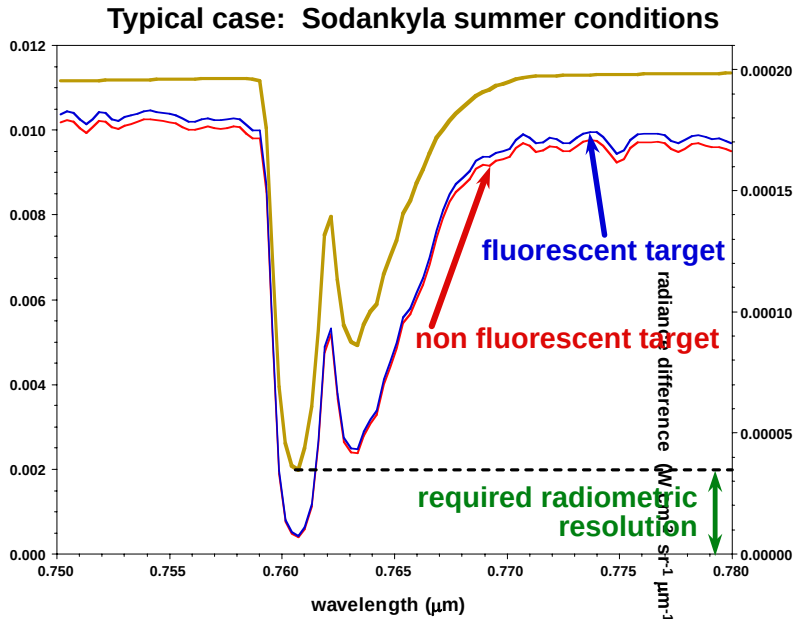

Figure 6.11. Variation in Top-Of-Atmosphere radiance signal for a fluorescent and a non-fluorescent targets, for a typical case corresponding to Sodankyla summer conditions.

In order to distinguish between actual fluorescence signal and small changes in surface reflectance, we have simulated also the satellite signal in the case of non-fluorescent targets but with a variation of 1% in surface reflectance. As indicated in Figure 6.12, such variation of 1% in surface reflectance produces a similar change in radiance levels, but spectrally different because of the different coupling of atmospheric effects to the case of surface reflection and surface emission.

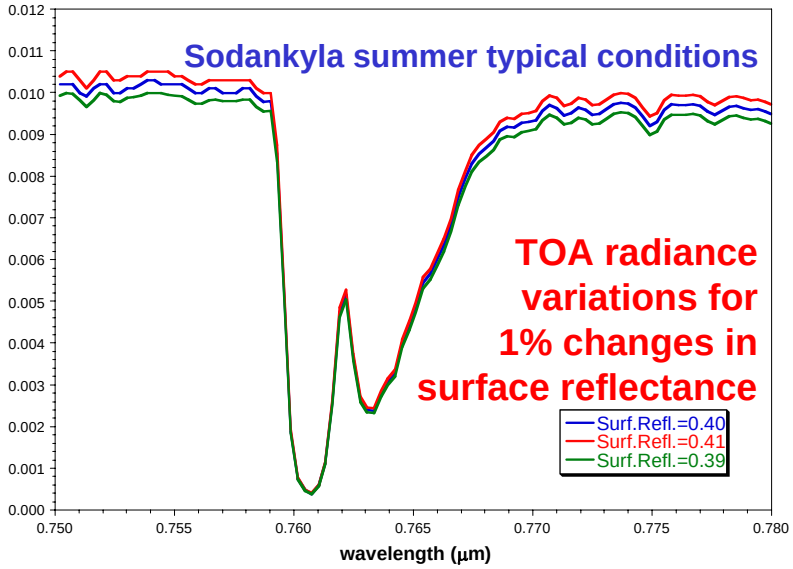

Figure 6.12. Variation in Top-Of-Atmosphere radiance signal for surface reflectance changes of 1% around a typical surface reflectance of 40%, for a typical case corresponding to Sodankyla summer conditions.

Thus, we conclude that an adequate radiometric resolution should allow to distinguish between fluorescence emission and surface reflectance changes in satellite measurements around the O2 absorption band (760 nm).

(e) Use of fluorescence measurements as input to models of CO2 fluxes

A complete database has been collected (also including target temperature, etc.) to allow future modelling of CO2 fluxes during SIFLEX by using standard and alternative inputs. In particular, parameters such as F687/F760, DPR (Double Peaks Ratio), and PRI can be tested as potential inputs to CO2 models, and the role of each parameters as input to such models should be identified since we have seen that they provide different, non-redundant information. Preliminary results are shown in Figure 6.13, although more work in needed to fully exploit the potential of the different measured photosynthetic indicators as potential inputs in CO2 flux model.

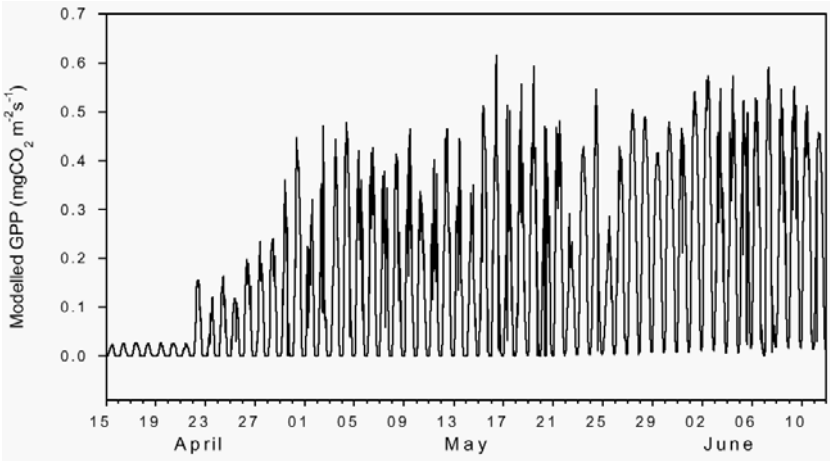

Figure 6.13. Gross Primary Production of the Scots pine canopy for the campaign period simulated by the optimal regulation model which uses measured Fv/Fm as parameter to describe the seasonal changes in biochemistry

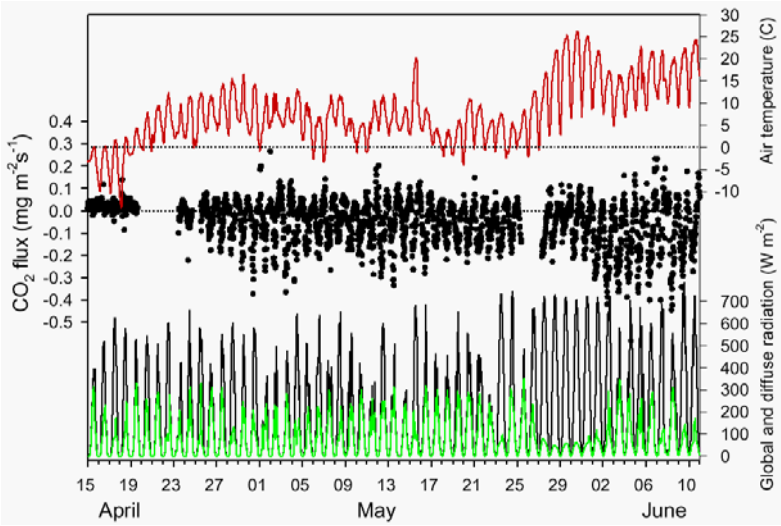

Fig. 6.14. Measured CO2 fluxes during SIFLEX. Positive CO2 fluxes denote net total respiration, negative values indicate net CO2 uptake by the forest

RECOMMENDATIONS

Some specific recommendations derived from the analysis of SIFLEX data can be summarised as follows:

(a) The need to derive absolute fluorescence values

Most current measurement techniques, including those used in SIFLEX, are based on relative values, by using a reference panel (white perfect diffuser) to which refer the relative measurements. There is a need to account for "absolute" fluorescence values without any external relative reference, by expressing the fluorescence levels in absolute radiance values. However, this required an extremely precise instrumental calibration, and quite accurate compensation of atmospheric effects. It remains a challenge for future experiments.

Field experiments under fully controlled conditions must be performed in order to determine such absolute values, and also to asses the role of the different environmental factors affecting the absolute fluorescence radiance levels.

(b) Need to improve the understanding of PRI variations

Due to the importance of PRI in tracking changes in canopy photosynthesis, there is a need to better interpret the observed PRI changes. It is known that PRI changes are due to a combination of different effects, some of then occurring in short time (the "quick phase") and some occurring over longer (weekly and even seasonal) time scales. Both changes have been observed in SIFLEX, but since PRI measurements was not a primary objective in SIFLEX such measurements were not planned to precisely measure and quantify the different changes. Future activities should focus to measure and characterise PRI variations under controlled and natural conditions, as well as to develop theoretical models that can explain such PRI changes by means of the underlying physiological processes at the leaf and at the canopy levels.

(c) Improvements in pigments analysis

One problem encountered in the analysis of SIFLEX data has been the high correlation between leaf pigments content and light levels at the time of leaf sampling. This has limited the analysis of fluorescence and PRI changes as a

function of the also varying pigment content in the canopy.
In future campaigns, leaf samples must be taken quite carefully in the same light conditions (preferably at night or keeping the samples in dark conditions before there are cut) to allow a proper interpretation of leaf pigment variations versus fluorescence levels. Due to the critical changes of pigments with light conditions, conclusions cannot be derived from samples taken under different illuminations.

(d) Accounting for canopy structural effects

Canopy structural effects must be accounted for, including:

- BRDF (reflectance anisotropy) description and analysis of effects on the resulting anysotropic fluorescence emission

- Illumination / shadows geometrical effects in instantaneous fluorescence measurements, and mostly to decouple the observed variations along the diurnal cycle between actual physiological changes and simple effects due to varying illumination.

- Intrinsic three-dimensional effects in fluorescence emissions, including reabsorptions along paths through the canopy due to the presence of leaves with chlorophyll in the paths from the emission point to the observed point. Such re-absorption effects also occur at the leaf level, but at the leaf level are more easily accounted for due to the relative simple leaf structure. At the canopy level, the description of re-absorption effects along intermediate paths remains as a challenge due to the need to account for the actual canopy structure.

(e) Hα versus oxygen band

Due to the difficulties in measurements within the oxygen absorption bands over varying atmospheric conditions, it is stressed the importance of looking for alternatives, such as Hα line, and compare fluorescence measurements in oxygen bands and in Hα lines in view of future airborne and spaceborne instruments.

(f) Future campaigns

As confirmed in SIFLEX, fluorescence in mono-vegetation cases mostly track PAR variations (in absence of stress conditions). Fluorescence changes are more significant in the case of spatial variations in multi-vegetation cases under same PAR conditions. Then, there is a need to use airborne sensors that

can measure spatial variations with the same illumination conditions. Hα methods should be tested as alternative (or complement) to O2 methods in future campaigns.

Finally, it must be emphasised that the main result from SIFLEX is the resulting database. The large amount of data collected during the SIFLEX experiment will for sure serve in future studies to better understand the observed variations in fluorescence levels as related to environmental conditions. The full in-depth analysis of the whole database will deserve future dedicated studies. Moreover, the lessons learn in SIFLEX should serve to prepare new campaigns more focused on particular aspects. The airborne fluorescence sensor AIRFLEX is an excellent opportunity to extend the SIFLEX results to other targets, and in particular to move from the analysis of temporal evolution in a fixed spatial location (that was the case in SIFLEX) to the analysis of spatial variability under the same instantaneous environmental conditions over extended areas, that was the main missing aspect in SIFLEX.

On the other hand, the current activities related to modelling leaf and canopy fluorescence emission provides an excellent opportunity to exploit SIFLEX data, since the models under development should reproduce the observed trends in SIFLEX data. The SIFLEX dataset is a tool for future modelling / validation studies.

References

Adams I. W, Demmig-Adams B. (1994) Carotenoid composition and dawn regulation of phutosystem II in three coniferous species during the winter. Physiol Plant 92: 451-458

Agati G, Cerovic ZG and Moya I (2000) The effect of decreasing temperature up to chilling values on the in vivo F685/F735 chlorophyll fluorescence ratio in Phaseolus vulgaris and Pisum sativum: The role of the Photosystem I contribution to the 735 nm fluorescence band. Photochem. Photobiol. 72: 75-84

Allen JF (1992). How does protein phosphorylation regulate photosynthesis? TIBS 17:12-17

Aurela, M., Laurila, T. & Tuovinen, J.-P. (2002) Annual CO_2 balance of a subarctic fen in northern Europe: The importance of the wintertime efflux. Journal of Geophysical Research 107D21, ACH-17, 1-12.

Aurela, M., Laurila, T. & Tuovinen, J.-P. (2001) Seasonal CO_2 balances of subarctic mire. Journal of Geophysical Research 106, 1623-1638.

Aurela, M., Tuovinen, J.-P. & Laurila, T. (2001) Net CO_2 exchange of a subarctic mountain birch ecosystem. Theoretical and Applied Climatology 70, 135-148.

Berk A., Anderson G.P., Acharya P.K,. Chetwynd J. H, Bernstein L. S., Shettle E.P., Matthew M.W., and Adler-Golden S.M. , MODTRAN 4 user's manual. Air Force Research Laboratory, Space Vehicles Directorate, Air Force Materiel Command, Hascom AFB, MA 01731-3010, 1999.

Bilger, W., Björkman, O. & Thayer, S.S. (1989) Light-induced spectral absorbance changes in relation to photosynthesis and the epoxidation state of xanthophyll cycle components in cotton leaves. Plant Physiology, 91, 542-551.

Bubier, J. L., Rock, B. R., Crill, P. M. (1997) Spectral reflectance measurements of boreal wetland and forest mosses. J. Geophys. Res., 102, 29483-29494.

Caselles C., Niclòs N., Valor E. ,Coll C. and Moya I. , "Air-canopy temperature difference and fluorescence emission," Proceedings of the FLEX Workshop, June 2002, ESTEC, Noordwijk, The Nertherlands.

Demmig-Adams, B. and Adams, W. W., III (1996) The role of xanthophylls cycle carotenoids in the protection of photosynthesis. Trends in Plant Science, 1, 21-26.

Evain, S., Camenen, L. and Moya, I. (2001), Three channels detector for remote sensing of chlorophyll fluorescence and reflectance from vegetation, In 8th International Symposium: Physical Measurements and Signatures in Remote Sensing, (M. Leroy, ed.) Aussois, France, 2001, CNES, pp. 395-400.

Evain, S., Flexas, J.[1], Moya, I. (2003) Remote sensing of non-photochemical quenching of chlorophyll fluorescence and canopy reflectance changes at 531 nm, Remote Sensing of Environment, submitted

Flexas J, Briantais J-M, Cerovic ZG, Medrano H and Moya I (2000) Steady-state and maximum chlorophyll fluorescence responses to water stress in grapevine leaves: A new remote sensing system. Remote Sens Environ 73: 283-297

Gamon, J.A., Field, C.B., Bilger, W., Björkman, O, Fredeen, A.L. & Peñuelas, J. (1990). Remote sensing of the xanthophyll cycle and chlorophyll fluorescence in sunflower leaves and canopies. Oecologia, 85, 1-7.

Gamon, J.A., Serrano, L. & Surfus, J.S. (1997).The photochemical reflectance index: an optical

indicator of photosynthetic radiation use efficiency across species, functional types, and nutrient levels. Oecologia, 112, 492-501.

Heber, U. (1969) Conformational changes of chloroplasts induced by illumination of leaves in vivo. Biochimica et Biophysica Acta, 180, 302-319.

Heber, U., Neimanis, S. & Lange, O.L. (1986) Stomatal aperture, photosynthesis and water fluxes in mesophyll cells as affected by the abscission of leaves. Simultaneous measurements of gas exchange, light scattering and chlorophyll fluorescence. Planta, 167, 554-562.

Laurila, T., Soegaard, H., Lloyd, C. R., Aurela, M., Tuovinen, J.-P. & Nordstroem, C. (2001). Seasonal variations of net CO_2 exchange in European Arctic ecosystems. Theoretical and Applied Climatology 70, 183-201.

Lichtenthaler H. K., Hak R. and Rinderle U. (1986), "The chlorophyll fluorescence ratio F690/F730 in leaves of different chlorophyll content", Photosynth. Res.,25,295-298

Moya I, Cerovic ZG, Evain S, Goulas Y, Ounis A and Stoll M-P (2001) Télédétection de l'activité photosynthétique : de la vérité terrain à la mesure satellitaire. In: Leroy M (Ed.), 8th International Symposium: Physical Measurements and Signatures in Remote Sensing, pp 319-332, Aussois, France: CNES.

Moya, I., Silvestri, M., Cinque, G. & Bassi, R. (2001) Time resolved fluorescence analysis of the photosystem II antanna proteins in detergent micelles and liposomes. Biochemistry, 40, 12552-12561.

Niclòs R., Caselles C., Rubio E., Coll C. , and Valor E. , "Precise and reliable sea surface temperature retrieval," Journal of Applied Metheorology (in press).

Niyogi, K.K. (1999) Photoprotection revisited: genetic and molecular approaches. Annual Review of Plant Physiology and Plant Molecular Biology, 50, 333-359.

Ottander, C., Campbell, D. and Öquist, G. (1995) Seasonal changes in Photosystem II organization and pigment composition in Pinus sylvestris. Planta, 197, 176-183.

Ounis A. Télédétection de la fluorescence des couverts végétaux induite par laser: application des techniques de corrélation temporelle microseconde et nanoseconde [PhD Thesis]. Université de Paris-Sud, 2001

Peñuelas, J., Gamon, J.A., Fredeen, A.L., Merino, J. & Field, C.B. (1994) Reflectance indices associated with physiological changes in nitrogen- and water-limited sunflower leaves. Remote Sensing of Environment, 48, 135-146.

Pietras C., Abuhassan N. K., Haeffelin G. , Brogniez G. , Legrand M. , and Buis J. P., "Development of a high precision thermal infrared field radiometer," Proceedings of 6th ISPRS Symposium, Val d'Isere, France, Jan. 17-21, pp. 809-815, 1994.

Rubio E., Caselles V., and Badenas C., "Emissivity measurements of several soils and vegetation types in the 8-14 mm wave band: Analysis of two field methods," Remote Sensing of Environment, vol. 59, pp. 490-521, 1997.

Sicard M., SpyakP. R. , Brogniez G. , Legrand M. , Abuhassan N. K., Pietras C. , and Buis J. P. , "Thermal infrared field radiometer for vicarious cross-calibration: characterization and comparisons with other field instruments," Optical Engineering, vol. 38(2), pp. 345-356, 1999.

Yamamoto, H.Y. & Kamite, L. (1972) The effects of dithiothreitol on violaxanthin de-epoxidation and absorbance changes in the 500-nm region. Biochimica et Biophysica Acta, 267, 538-543.



FINNISH METEOROLOGICAL INSTITUTE